AD-A085 708 AIR FORCE INST OF TECH WRIGHT-PATTERSON AFB OH SCHOO--ETC F/G 9/5
EFFECTS OF ADAPTIVE ANTENNA ARRAYS ON BROADBAND SIGNALS.(U)
JUN 80 W A RISKI

UNCLASSIFIED AFIT/GE/EE/80-4 NL

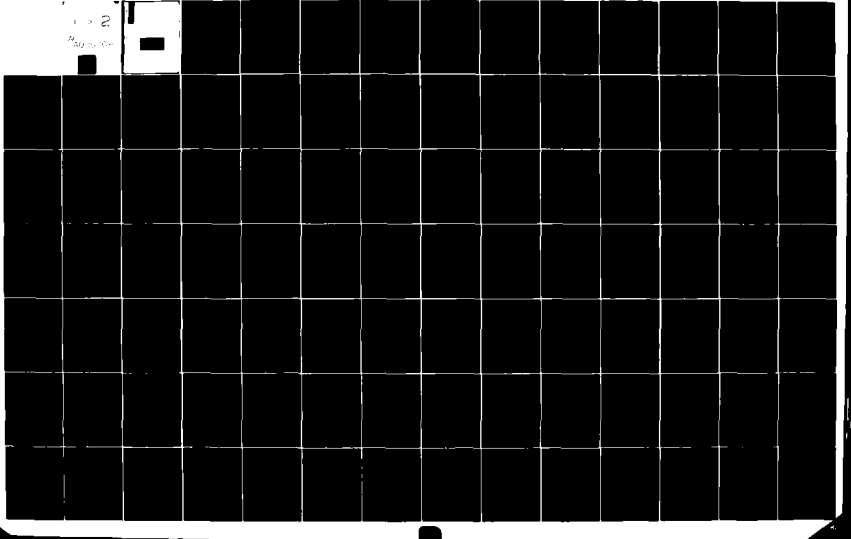

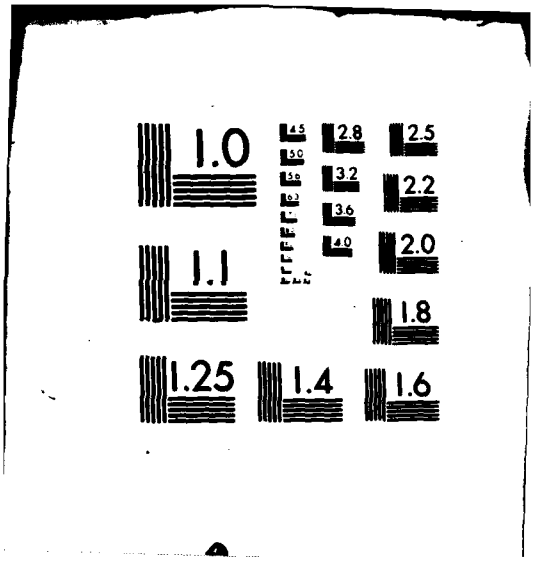
1.0
1.1
1.25
1.4
1.6
1.8
2.0
2.2
2.5
2.8
3.2
3.6
4.0
4.5
5.0

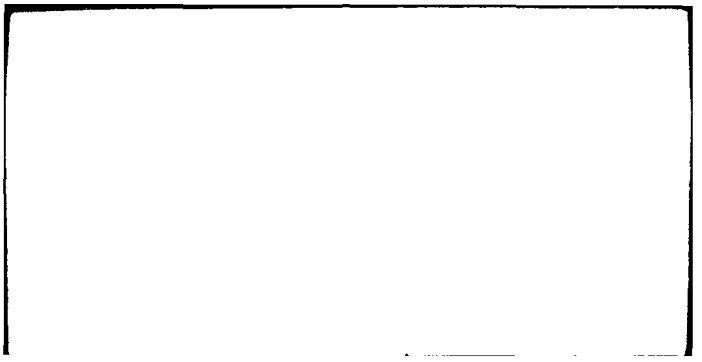

(14) AFIT/GE/EE/80-4

(11) Jun 80

(12) 164

(6) EFFECTS OF ADAPTIVE ANTENNA ARRAYS ON BROADBAND SIGNALS.

(9) master's THESIS

AFIT/GE/EE/80-4

(10) William [redacted] Riski
~~Captain~~ USAF

Artman

DTIC
ELECTE
JUN 13 1980
S
A

Approved for public release; distribution unlimited.

012225

AFIT/GE/EE/80-4

EFFECTS OF ADAPTIVE ANTENNA ARRAYS ON BROADBAND SIGNALS

THESIS

Presented to the Faculty of the School of Engineering
of the Air Force Institute of Technology
Air Training Command
in Partial Fulfillment of the
Requirements for the Degree of
Master of Science

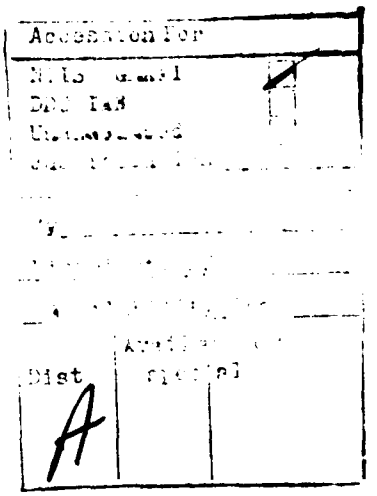

by
William A. Riski, B.S.
Captain USAF
Graduate Electrical Engineering
June 1980

Approved for public release; distribution unlimited.

Preface

The first step in completing a thesis is to choose either a topic or an advisor. I chose Capt. Stanley R. Robinson as an advisor. It was an easy decision, for his fame preceded him. Together we chose to continue the research on antenna arrays begun by Capt. Edward Raska Jr. and sponsored by Major Jurgen O. Gobien of the Rome Air Development Center. This previous work had led to some interesting discoveries; phase steered antenna arrays distort an incoming broadband signal such that the output is the signal plus its first time derivative. The purpose of this continuing study was to investigate the effects of adding tapped delay lines to the array and adapting the array to place a null on jamming sources.

I spent many long hours gaining some knowledge of adaptive antenna arrays. Also included was the usual pleasure of writing a computer program to support the numerical analysis to be done. I thank Capt. Robinson for bringing me back on track the many times I became infatuated by computer plots which led nowhere. Eventually the interesting research ended and the drudgery of writing began. Though this phase took much too long, I am especially thankful that Capt. Robinson continued with his encouragement and support.

I wish to also thank Maj. Carl and Lt. Col. Carpinella for the time they devoted to reading my draft and discussing this project and its goals. It is truly unfortunate that Capt. Robinson has decided to leave this institution and

move on to other endevors. I wish him well and extend my thanks once more.

Finally, I am thankful to my wife, Laura, for her love and patience not only during this research effort but during this entire academic program, and beyond.

William A. Riski

Contents

Preface ii

List of Figures vi

List of Tables. viii

Abstract. ix

I. Introduction 1

II. System Models. 5

A. Signal and Array Equation. 5
B. Frequency Response 15
C. Signal of Interest 20
D. Performance. 24

III. Adaptive Weights 29

A. Optimum Weights. 29
B. Noise Environment. 31
C. Noise Covariance Matrix. 33
D. Karhunen-Loève Expansion 35
E. Numerical Analysis of Model. 44

IV. Antenna Arrays without Adaptive Weights. 48

A. Linear Array 48
B. Linear, Equally-Spaced Array 50
C. Transfer Function. 53
D. Transfer Function with Tapped Delay-Lines. . . 62

V. Antenna Arrays with Adaptive Weights 73

A. Linear Array Adapted to Narrowband Jammers 73
1. Phase Response 75
2. Frequency Response for a Jammer at $\theta = 10^0$. 77
3. Frequency Response for a Jammer at $\theta = 50^0$ 81
4. Frequency Response for Multiple Jammers. . 91
B. Linear Array Adapted to Broadband Jammer . . . 96
1. Frequency Response for a Jammer at $\theta = 10^0$. 98
2. Frequency Response for a Jammer at $\theta = 50^0$. 101

VI. Conclusions and Recommendations 113

Bibliography 117

Appendiees 119

Appendix A: Perturbation Analysis 119
Appendix B: Phase Response Figures. 122
Appendix C: Frequency Response Figures. 135

Vita 151

List of Figures

Figure		Page
1	General System Model	7
2	Adaptive Array Model	9
3	Pseudo-Noise Waveform.	21
4	Autocorrelation Waveform	23
5	Power Spectral Density of Broadband Jammer . . .	43
6	Frequency Response	55
7	Phase Response	56
8	Polar Plot of $\|A(\theta)\|$	58
9	Polar Plot of $\|B(\theta)\|$	59
10	Polar Plot of $\|C(\theta)\|$	60
11	Plot of the Ratio $\left\|\frac{A(\theta)}{B(\theta)}\right\|$	61
12	Generic Frequency Response of Transfer Functions	63
13	Frequency Response	65
14	Phase Response	66
15	Polar Plot of $\|A(\theta)\|$	68
16	Polar Plot of $\|B(\theta)\|$	69
17	Polar Plot of $\|C(\theta)\|$	70
18	Plot of the Ratio $\left\|\frac{A(\theta)}{B(\theta)}\right\|$	71
19	Frequency Response	78
20	Frequency Response	80
21	Frequency Response	82
22	Frequency Response	83
23	Frequency Response	87
24	Polar Plot of $\|A(\theta)\|$	88

Figure		Page
25	Polar Plot of $\|B(\theta)\|$	89
26	Polar Plot of $\|C(\theta)\|$	90
27	Frequency Response	92
28	Frequency Response	94
29	Frequency Response	95
30	Frequency Response	97
31	Frequency Response	99
32	Frequency Response	100
33	Frequency Response	103
34	Frequency Response	104
35	Frequency Response	105
36	Frequency Response	106
37	Frequency Response	110

List of Tables

Table		Page
I	Broadband Jammer Correlation Function	47
II	Taylor Series Coefficients for Narrowband Jammer at 10^0.	77
III	Taylor Series Coefficients for Narrowband Jammer at 50^0.	84
IV	Frequency Response for Narrowband Jammer at 50^0 .	85
V	Taylor Series Coefficients for Broadband Jammer at 10^0.	102
VI	Taylor Series Coefficients for Broadband Jammer at 50^0.	102
VII	Weights for Broadband Jammer at 50^0	108
VIII	Transfer Function of Delay Line for Broadband Jammer at 50^0	108
IX	Weights for Narrowband Jammer at 50^0.	111

Abstract

This paper develops a complex baseband model for an adaptive array with N isotropic elements and T tapped delay lines behind each element. Three aspects of arrays are represented: spatial and temporal propagation delays and the weighting coefficients. The model is used to determine the steady state effect of arrays on wideband signals. Optimum weights are calculated based on the noise covariance matrix produced by single and multiple narrowband jammers and single broadband jammers. It is shown that discrete spectral lines can be used to model a broadband jammer. For a jammer with 4% f_0 bandwidth, this approximation yields a correlation function which is accurate to within 0.53%. For a linear, equally spaced adaptive array the output consists of the input signal and its first time derivative. This first derivative distortion is reduced by the addition of tapped delay lines only when the noise environment contains broadband jammers. This performance improvement is quantified by increased null depth. The improvement, for a 4% f_0 bandwidth jammer, was 6.2 db with a jammer located at 10^0 and 2.5 db for a jammer at 50^0.

EFFECTS OF ADAPTIVE ANTENNA ARRAYS ON BROADBAND SIGNALS

I Introduction

Adaptive antenna arrays have received considerable attention in recent years. One application of some interest is their use in communications systems where reducing the effects of undesired sources of interference yields improved system performance (Ref 17,6). In an adaptive array, phase and amplitude of the signal at each receiving antenna element is weighted and the resulting signals summed to produce the array output. The values of the element weights are determined by an algorithm which can act to steer the main antenna beam, scan the beam across a target, stear nulls in the direction of interfering signals, or meet several other system requirements (Ref 14:212-213). Not all these requirements can be met concurrently, but algorithms exist to steer the main beam in the direction of a desired signal while steering nulls in the direction of interfering signals. However, satisfactory performance requires that the interfering signals be much stronger than the desired signal. If the interference is weak or absent, the desired signal itself may have a null steered in its direction. In this situation, we can greatly improve the adaptive arrays performance by being able to distinguish between a

desired signal and the interference. The new algorithm can then be constrained to avoid nulling the desired signal while still nulling the interferences.

An information transmission technique whose signal structure can be distinguished from undesired signals is spread spectrum modulation. This technique employs a pseudo-noise binary phase shift keying (PN-BPSK) modulation scheme which results in a transmitted signal whose spectrum is orders of magnitude wider than the information spectrum of the unmodulated signal. The pseudo-noise (PN) coded sequence has a time-autocorrelation structure with a distinctive peak. It is this correlation structure in the transmitted signal which is exploited to differentiate between the desired signal and undesired signals. Current technology permits the use of PN-BPSK spread spectrum signals in conjunction with adaptive antenna arrays (Ref 1).

An antenna array acts as both a spatial and temporal filter. For an incident signal at a fixed arrival angle, the array can distort the signals it receives, especially if they are broadband signals. It is important to characterize this distortion effect, since digital receivers using correlator detectors can be quite sensitive to phase and amplitude distortion. Distortion can be divided into two categories: static and dynamic. Static effects are inherent in the frequency-sensitive nature of the antenna array. Dynamic effects are due to the adaptive nature of the array and the resultant time varying response it produces. In this paper we shall

limit ourselves to the static distortion effects.

Recent analysis has begun in this area (Ref 11). However, this work addresses antenna arrays without adapted weights or tapped delay lines. In this paper we will calculate weights adapted to a noisy environment and use the static value of these weights in the array model. The steady-state response of the adapted antenna array will then be analyzed. In addition, tapped delay line filters will be placed behind each antenna element and the response of the array analyzed. The addition of tapped delay-lines allows the associated weights to adapt to the bandwidth of a noise source. This results in a broader antenna pattern null in the direction of that source.

In Chapter II the analysis is begun by introducing the various models and assumptions that are the basis for the ensuing work. The basic properties of an adaptive array are introduced. From this, a general transfer function equation is derived. The chapter ends with an analysis of conditions necessary for distortionless transmission of a signal through the array.

In Chapter III we begin with a discussion of optimum adaptive weights and the noise signals which drive these weights. The noise covariance matrix used in calculating the optimum weights is discussed with respect to narrowband and broadband jammers. A Karhunen-Loève expansion is used to derive a representation for the correlation function of a

broadband jammer based on discrete spectral lines. The chapter ends with a numerical analysis of the correlation model.

In Chapter IV we look at the transfer function of a linear, equally spaced array with phase steering. Several graphical results are analyzed for arrays with and without tapped delay-lines.

In Chapter V we extend the transfer function analysis to arrays adapted to narrowband and broadband jammers. The effects of tapped delay lines and jammer bandwidth on the output signal's distortion are investigated.

Chapter VI contains conclusions and recommendations.

II System Models

This chapter introduces a complex baseband model for the desired signal and adaptive array transfer function. The frequency response of the array is further analyzed using a Taylor series expansion. From this we develop performance criteria associated with signal distortion caused by the array.

A. Signal and Array Equation

The desired signal is written

$$\mathcal{s}(t) = V(t)\cos[2\pi f_0 t + \phi(t)] \tag{1}$$

where $V(t)$ and $\phi(t)$ are amplitude and phase, respectively, of an rf carrier at center frequency f_0. This can also be written as

$$\mathcal{s}(t) = \mathrm{Re}\left\{s(t)e^{[-j2\pi f_0 t]}\right\} \tag{2}$$

where the complex baseband representation of the signal is

$$s(t) = V(t)e^{[j\phi(t)]} \tag{3}$$

and $\mathrm{Re}\{\cdot\}$ denotes the real part of the enclosed quantity. The center frequency term in (2) will be ignored from now on and only the complex representation of the signal written. The complex representation contains all the information of the signal $\mathcal{s}(t)$ centered at f_0 since modulation of $\mathcal{s}(t)$

would either be amplitude modulation or phase modulation. In either case, the information is contained in $V(t)$ or $\phi(t)$, respectively. Therefore, there is an implicit time dependence of $e^{[-j2\pi f_0 t]}$ when we use the complex baseband representation $s(t)$ (Ref 9:121).

Consider the geometry and system shown in Figure 1. The configuration is for a one-dimensional array geometry. The signal impinging on the antenna array elements is assumed to have originated from a point source in the far field, or Fraunhofer, region of the array. This region is defined to begin at a distance of L^2/λ from the array where L is the largest array dimension and λ is the wavelength of the wave propagating from the point source (Ref 14:12). For these conditions, the wavefront striking the array surface is a plane wave (Ref 9:124). It is assumed here that the equiphase surface of the plane wave is also an equiamplitude surface. Therefore the signal at the array is a uniform plane wave. This assumption is valid since any spatial variations in the plane wave can be expected to be slowly varying in relation to the delays it experiences in propagating between the array elements at the rf frequencies of interest. The signal representation in Eq.(3) is valid in the time-frame of the array surface.

For the antenna array, our primary interest is in modeling the propagation and adaption effects under steady state conditions. In addition, the array is assumed to be "ideal".

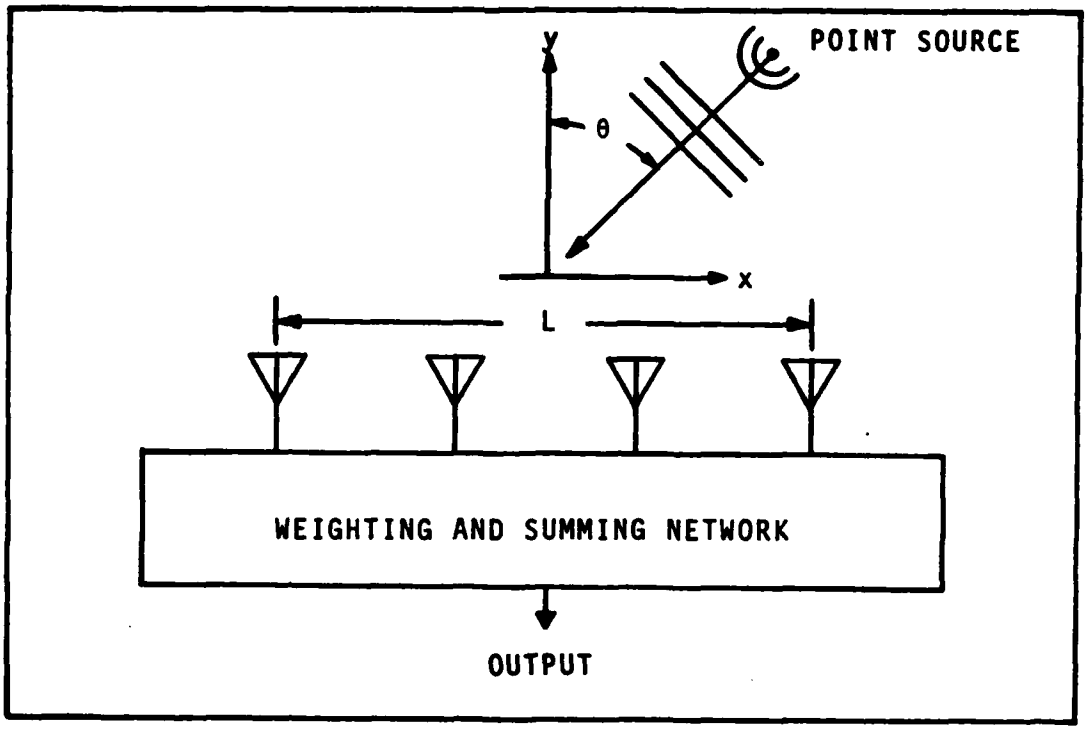

Figure 1. General System Model

The assumptions which define an "ideal" array are first, all antenna elements are isotropic in nature. Second, mutual coupling effects between elements are ignored since the array has few elements. Third, practical issues of circuit element nonlinearities, filtering and dispersive effects, etc. are ignored. The analysis will consider an ideal adaptive array as a filter and identify the fundamental distortion effects it produces. Once identified, the limitations above can be removed and their impact compared to the baseline developed here.

There are three effects to model in the adaptive antenna array: spatial, temporal, and adaptive. Spatial effects

are represented as time delays experienced by the signal as it propagates across antenna elements. These delays are dependent upon the angle of arrival θ of the signal. Temporal effects are represented as time delays experienced by the signal as it propagates down a tapped delay-line behind an element and are not angle dependent. Adaptive effects are modelled as a complex term used as a multiplier on the signal at each antenna port. These complex terms are referred to as adaptive weights, weighting coefficients, or just weights. An antenna port can be either an element or a tap on a delay line. Therefore an array with four elements and three taps per element has twelve ports. The weights are dependent upon the desired signal's and jamming signal's statistics, power, and geometries relative to the array. Figure 2 refines Figure 1 by detailing the array configuration. The notation of Figure 2 is listed below:

$w_{i,g}$ $\triangleq$ Complex adaptive weight at the port defined by the i^{th} element and g^{th} tap on the delay line behind that element.

Δ $\triangleq$ Delay between taps in units of meters.

N $\triangleq$ Total number of antenna elements.

T $\triangleq$ Total number of taps per delay line.

$y(t)$ $\triangleq$ Array output.

$H_M(f)$ $\triangleq$ Matched filter transfer function, matched to the desired signal.

$r(\tau)$ $\triangleq$ Array output after matched filter.

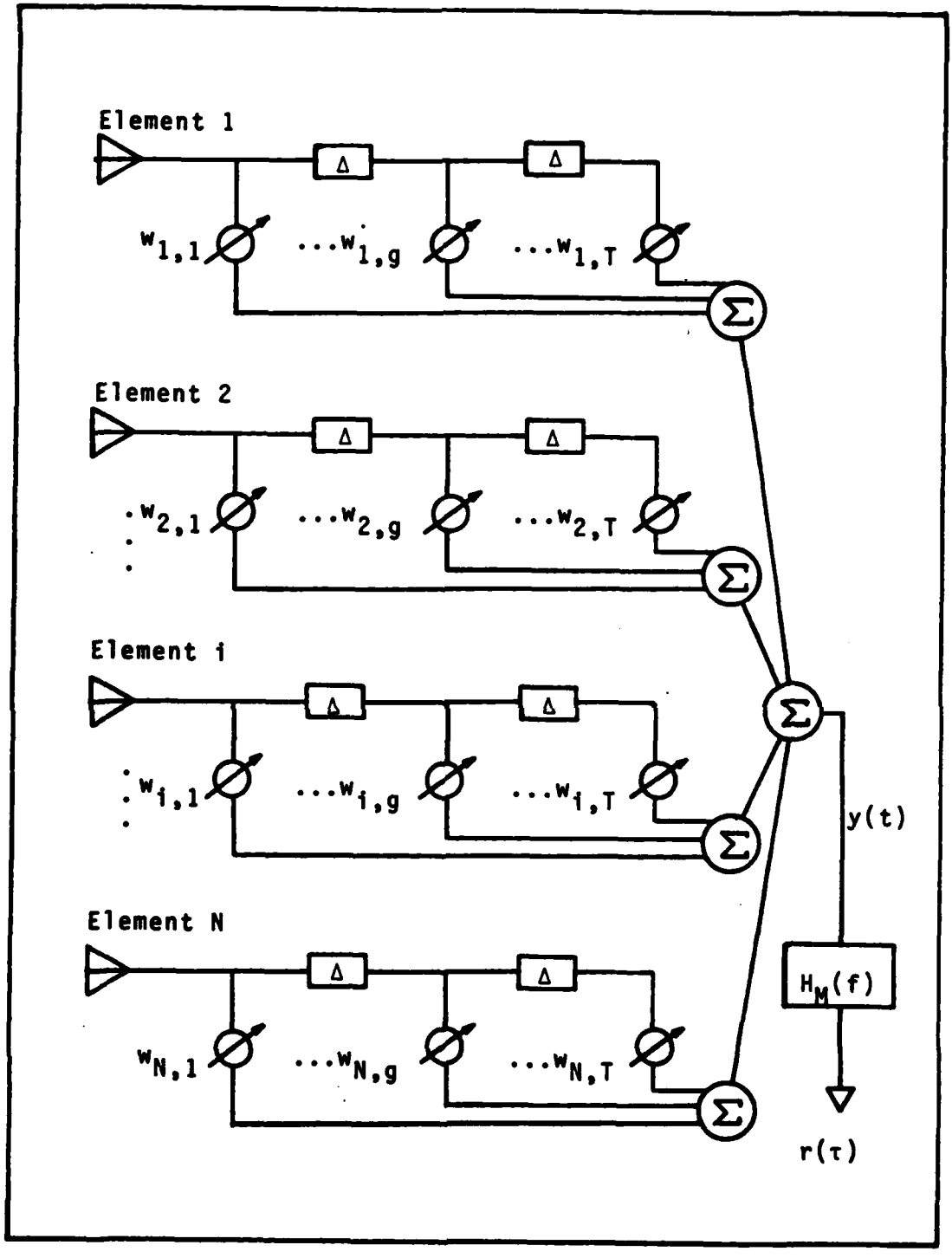

Figure 2. Adaptive Array Model

The total propagation delay of a signal from an antenna port to a reference point can be represented as a time delay $t_{i,g}$ where i refers to the i^{th} element and g refers to the g^{th} tap on a delay line. This delay can be factored into a spatial delay dependent on signal arrival angle and a fixed temporal delay

$$t_{i,g} \triangleq t_i(\theta)+t_g \tag{4}$$

The assumptions used to identify the far field region of an array also lead to an approximation for $t_i(\theta)$. It is

$$t_i(\theta) \simeq \frac{x_i \sin(\theta)}{c} \tag{5}$$

where x_i is the distance from the reference point to the i^{th} element and c is the velocity of light. As shown in Figure 1, the direction of arrival of the signal θ is measured with respect to the array normal. This convention results in the array broadside corresponding to $\theta=0^0$.

Temporal delay t_g corresponds to the propagation delay experienced by a signal in travelling along a delay line from an antenna element $(g\underline{\Delta}1)$ to tap g (see Figure 2). The delay is dependent on the distance between taps and not signal arrival angle. The temporal delay is

$$t_g \triangleq \frac{y_g}{c} \tag{6}$$

where y_g is the distance from the reference point to the

g^{th} tap. The reader should not infer from the use of x_i and y_g that the array is two-dimensional.

The distances to a port are represented in a rectangular coordinate system. The reference point or origin is defined as element one, tap one (i.e. i=1,g=1) .

The complex adaptive weights contain an amplitude and phase term. Both terms are independent of time since transient effects are not within the scope of this research effort. The weight at the i^{th} element and g^{th} tap (i.e. port i,g) is defined by

$$w_{i,g} \triangleq G_{i,g} \exp(j\alpha_{i,g}) \tag{7}$$

where $G_{i,g}$ and $\alpha_{i,g}$ are real numbered values determined by the equations discussed in Chapter III.

Since the signal at port i,g is delayed by amount $t_{i,g}$, we can represent it as

$$\begin{aligned} \Delta_{i,g}(t) &= \Delta(t-t_{i,g}) \\ &= \mathrm{Re}\{s(t-t_{i,g})\exp(-j2\pi f_0(t-t_{i,g}))\} \end{aligned} \tag{8}$$

The complex baseband representation for the desired signal at port i,g is

$$s_{i,g}(t) = s(t-t_{i,g})\exp(+j2\pi f_0 t_{i,g}) \tag{9}$$

Note that with complex baseband notation, a delay results in

an additional phase term. The adaptive antenna array output is the summation of the signals at each port, as defined in Eq.(9), multiplied by their associated weight, defined in Eq.(7). The array output is

$$y(t) = \sum_{i=1}^{N} \sum_{g=1}^{T} w_{i,g} s(t-t_{i,g}) \exp(+j2\pi f_0 t_{i,g}) \qquad (10)$$

It is apparent from Figure 2 that the origin of the coordinate system is not the geometric center, or phase center, of the array model (Ref 15:72). The phase center of an array is defined as the point at which the sum of the time delays to each port is zero. To isolate the effects of this choice of origin within the array representation, a phase center term t_c must be factored out. Propagation delay t_c is a constant, for a given angle θ, which is a measure of the difference between the array's phase center and the arbitrarily chosen coordinate system origin. The phase center is derived from

$$\sum_{i=1}^{N} \sum_{g=1}^{T} (t_i + t_g - t_c) = 0 \qquad (11)$$

$$\sum_{i=1}^{N} \sum_{g=1}^{T} (t_i + t_g) = \sum_{i=1}^{N} \sum_{g=1}^{T} t_c = NTt_c \qquad (12)$$

Solving for the phase center term yields

$$t_c = \frac{1}{NT} \sum_{i=1}^{N} \sum_{g=1}^{T} (t_i + t_g)$$

$$= \frac{1}{NT} \sum_{i=1}^{N} \sum_{g=1}^{T} t_{i,g} \qquad (13)$$

Factoring t_c out of the array output yields

$$y(t) = \exp(j2\pi f_0 t_c) \sum_{i=1}^{N} \sum_{g=1}^{T} w_{i,g} s(t - t_{i,g} + t_c)$$

$$\exp(j2\pi f_0 (t_{i,g} - t_c)) \qquad (14)$$

This factorization allows us to separate the effects of our choice of coordinate system origin from the effects inherent in the generic array model itself. The first exponential corresponds to a constant phase shift. It is a function, through t_c , of the relationship between the signal location, phase center location, and the location of the origin of the coordinate system. In addition, t_c results in a constant time delay of the signal. Writting Eq.(14) in the frequency domain yields

$$Y(f) = e^{\left[j2\pi(f+f_0)t_c\right]} \sum_{i=1}^{N} \sum_{g=1}^{T} w_{i,g} S(f)$$

$$e^{\left[j2\pi(f+f_0)(t_{i,g} - t_c)\right]} \qquad (15)$$

where Y(f) and S(f) are the Fourier transforms of y(t) and s(t) respectively. The system transfer function,

$H(f,\theta)$, is defined as the ratio of output to input forcing functions. From Eq.(15) the transfer function of an adaptive antenna array is

$$H(f,\theta) = e^{(j2\pi(f+f_0)t_c)} \sum_{i=1}^{N} \sum_{g=1}^{T} w_{i,g} e^{(j2\pi(f+f_0)(t_{ig}-t_c)} \quad (16)$$

The dependence of this function on frequency is shown explicitly. Its dependence on signal arrival angle θ is implicit in $t_{i,g}$ as was shown in Eq.(5). The reader is reminded at this point that we still are working with complex baseband notation. Therefore frequency f is still defined as a frequency offset from f_0 . The transfer function is dependent on several other parameters which are defined by a particular system (signal and array) configuration. These parameters are the weighting coefficients ($G_{i,g}$ and $\alpha_{i,g}$) and array geometry (x_i,y_g,N, and T) . (See Eqs.(7), (4), (5), and (6)). Although $H(f,\theta)$ is dependent on these parameters, they are all fixed, for a given system, in the steady state analysis of subsequent chapters.

One of the main objectives of this thesis is to investigate the distortion experienced by wideband signals as they pass through an adaptive array. It is the analysis of Eq(16) which will reveal any distortion. $H(f,\theta)$ must meet two conditions for distortionless transmission of signals. First, its amplitude response ($|H(f,\theta)|$) must be constant over the frequency spectrum of the desired signal. Second, its phase

response $\left(\arg \angle H(f,\theta)\right)$ must be linear over the same frequency spectrum. These conditions will result in all spectral components of the input signal having the same attenuation and phase shift at the array output. In the time domain, the output signal will be a scaled, delayed replica of the input signal.

B. Frequency Response

To explore the frequency dependence of $H(f,\theta)$ further, the function is expanded into a Taylor series about $f=0$. (Since the expression is in complex baseband representation, this corresponds to expanding physical quantities about the center frequency f_0.) It is assumed here that the adaptive weights are independent of frequency f. This corresponds to steering the array at center frequency f_0. The series is

$$H(f,\theta) = e^{[j2\pi(f+f_0)t_c]} \sum_{i=1}^{N} \sum_{g=1}^{T} w_{i,g} e^{[j2\pi f_0(t_{i,g}-t_c)]} \Big\{ 1 + (j2\pi f(t_{i,g}-t_c)) + \frac{(j2\pi f(t_{i,g}-t_c))^2}{2!} + \ldots + \frac{(j2\pi f(t_{i,g}-t_c))^n}{n!} + \ldots \Big\} \quad (17)$$

$$\triangleq e^{[j2\pi(f+f_0)t_c]}\{A(\theta)+(j2\pi f)B(\theta)+(j2\pi f)^2C(\theta)+\ldots\} \qquad (18)$$

where

$$A(\theta) \triangleq \sum_{i=1}^{N}\sum_{g=1}^{T} w_{i,g}\, e^{[j2\pi f_0(t_{i,g}-t_c)]} \qquad (19)$$

and

$$B(\theta) \triangleq \sum_{i=1}^{N}\sum_{g=1}^{T} w_{i,g}(t_{i,g}-t_c)\, e^{[j2\pi f_0(t_{i,g}-t_c)]} \qquad (20)$$

and

$$C(\theta) \triangleq \sum_{i=1}^{N}\sum_{g=1}^{T} w_{i,g}\left(\frac{t_{i,g}-t_c}{2}\right)^2 e^{[j2\pi f_0(t_{i,g}-t_c)]} \qquad (21)$$

If we define β *as the* bandwidth of the desired signal $s(t)$, then conditions for distortionless transmission by filter $H(f,\theta)$ can be stated more specifically (Ref 13:351-355). First, a constant amplitude *response is achieved if*

$$|f(t_{i,g}-t_c)| << 1 \quad \text{for} \quad f \quad \text{in} \quad \beta \quad \text{and all} \quad i,g \qquad (22)$$

This is apparent from Eq.(16). Secondly, another condition becomes apparent once we have performed the series expansion in Eq.(18)

$$\left|\frac{2\pi f B(\theta)}{A(\theta)}\right| << 1 \quad \text{for all} \quad f \quad \text{in} \quad \beta \qquad (23)$$

The condition of Eq.(22) would be sufficient for a constant amplitude response if $H(f,\theta)$ could be completely represented by the first term in the Taylor series; i.e. $H(f,\theta) = A(\theta)$. This is true for input signals which are monochromatic; i.e. $f=0$. Nearly all antenna work makes this assumption or assumes the signal is narrowband enough to be validly modelled as monochromatic. The common nomenclature for this first term $(A(\theta))$ is the array factor. It is used to determine many properties of arrays including the radiation pattern of the array, the main lobe location and beamwidth, null location, and sidelobe characteristics (Ref 14:chapter 1). The frequency response of an array in the vicinity of a null is often analyzed and the results then referred to as the radiation pattern. Though this is not absolutely correct, a strong duality exists between the frequency response and antenna pattern in the vicinity of a null. Appendix A contains a perturbation analysis which explains this relationship.

The second condition (Eq(23)) implies that meeting the first condition alone does not result in distortionless transmission. In the vicinity of an antenna pattern null, the first term approaches zero while the second term may not. In this case the transfer function is dominated by the second

term which has linear variation with frequency across the band of interest. A performance measure of this situation is developed in a later section and is used to analyze several system configurations in subsequent chapters. This second condition of distortionless transmission can be extended to a third condition by requiring that

$$\left|\frac{(2\pi f)^2 C(\theta)}{A(\theta)}\right| << 1 \quad \text{for all} \quad f \quad \text{in} \quad \beta \tag{24}$$

If $A(\theta)$ and $B(\theta)$ both approached zero then $H(f,\theta)$ would be determined by this third term in the series. It will be shown in later chapters that the magnitude of $C(\theta)$ is negligible, as compared to $A(\theta)$ or $B(\theta)$.

The effect of the higher order terms in the transfer function upon the desired signal can be interpreted in the time domain by recalling the differentiation theorem of Fourier transforms. Using Eq.(18) and (15) yields

$$\begin{aligned} Y(f) &= S(f)H(f) \\ &= S(f)[A(\theta)+(j2\pi f)B(\theta)+(j2\pi f)^2 C(\theta)+\ldots]e^{[j2\pi(f_0+f)t_c]} \end{aligned} \tag{25}$$

In the time domain this is

$$y(t) = \left\{A(\theta)s(t-t_c)+B(\theta)\frac{ds(t-t_c)}{dt} + C(\theta)\frac{d^2s(t-t_c)}{dt^2} + \ldots + \frac{d^ns(t-t_c)}{dt^n}\right\} \frac{1}{n!} \sum_{i=1}^{N} \sum_{g=1}^{T} w_{i,g}(t_{i,g}-t_c)^n e^{[j2\pi f_0(t_{i,g}-t_c)]} e^{j2\pi f_0 t_c} \quad (26)$$

Recall that with complex baseband notation a monochromatic signal is written as a complex constant. Thus it has no derivatives and the output of the array is just the first term of the series in Eq.(26)(including the constant phase offset due to the phase center exponential term). However for broadband signals Eq(26) shows that the array output is the sum of the signal and all of its time derivatives. This characterization of the actual waveform distortion experienced by a broadband signal as it is processed by an antenna array was first derived and studied by Raska for arrays without adaptive weights and without tapped delay lines (Ref 11). Similar analysis exists for multipath effects on a communication channel (Ref 13:351-355).

As Eq(26) reveals, the distortion in the array output consists of all n^{th} order derivatives of the input signal. The following section describes a particular signal of interest and its first time derivative.

C. Signal of Interest

Several types of modulation can be used to spread an information signal to produce a spread spectrum signal. We will only consider direct sequence modulation (Ref 5:3). This is defined as modulation of a carrier by a digital code sequence whose bit rate is much higher than the information signal bandwidth. To recover the information signal at a receiver, the spread spectrum signal is modulated again with the same digital code sequence. This compresses the information back down to its original bandwidth. The type of code sequence used for modulation, and which must be known at the receiver, is called a pseudo-noise (PN) code.

A pseudo-noise signal can be thought of as a train of ±1 pulses that switch states randomly at a high rate (such as 5M Hz). The pulse train, $p(t)$, becomes periodic after some fixed number of pulses has passed. An n-bit shift register, with proper feedback connections, can produce a PN code of length 2^n-1 bits. The entire periodic sequence is called a code word, with each bit of the code referred to as a chip (Figure 3). PN codes have two properties of particular interest which led to the implementation of correlation receivers for demodulation of spread spectrum signals (Ref 5:55). First, the distribution of bits within a PN code word is random. Second, the code word has an autocorrelation with a peak only at the zero shift point. Its value is nearly zero if the time shift is a full chip width or greater. These

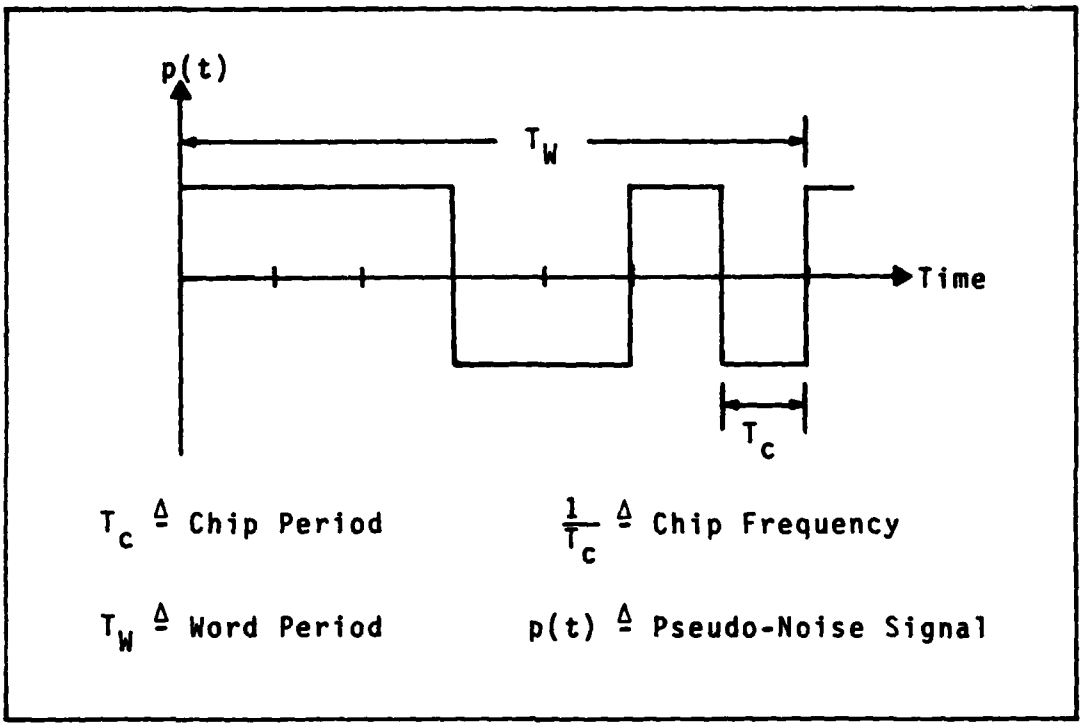

Figure 3. Pseudo-Noise Waveform

two properties are related since only a truly random code would have an autocorrelation function which approaches a delta function. Because the correlation function of a PN code resembles a delta function, it looks like white noise when used to drive a system whose bandwidth is small compared with the inverse chip period (thus the name "pseudo-noise" code). The correlation peak provides an excellent signal discriminant to be used in receiver design, and adaptive weight algorithms. Correlation receivers perform a correlation of the received signal with the PN code and use the resultant correlation peak for synchronization. If an adaptive array distorts the received spread spectrum signal

enough, the pseudo-noise code characteristics of the signal can be lost and the correlation receiver will produce a distorted correlation waveform. If distortion is enough to prevent synchronization between the signal's PN code and the receiver's PN code, the receiver will be unable to recompress the received signal down to its original bandwidth and the information will be lost. Therefore, instead of looking at the spread spectrum signal directly, we will investigate the effects of the adaptive array on the correlation function of the PN code.

The autocorrelation function of a PN sequence is a triangular waveform of height CT_c and width T_c, where T_c is still the chip period and C is the code length ($C=2^n-1$) (Ref 5:64-67). This waveform can be normalized by 1/C to remove the code length dependence (Figure 4). In Figure 2 we have the array output passing through a filter matched to the input $s(t)$. Filtering the signal by this matched filter is equivalent to the correlation operation performed in a receiver. The Fourier transform of a matched filter is

$$H_M(f) = S^*(f) \tag{27}$$

where $S^*(f)$ is the conjugate of the Fourier transform of signal $s(t)$. Using Eq.(25) the output is written

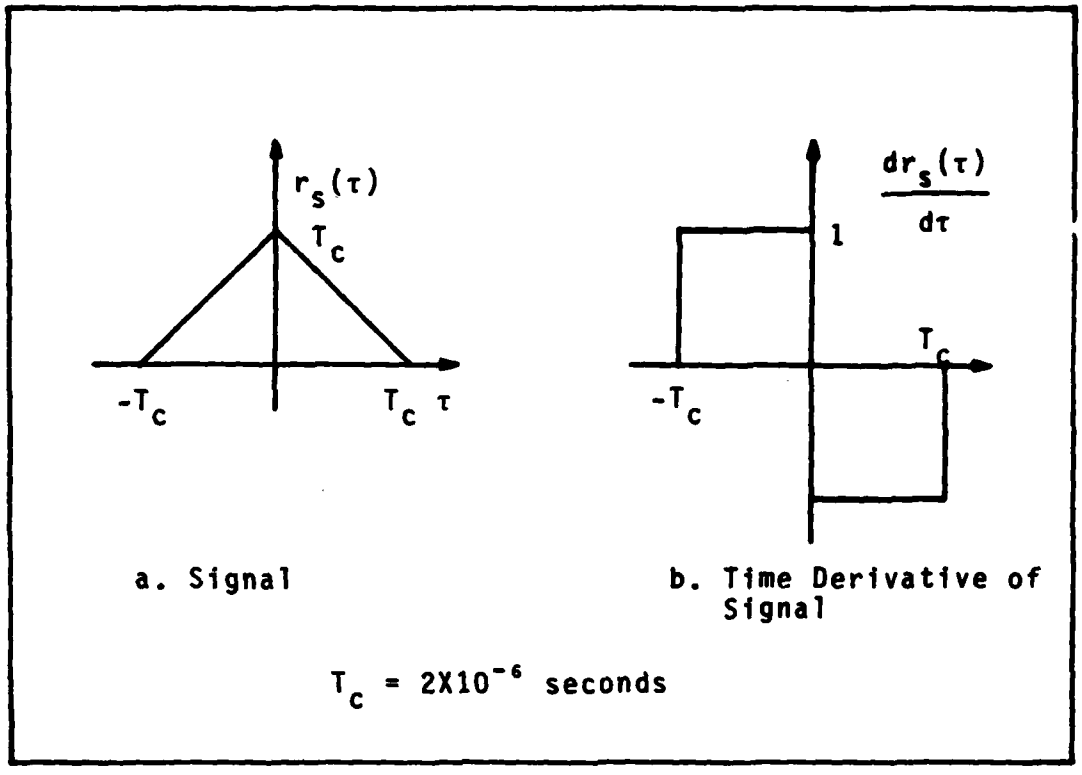

Figure 4. Autocorrelation Waveform

$$R(f) = Y(f)H_M(f)$$

$$= Y(f)S^*(f)$$

$$= S(f)H(f,\theta)S^*(f)$$

$$= |S(f)|^2 H(f,\theta) \qquad (28)$$

where $|S(f)|^2$ is the transform of the autocorrelation function of the desired signal, and $R(f)$ is the transform of the output correlation function. Substituting Eq(18) for $H(f,\theta)$ and taking the inverse transform into the time domain yields

$$r(\tau) = \left\{A(\theta)r_s(\tau-t_c)+B(\theta)\frac{dr_s(\tau-t_c)}{d\tau} + C(\theta)\frac{d^2r_s(\tau-t_c)}{d\tau^2} + \ldots\right\}e^{(j2\pi f_0 t_c)} \qquad (29)$$

where $r_s(\tau)$ is the autocorrelation function of the desired signal, $s(t)$. The distorted matched filter output is seen to be a complex weighted sum of the desired signal's autocorrelation function and its derivatives. The results of Eq.(26) and Eq.(29) are equivalent with respect to signal distortion. In Eq.(26), the desired signal is very general in nature. Equation (29) assumes that we have added a matched filter to the array and therefore the desired signal is an autocorrelation function. The definition of $H(f,\theta)$ is unchanged in either case since it is of course independent of the signal waveform. To quantify the distortion due to $H(f,\theta)$, the signal of Figure 4 will be used to illustrate a performance criteria.

D. Performance

The condition of Eq.(23) can be used to give a measure of the angular displacement around the array where the output of the array is dominated by the first derivative of the desired signal. This condition is dependent on the particular signal of interest, since it is evaluated only for frequencies within the bandwidth of the signal, β . From Eq.(29), we

can see that an equivalent time domain condition is that

$$\left|\frac{dr_s(\tau-t_c)B(\theta)}{r_s(\tau-t_c)A(\theta)}\right| \ll 1 \qquad (30)$$

Rearranging and defining a threshold η we get

$$\left|\frac{A(\theta)}{B(\theta)}\right| \geq \frac{\eta\frac{dr_s(\tau-t_c)}{d\tau}}{r_s(\tau-t_c)} \qquad (31)$$

where η is a time-bandwidth product. For the correlation function of spread spectrum signals, shown in Figure 4, we see that near $\tau=0$ the ratio of the signal derivative to the signal is

$$\frac{\frac{dr_s(\tau-t_c)}{d\tau}}{r_s(\tau-t_c)} = \frac{1}{T_c} \qquad (32)$$

From the Fourier transform of $r_s(\tau)$, the first zero crossing occurs at frequency $1/T_c$. Since $r_s(\tau)$ is not band-limited, we cannot uniquely specify its bandwidth. The question now becomes what filter bandwidth is sufficient to pass the signal undistorted. Dixon has shown that power spectrum of the form $\left(\frac{\sin x}{x}\right)^2$ contain 90 percent of their total power within the main lobe. However, if the filter bandwidth is restricted to the signals main lobe, the sharply peaked triangular shape of the signal is rounded off (Ref 5:20-21). The

designer of an antenna array-correlation receiver system must decide on the correlation pulse distortion which is acceptable. This will determine the array filter bandwidth. A wider filter bandwidth results in an output signal of higher fidelity. The necessary bandwidth can be defined in terms of the number of sidelobes included from the $(\sin x/x)^2$ power spectrum. The signal bandwidth is

$$\beta = \frac{\eta}{T_c} \tag{33}$$

With this signal bandwidth the filter bandwidth must be at least η/T_c . Looking at Eq.(31), we now have

$$\left|\frac{A(\theta)}{B(\theta)}\right| \geq \frac{\eta}{T_c} = \beta \tag{34}$$

The ratio on the left is interpreted as the array filter bandwidth as a function of signal arrival angle. Eq.(34) states that the filter bandwidth must be at least as large as the signal bandwidth.

Using the specific values in Figure 4 for T_c , and assuming that the bandwidth of the correlation pulse is defined as including the main lobe and four sidelobes of its power spectrum, we have

$$\left|\frac{A(\theta)}{B(\theta)}\right| \geq \frac{\eta}{T_c} = \frac{10}{2\text{x}10^{-6}} = 5\text{x}10^{6}\text{Hz} \tag{35}$$

Taking logarithms yields

$$\log \frac{A(\theta)}{B(\theta)} \geq 6.7 \tag{36}$$

This threshold will be used as a benchmark in the analysis of Chapter IV.

Eq.(24) identified another condition for distortionless transmission of a signal through the array. It is that

$$\left|\frac{A(\theta)}{C(\theta)}\right| \geq \frac{\frac{d^2 r_s(\tau - t_c)}{d\tau^2}}{r_s(\tau - t_c)} \tag{37}$$

It is apparent from Figure 4 that for the PN-BPSK signal of interest the right side of this equation evaluates to 10^6 . Later chapters will show that this condition is always met for the scenarios analyzed.

For the second time derivative term to be insignificant a condition to be met is

$$\left|\frac{B(\theta)}{C(\theta)}\right| \geq \frac{\frac{d^2 r_s(\tau - t_c)}{d\tau^2}}{\frac{dr_s(\tau - t_c)}{d\tau}} \tag{38}$$

For the signal of interest the right side of this equation evaluates to 0.5 . Research has been done into the auto-correlation functions and their time derivatives, for other modulation techniques (Ref 3). The performance expressions

in Eqs.(34), (37), and (38) were evaluated for these modulation types. The values obtained are on the same order of magnitude as those shown here for PN-BPSK signals. Therefore results based on these values are valid for several common modulation techniques. In Chapter III we derive the expressions used to determine the adaptive weight values. They are based on the array geometry and the power, bandwidth, location and stochastic nature of the desired signal and noise sources.

III Adaptive Weights

This chapter begins with an introduction to adaptive arrays. The widely accepted equation for optimum weights is presented. It is based on the use of a noise covariance matrix. The noise environment represented in this research is analyzed by using a Karhunen-Loève expansion. This leads to a representation for broadband jamming sources which is used in subsequent chapters to calculate the optimum weights.

A. Optimum Weights

The most widely used objective in calculating the weights is to minimize array output noise power, where the noise consists of both thermal noise and jammer noise. This is done by using weights which result in the array's receiving antenna pattern having nulls in the direction of jamming sources.

In order to maximize signal and minimize noise out of the array, some a priori knowledge is necessary with which to distinguish the signal from the noise. This discriminant can include information either about the signal or noise, or can rely on their differences. Some useful discriminants are the signal waveform, spectral differences between signal and noise, directions of arrival, polarizations, and power levels (Ref 8:13). One or several of these can be used such that only the interference is cancelled. Direction of arrival of the desired signal is used in this paper.

It has been shown that the set of optimum weights is given by

$$\vec{\bar{W}} = \vec{\bar{\Phi}}^{-1} \vec{\bar{W}}_q \tag{39}$$

where the covariance matrix $\vec{\bar{\Phi}}$ is a matrix of cross-covariances and autocovariances of the input noise signals at each antenna port (Refs 17,6,12). Subsequent sections of this chapter develop a representation for the noise signals which is used to explicitly define the covariance matrix. The column vector of optimum weights $\vec{\bar{W}}$ is defined as

$$\vec{\bar{W}} = \begin{bmatrix} w_{1,1} \\ w_{1,2} \\ \vdots \\ w_{i,g} \\ \vdots \\ w_{N,T} \end{bmatrix} \tag{40}$$

The quiescent weights $\vec{\bar{W}}_q$ are chosen to steer the main antenna array beam in the direction of arrival of the desired signal, independent of the jammer environment (e.g. in a "quiescent" environment). This direction of arrival is assumed known a priori. The quiescent weights are determined explicitly in the next chapter (see Eq(75) and (78)).

One of the differences between various adaption algorithms is the information which is known a priori. It is to be expected that as the estimates for the unknown information

improves, the weights calculated from algorithms converge to the optimum weights defined in Eq(39) (Ref 12:19). Since the scope of this paper is limited to analyzing the steady state response of the antenna array transfer function, the optimum weights are simulated assuming known signal parameters. Therefore the results of this paper are independent of the adaption algorithm used.

The emphasis in the rest of this chapter is on developing explicit expressions for $\vec{\Phi}$. If the noise environment only contains monochromatic jammers, then $\vec{\Phi}$ can be calculated given the thermal noise power and the power, frequency, and direction of arrival of all jammers. This simplifies the numerical evaluation of the optimum weights. The next section evaluates the covariance matrix for the general case of a jammer with bandwidth. It is then shown that for large time-bandwidth products, monochromatic jammers can be used to adequately approximate a broadband jammer.

B. Noise Environment

The noise signals include both directional noise sources, which propagate as uniform plane waves, and thermal noise at the front end of the array, which is assumed independent from one antenna element to the next. Each of the M spatially discrete jamming sources is assumed uncorrelated with all other jammers. The jamming signals are defined at rf frequency as

$$\underset{\sim}{\mathcal{J}}_m(t) = \underset{\sim}{\xi}_m(t)\cos\left[2\pi f_0 t \underset{\sim}{\rho}_m(t) - \underset{\sim}{\sigma}_m\right]$$

$$m=1,2,\ldots,M \qquad (41)$$

The modulation $\underset{\sim}{\xi}_m(t)$ and $\underset{\sim}{\rho}_m(t)$ are sample functions from independent random processes. The independent random variables $\underset{\sim}{\sigma}_m$, which are uniformly distributed on $[0,2\pi]$, are added to ensure stationarity [Ref 10:303]. The random processes are also assumed ergodic. In complex baseband notation the m^{th} jammer is

$$\underset{\sim}{J}_m(t) = \underset{\sim}{\xi}_m(t)\exp\left[j\underset{\sim}{\rho}_m(t) + \underset{\sim}{\sigma}_m\right] \qquad (42)$$

The expected value of $\underset{\sim}{J}_m(t)$ is zero. The zero-mean thermal noise is modelled as bandlimited noise with one-sided power spectral density of N_0 watts/m^2-sec. The bandwidth of this noise is assumed large as compared to the bandwidth of the array. Therefore the propagation delays between antenna elements and between taps on a delay line are assumed larger than the coherence time of the thermal noise. The autocorrelation function of the noise is then a delta function of height N_0 and the cross-correlation between any two ports is zero.

The elements of the noise covariance matrix are a function of phase differences between ports, and therefore time delay differences. The use of the double subscript (i,g) leads to

cumbersome notation. Therefore for the rest of this chapter the delay associated with the m^{th} jammer at port i,g will be denoted as t_{mk} where k=1,2,...,K. The term K equals NxT , the total number of ports. The delay at a different port will be denoted as $t_{mk'}$. Since the noise covariance matrix is a function of phase differences, the phase center of the antenna array does not need to be considered as it was in Eq.(14). Therefore the coordinate system by which the delays t_k are determined is irrelevant, as long as we are consistent. In the computer simulation used to support the following chapters, the coordinate system is the same as that described in Chapter II.

Using this notation, the total noise signal at port k is

$$\underset{\sim}{N}_k(t) = \sum_{m=1}^{M} \underset{\sim}{J}_m(t-t_{mk})\exp[j2\pi f_0 t_{mk}] + \underset{\sim}{n}_k(t) \qquad (43)$$

where $\underset{\sim}{n}(t)$ is the complex baseband representation for the thermal noise. Note that t_{mk} is dependent on the array geometry and jammer location.

C. Noise Covariance Matrix

The noise covariance matrix $\vec{\Phi}$ is composed of the expected value between the noise signal at port k and every other port, for all k . The noise signal of Eq.(43) is used in evaluating the expectation. Since both $\underset{\sim}{J}_m(t)$ and $\underset{\sim}{n}(t)$

are random processes with zero mean, the matrix is actually a correlation matrix. Using a superbar "$\overline{\quad}$" to denote ensemble average, the covariance matrix is written

$$\vec{\Phi} \triangleq \begin{bmatrix} \overline{N_1^*(t)\,N_1(t)} & \overline{N_1^*(t)\,N_2(t)} & \overline{N_1^*(t)\,N_3(t)} & \cdots & \overline{N_1^*(t)\,N_K(t)} \\ \overline{N_2^*(t)\,N_1(t)} & \overline{N_2^*(t)\,N_2(t)} & & & \\ & & \overline{N_k^*(t)\,N_k(t)} & & \\ \overline{N_K^*(t)\,N_1(t)} & & & & \overline{N_K^*(t)\,N_K(t)} \end{bmatrix} \tag{44}$$

Each element of this matrix consists of the sum of autocorrelation functions for each jammer, and the autocorrelation function of the thermal noise, evaluated at a time differential τ . The time differential is the difference between the time delay t_{mk} to port k and the delay $t_{mk'}$ to port k' i.e. the kk' entry of the matrix.

Consider the case of one jammer $(M=1)$. Evaluating the kk' entry due to only this emitter yields

$$\overline{\underset{\sim}{J}(t-t_k)e^{(j2\pi f_0 t_k)} * \underset{\sim}{J}(t-t_{k'})e^{(j2\pi f_0 t_{k'})}}$$

$$= e^{(j2\pi f_0(t_k-t_{k'})} \overline{\underset{\sim}{J}(t-t_k)^* \underset{\sim}{J}(t-t_{k'})}$$

$$= e^{(j2\pi f_0(t_k-t_{k'})} R_J(t_{k'}-t_k) \qquad (45)$$

However

$$R_J(t_{k'}-t_k) \triangleq \int_{-\infty}^{\infty} S_J(f)e^{j2\pi f(t_{k'}-t_k)}df \qquad (46)$$

where $R_J(\cdot)$ is the autocorrelation function of $\underset{\sim}{J}(t)$ and $S_J(f)$ is the associated power spectral density. The kk' entry of $\vec{\Phi}$ with M jammers and thermal noise is then

$$\overline{\underset{\sim}{N}_k(t)^* \underset{\sim}{N}_{k'}(t)} = \sum_{m=1}^{M} R_{J_m}(t_{mk'}-t_{mk})$$

$$e^{(j2\pi f_0(t_{mk}-t_{mk'})} + N_0\delta_{kk'} \qquad (47)$$

where $\delta_{kk'}$ is a Kronecker Delta function.

D. Karhunen-Loève Expansion

Equation (47) was implemented in a computer program assuming the jammers were monochromatic signals. It was later decided to investigate the effects of broadband

jammers on the results. The derivation to follow showed that the narrowband jammer implementation could be used since the correlation function of a broadband random process can be approximated using discrete spectral lines.

Consider the following model expansion of the complex random process $\mathcal{J}(t)$ along a complete orthonormal (CON) set of basis functions $\{\psi_m(t)\}$ over a finite time interval $-T'/2,\ T'/2$,

$$\mathcal{J}(t) = \underset{M\to\infty}{\text{l.i.m.}} \sum_{m=-M}^{M} \mathcal{J}_m \psi_m(t) \tag{48}$$

for $-T'/2<t<T'/2$

$$\text{where} \qquad \mathcal{J}_m = \int_{\frac{-T'}{2}}^{\frac{T'}{2}} \mathcal{J}(t)\psi_m^*(t)dt \tag{49}$$

The notation "l.i.m." denotes limit in the mean, implying a mean-square convergence of the sum in Eq.(48) and m is the integer index of the m^{th} temporal mode. Note that $\{\psi_m(t)\}$ is a set of complex functions yet to be specified. In addition, since $\mathcal{J}(t)$ is assumed to be a zero-mean, complex random process, $\{\mathcal{J}_m\}$ are zero-mean, complex random variables.

By proper selection of basis functions $\{\psi_m(t)\}$ it is possible to expand $\mathcal{J}(t)$ so that the coefficients of the

expansion $\{\mathcal{J}_m\}$ are pair-wise uncorrelated,

$$\left(\overline{\mathcal{J}_m \mathcal{J}_{m'}^*}\right) = \left(\overline{\mathcal{J}_m}\right)\left(\overline{\mathcal{J}_{m'}^*}\right) = 0 \tag{50}$$

for $m \neq m'$.

A necessary and sufficient condition for the $\{\mathcal{J}_m\}$ to be uncorrelated is that the basis functions $\{\psi_m(t)\}$ are the solutions to the Fredholm equation (Ref 16:180)

$$\gamma_m \psi_m(t) = \int_{\frac{-T'}{2}}^{\frac{T'}{2}} R_J(t,t')\psi_m(t')dt' \tag{51}$$

for $-T'/2<t<T'/2$.

The numbers $\{\gamma_m\}$ are the real eigenvalues associated with the eigenfunctions $\{\psi_m(t)\}$ for all integers $m(-\infty<m<\infty)$. The series expansion of $\mathcal{J}(t)$ on a CON set of eigenfunctions over an interval yielding uncorrelated random coefficients is known as a Karhunen-Loève (KL) expansion. If the basis functions $\{\psi_m(t)\}$ of Eq.(48) are solutions to the Fredholm Eq.(51) then the model expansion of $\mathcal{J}(t)$ is such an expansion.

Results from linear integral equation theory lead to several properties of integral equations (such as the Fredholm equation above). One of these properties is known as Mercer's Theorem (Ref 16:180-181). It states that any square integrable kernel $R_J(t,t')$ of Eq.(51) may be expanded in a

series.

$$R_J(t,t') = \sum_{m=-\infty}^{\infty} \gamma_m \psi_m(t) \psi_m^*(t') \qquad (52)$$

for $-T'/2<t,t'<T'/2$

where the convergence is uniform for $-T'/2<t,t'<T'/2$. It can be shown that if the correlation function of a zero-mean, complex random process $\underset{\sim}{J}(t)$ can be expanded in a form of Eq.(52) the model expansion given in Eq.(48) will converge in the mean-square sense (Ref 7:409).

For stationary random processes characterized over long time intervals $|-T'/2,T'/2|$, it can be shown that the eigenvalues $\{\gamma_m\}$ and associated eigenfunctions $\{\psi_m(t)\}$ which are solutions to the Fredholm Eq.(51) can be approximated by (Ref 16:205-207)

$$\gamma_m \simeq \frac{1}{T'} S_J\left(\frac{m}{T'}\right) , \qquad (53)$$

and

$$\psi_m(t) \simeq \exp[j2\pi \frac{m}{T'} t] \qquad (54)$$

for $-T'/2<t<T'/2$.

Here T' is again the characterization interval in seconds and $S_J\left(\frac{m}{T'}\right)$ is the power spectrum of the complex random process, defined in Eq.(46), sampled at frequencies $\frac{m}{T'}$ Hertz.

The magnitude of T' needed for the approximation to

be valid depends on how quickly $S_J(f)$ varies near frequency $\frac{m}{T'}$. For smooth spectra, long T' means long compared to the fluctuations of the jamming signals envelope

$$T' >> \frac{1}{\beta_J} \tag{55}$$

where β_J is the jamming signals bandwidth.

Therefore if T' is several times greater than $\frac{1}{\beta_J}$ then the basis functions $\{\psi_m(t)\}$ of the expansion over a time interval of length T' became the complex exponentials of a Fourier series expansion. It can be shown that the coefficients of these complex exponentials became uncorrelated as the interval T' gets long (Ref 4:94). The eigenvalues $\{\gamma_m\}$ become samples of the power spectrum $S_J(f)$ evaluated at the harmonic frequencies of the Fourier series expansion.

Thus, for long characterization time T', the Karhunen-Loève expansion for $\underline{J}(t)$ becomes

$$\underline{J}(t) = \sum_{m=-\infty}^{\infty} \underline{J}_m e^{j2\pi\frac{m}{T'}t} \tag{56}$$

for $-T'/2<t<T'/2$

where

$$\underline{J}_m = \frac{1}{T'} \int_{\frac{-T'}{2}}^{\frac{T'}{2}} \underline{J}(t) e^{-j2\pi\frac{m}{T'}t} dt \tag{57}$$

The expected value of the energy of $\underset{\sim}{J}(t)$ in time interval $[-T'/2, T'/2]$ is defined as

$$E \triangleq \int_{\frac{-T'}{2}}^{\frac{T'}{2}} \underset{\sim}{J}(t)\underset{\sim}{J}(t)^* dt$$

$$= T' \sum_{m=-\infty}^{\infty} \overline{\underset{\sim}{J}_m \underset{\sim}{J}_m^*} \qquad (59)$$

where the modal expansion for $\underset{\sim}{J}(t)$ has been used. Using Mercer's theorem Eq.(52), the mean energy of the process for long characterization time T' is

$$E = \sum_{m=-\infty}^{\infty} S_J(\tfrac{m}{T'}) \qquad (60)$$

Equating each term in Eq.(59) and (60) and using Eq.(50) produces

$$\overline{\underset{\sim}{J}_m \underset{\sim}{J}_{m'}^*} = \frac{1}{T'} S_J(\tfrac{m}{T'}) \delta_{mm'} \qquad (61)$$

where $\delta_{mm'}$ is again the Kronecker delta. Therefore, for long characterization intervals, the mean-square value of each expansion coefficient $\{J_m\}$ is the power spectrum evaluated at the coefficient's harmonic frequency.

Since the modal expansion coefficients have been chosen so as to be pairwise uncorrelated, the correlation function of the complex random process $\underset{\sim}{J}(t)$ can be written

$$R_J(t,t') = \overline{\underline{J}(t)\underline{J}(t')^*}$$

$$= \sum_{m=-\infty}^{\infty} \frac{1}{T'} S_J(\frac{m}{T'})\exp[j2\pi\frac{m}{T'}(t-t')] \qquad (62)$$

for $-T'/2<t<T'/2$

Note the similarity between this expression and Eq.(47). Equation (62) can be considered as an entry in the noise covariance matrix produced by an infinite number (depending on $S_J(\cdot)$) of narrowband jammers. To emphasize this we will start with Eq.(47) and apply it to a group of narrowband jammers chosen to represent a single broadband jammer.

Narrowband jammers which are not necessarily at center frequency yield a noise signal at port k of

$$\underline{N}_k(t) = \sum_{m=1}^{M} \underline{J}_m e^{[+j2\pi(f_0-f_m)t_{mk}]} + \underline{n}_k(t) \qquad (63)$$

where f_m is an offset frequency from center frequency for the m^{th} jammer. This leads to the kk' entry in the covariance matrix, from Eq.(47), as

$$\overline{\underline{N}_k(t)^*\underline{N}_{k'}(t)} = \sum_{m=1}^{M} \overline{|\underline{J}_m|^2} e^{(j2\pi(f_0-f_m)(t_{mk}-t_{mk'}))} + N_0\delta_{kk'} \qquad (64)$$

We choose to model a single broadband jammer as a sum of

narrowband jammers each at a different frequency but all at the same spatial location (i.e. $t_{mk}=t_k$ and $t_{mk'}=t_{k'}$ for all m). The broadband jammer is assumed to have a flat power spectral density. Therefore each discrete spectral line has equal power P_N (i.e. $P_N=\overline{|J_m|^2}$ for all m). From Eq.(64), the kk' entry in the covariance matrix due to jammers alone, becomes

$$R_{kk'}(\tau) = \sum_{m=1}^{M} P_N e^{(j2\pi(f_0-f_m)\tau)} \tag{65}$$

The frequency offsets are defined to be

$$f_m = \frac{\beta_J}{2} - (m-1)\partial f, \quad m=1,2,\ldots,M \tag{66}$$

where ∂f is the spacing between discrete spectral lines (see Figure 5).

To equate the results of the Karhunen-Loève expansion in Eq.(62) with Eq.(65) it is assumed that the power spectrum in Figure 5 is for process $J(t)$, and that

$$\frac{1}{T'} \triangleq \partial f = \frac{\beta_J}{M-1} \tag{67}$$

The correlation function of Eq.(62) can be written

$$R_J(\tau) = \sum_{m=1}^{M} \frac{\beta_J}{M-1} \frac{P_J}{\beta_J} e^{(j2\pi f_m \tau)} \tag{68}$$

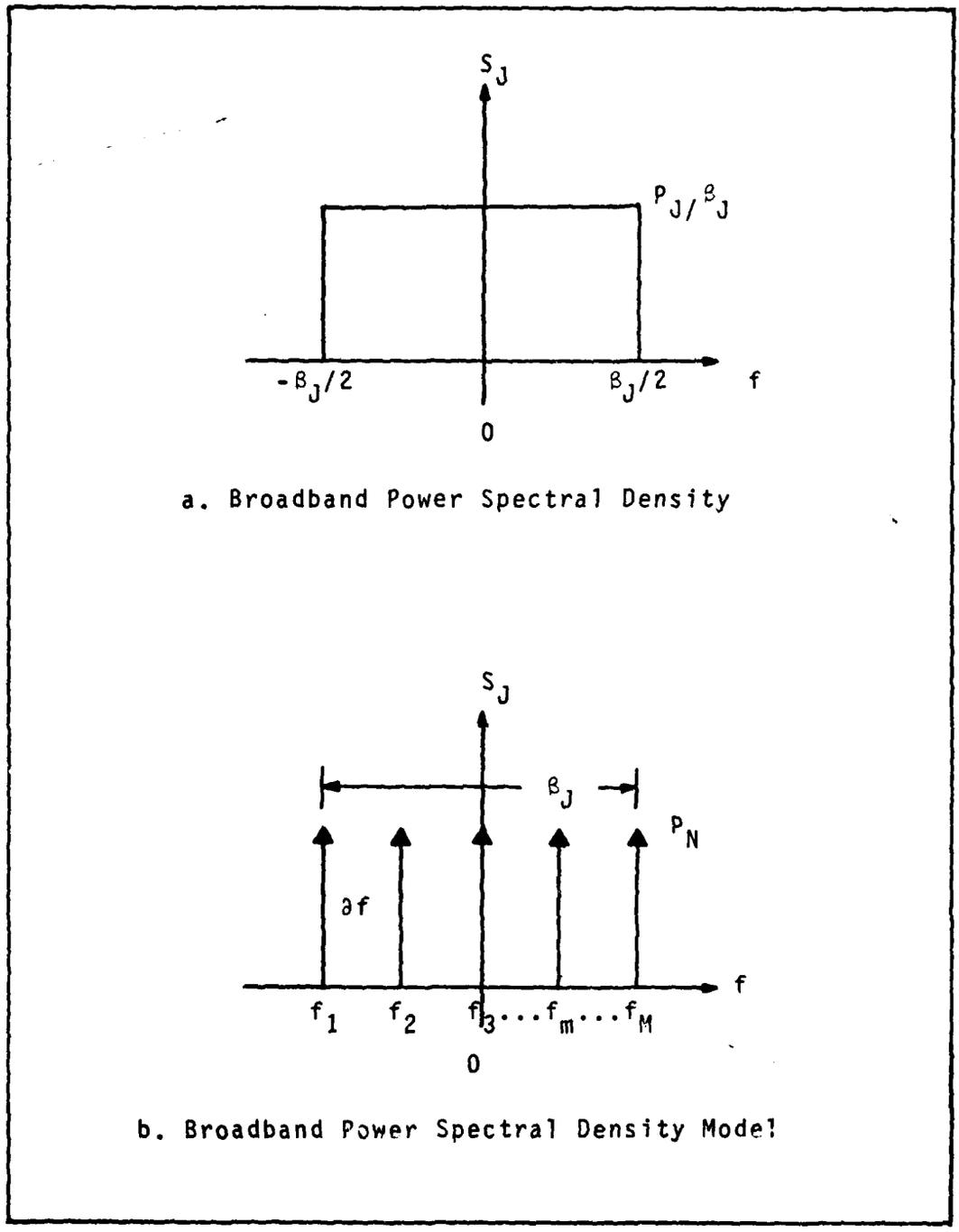

Figure 5. Power Spectral Density of Broadband Jammer

Exploiting the symmetry of the correlation function and incorporating the phase term associated with complex baseband representation, yields

$$R_J(\tau) = \sum_{m=1}^{M} \frac{P_J}{(M-1)} e^{(j2\pi(f_0-f_m)\tau)} \qquad (69)$$

This expression is nearly equivalent to Eq.(65). They differ only in the weight placed on each spectral component (i.e. $P_J/(M-1)$ versus P_N).

Note that the total power in $\mathcal{J}(t)$ from Figure 5a. is P_J . In implementing Eq.(65) in the computer program used later the power in each spectral line was chosen as

$$P_N = \frac{P_J}{M} \qquad (70)$$

so that the total power in $\mathcal{J}(t)$ is P_J .

From Eq.(69), the total power in $\mathcal{J}(t)$ is $\frac{M}{(M-1)} P_J$. Note that as the number of spectral lines becomes large, this expression approaches P_J . Therefore for large M Eq.(65) is equivalent to Eq.(69).

Summarizing, it has been shown that a Karhunen-Loève expansion of $\mathcal{J}(t)$ supports the approximation of the correlation function for a broadband jammer by discrete spectral lines. To quantify this approximation, a numerical analysis follows.

E. Numerical Analysis of Model

The correlation function approximation of Eq.(65) can be

written in closed form. Using a geometric series identity and Eq.(66), we get

$$R_{kk'}(\tau) = P_N e^{(j2\pi f_0 \tau)} \frac{\sin(M2\pi \partial f \frac{\tau}{2})}{\sin(2\pi \partial f \frac{\tau}{2})} \tag{71}$$

Normalizing this expression by total power yields

$$\frac{R_{kk'}(\tau)}{R_{kk'}(\tau)|_{\tau=0}} = \frac{1}{M} e^{(j2\pi f_0 \tau)} \frac{\sin(M2\pi \partial f \frac{\tau}{2})}{\sin(2\pi \partial f \frac{\tau}{2})} \tag{72}$$

The complex baseband correlation function is defined in Eq.(45) for a single broadband jammer at center frequency. Using the power spectral density in Figure 5a., Eq.(46) evaluates to

$$R_J(\tau) = P_J \frac{\sin(\pi \tau \beta_J)}{(\pi \tau \beta_J)} \tag{73}$$

Substituting Eq.(73) into Eq.(45) and normalizing by the total power, produces

$$\frac{R_{kk'}(\tau)}{R_{kk'}(\tau)|_{\tau=0}} = e^{j2\pi f_0 \tau} \frac{\sin(\pi \tau \beta_J)}{(\pi \tau \beta_J)} \tag{74}$$

Inspection of Equations (72) and (74) reveal that the complex correlation functions have equal phase information, since the exponential terms are identical. The envelopes of these

complex functions both approach unity for small arguments of the sine function. The worst case analysis is for maximum time delay differential (τ max). This occurs when the jammer is located at $\theta=90^0$ (endfire) and the correlation function is evaluated for signals at ports located at opposite extremes of the array. In Figure 2 this would be port 1,1 and port N,T. Table I shows the percent error between the approximate correlation function (Eq.(72)) and the actual correlation function (Eq.(74)). The calculations are for two jammer bandwidths and two array geometries using τmax. The errors are very small (less than 2%). The conclusion is that Eq.(72) is a good approximation for the correlation function of a broadband jammer.

Equation (64) is implemented in the computer simulation used to produce the results discussed in subsequent chapters. The covariance matrix depends on three jammer parameters, which can be different for each jammer. These parameters are total power ($\overline{|J_m|^2}$) , frequency offset (f_m) , and spatial location (θ_m) .

The analysis of transfer functions for a linear, equally spaced array begins in Chapter IV. No noise sources are present; the quiescent weights are chosen for phase steering of the array's main beam.

Table I. Broadband Jammer Correlation Function

	Parameters	Correlation Function $R_J(\tau) = \frac{\sin(\pi\tau\beta_J)}{(\pi\tau\beta_J)}$	Approximate Correlation Function $R_J(\tau) \simeq \frac{1}{M}\frac{\sin(M\pi\tau\delta f)}{\sin(\pi\tau\delta f)}$	Percent Error $\frac{3-4}{3}$ X100
N=4 T=3 $\tau=\lvert t_{1,1}-t_{4,3}\rvert$ $=2/f_0$	$\beta_J=4\%f_0$ M=5	0.9895	0.9843	0.53%
	$\beta_J=10\%f_0$ M=11	0.9355	0.9229	1.35%
N=2 T=3 $\tau=\lvert t_{1,1}-t_{2,3}\rvert$ $= 1/f_0$	$\beta_J=4\%f_0$ M=5	0.9974	0.9956	0.18%
	$\beta_J=10\%f_0$ M=11	0.9836	0.9804	0.33%
Column 1	2	3	4	5

$\partial f = 1\%f_0$
$f_0 = 350\text{MHz}$

IV Antenna Arrays without Adaptive Weights

In this chapter the transfer function of an antenna array with weighting coefficients chosen for phase steering is analyzed. First, an expression for the transfer function is developed, assuming phase steering at center frequency. Second, several assumptions are made about the array's geometry which allow the transfer function to be expressed in a closed form. Third, for a given steering angle, the transfer function for an array without tapped delay lines behind each element is compared to the transfer function for an array with delay lines.

A. Linear Array

A common steering technique used extensively today is based upon electrically steering the main beam of an antenna array. Phase steering, as it is entitled, is done by delaying the signal at each array port by a specific amount. This changes the arrival angle at which all signals (at the array's output) are in phase, from broadside to some steering angle θ_s.

For phase steering, the weighting coefficients at each port vary in phase only, not amplitude. In other words

$$\vec{W}_q = W_{i,g} \triangleq G_{i,g} e^{j\alpha_{i,g}} = e^{j\alpha_{i,g}} \qquad (75)$$

$$\text{for } i=1,2,\ldots,N \ , \quad g=1,2,\ldots,T$$

The transfer function of Eq.(16) now becomes

$$H(f,\theta) = e^{j2\pi(f+f_0)t_c} \sum_{i=1}^{N} \sum_{g=1}^{T} e^{j[2\pi(f+f_0)(t_{i,g}-t_c)+\alpha_{i,g}]} \quad (76)$$

The Taylor series representation is then

$$H(f,\theta) = e^{j2\pi(f+f_0)t_c} \sum_{i=1}^{N} \sum_{g=1}^{T} e^{j[2\pi f_0(t_{i,g}-t_c)+\alpha_{i,g}]} \; X$$

$$\left\{1+j2\pi f(t_{i,g}-t_c) + \frac{(j2\pi f(t_{i,g}-t_c))^2}{2} + \ldots\right\} \quad (77)$$

Steering the antenna array's main beam in direction θ_s is defined by the transfer function of Eq.(76) having a maximum amplitude when $\theta=\theta_s$. The transfer function has a maximum amplitude when the exponential term within the summation of Eq.(76) has a value of one. The proper choice of weights for steering in direction θ_s is then

$$e^{j\alpha_{i,g}} = e^{-j2\pi f_0(t_{i,g_s}-t_{c_s})} \quad (78)$$

where t_{i,g_s} is the propagation delay $t_{i,g}$ for steering angle θ_s , and t_{c_s} is the phase center delay t_c for steering angle θ_s . Substituting the proper phase steering weights into Eq.(76) yields

$$H(f,\theta) = e^{j2\pi(f+f_0)t_c} \sum_{i=1}^{N} \sum_{g=1}^{T} e^{j[2\pi f(t_{i,g}-t_c)+2\pi f_0((t_i-t_{i_s}) - (t_c-t_{c_s}))]} \quad (79)$$

The Taylor series prepresentation is

$$H(f,\theta) = e^{j2\pi(f+f_0)t_c} \sum_{i=1}^{N} \sum_{g=1}^{T} e^{j2\pi f_0\left[(t_i-t_{i_s})-(t_c-t_{c_s})\right]} \; x$$

$$\left\{1+j2\pi f(t_{i,g}-t_c) + \frac{(j2\pi f(t_{i,g}-t_c))^2}{2} + \ldots\right\} \quad (80)$$

Equation (79) is the general expression for the transfer function of a phase steered array, assuming steering at center frequency.

B. Linear, Equally-Spaced Array

The transfer function of Eq.(79) can be simplified further by assuming that the array of interest has equally spaced elements and equally spaced taps on the delay lines. Using Eq.(4) the propagation delay at port i,g is

$$t_{i,g} = \frac{(i-1)d \sin\theta}{c} + \frac{(g-1)\Delta}{c} \qquad (81)$$

$$= \frac{(i-1)\Gamma \sin\theta}{f_0} + \frac{(g-1)\delta}{f_0} , \qquad (82)$$

$$i=1,2,\ldots,N \quad g=1,2,\ldots,T$$

The terms are defined as

$d = \Gamma\lambda_0$ = spacing between antenna elements in meters

Γ = spacing between antenna elements in units of fractional wavelength at f_0

N = number of antenna elements

$\Delta = \delta\lambda_0$ = delay between taps in meters

δ = delay between taps in units of fractional wavelength at f_0

T = number of delay line taps

λ_0 = wavelength at f_0

Note that with this notation, an array with no tapped delay lines corresponds to the number of taps T equal to 1 .

The transfer function can be written in closed form using a geometric series identity. Equation (79) reduces to

$$H(f,\theta) = e^{j2\pi(f+f_0)(\frac{N-1}{2}\frac{d}{c}\sin\theta + \frac{T-1}{2}\frac{\Delta}{c})} \frac{\sin N(\pi(f+f_0)\frac{d}{c}\sin\theta - \pi f_0\frac{d}{c}\sin\theta_s)}{\sin(\pi(f+f_0)\frac{d}{c}\sin\theta - \pi f_0\frac{d}{c}\sin\theta_s)} \frac{\sin T(\pi f\frac{\Delta}{c})}{\sin(\pi f\frac{\Delta}{c})} \qquad (83)$$

Note that for this antenna geometry we have

$$t_c = \frac{N-1}{2}\frac{d}{c}\sin\theta + \frac{T-1}{2}\frac{\Delta}{c} \tag{84}$$

Looking at Eq.(83), the leading exponential term is just the phase center term which is also the leading term in Eq.(79).

Several observations can be made about the phase response of the transfer function identified by Eq.(83). First, the choice of steering angle θ_s has no effect on the phase response. Second, the response has a constant phase offset associated with f_0, plus a term dependent on frequency deviation f. In the time domain, this response results in a constant phase shift of the array output plus a simple time delay of the output signal. The important point is that the phase response does not have second (or higher) order frequency dependent terms and therefore does not lead to distortion of the array output signal.

To separate the effects of tapped delay lines, the transfer function of Eq.(83) is written

$$H(f,\theta) = H_E(f,\theta)H_D(f) \tag{85}$$

where

$$H_E(f,\theta) \triangleq e^{j2\pi(f+f_0)(\frac{N-1}{2}\frac{d}{c}\sin\theta)} \times \frac{\sin N(\pi(f+f_0)\frac{d}{c}\sin\theta - \pi f_0\frac{d}{c}\sin\theta_s)}{\sin(\pi(f+f_0)\frac{d}{c}\sin\theta - \pi f_0\frac{d}{c}\sin\theta_s)} \tag{86}$$

and

$$H_D(f) \triangleq e^{j2\pi(f+f_0)(\frac{T-1}{2}\frac{\Delta}{c})} \quad X \quad \frac{\sin T\,(\pi f \frac{\Delta}{c})}{\sin\,(\pi f\frac{\Delta}{c})} \qquad (87)$$

The effects of the tapped delay lines are now entirely within $H_D(f,)$. Note that when there are no taps (i.e. T=1) $H_D(f,)$ reduces to unity and the transfer function of a linear, equally spaced array without tapped delay lines is defined by $H_E(f,\theta)$. To investigate the frequency response of $H(f,\theta)$, the response without taps (i.e. $H_E(f,\theta)$) is first reviewed then the impact due to $H_D(f)$ is anticipated and finally the total frequency response is analyzed.

C. Transfer Function

$H_E(f,\theta)$ in Eq.(86) defines the transfer function of interest. The results for the rest of this paper assume broadside steering (i.e. θ_s=0) . With this assumption, the transfer function becomes

$$H_E(f,\theta) = e^{j2\pi(f+f_0)(\frac{N-1}{2}\frac{d}{c}\sin\theta)} \quad X \quad \frac{\sin N(\pi(f+f_0)\frac{d}{c}\sin\theta)}{\sin(\pi(f+f_0)\frac{d}{c}\sin\theta)} \qquad (88)$$

The function has been analyzed by Raska (Ref 11). His results are based on the closed form solution of the Taylor series expansion terms. They were verified by implementing the open form transfer function and coefficients of Eqs (16)

through (21). For a linear equally spaced array without taps these coefficients are

$$A(\theta) = \sum_{i=1}^{N} e^{j2\pi f_0[(i-1)\frac{d}{c}\sin\theta - \frac{(N-1)}{2}\frac{d}{c}\sin\theta]} \tag{89}$$

$$B(\theta) = \sum_{i=1}^{N} [(i-1)\frac{d}{c}\sin\theta - \frac{(N-1)}{2}\frac{d}{c}\sin\theta] \; X \; e^{j2\pi f_0[(i-1)\frac{d}{c}\sin\theta - \frac{(N-1)}{2}\frac{d}{c}\sin\theta]} \tag{90}$$

$$C(\theta) = \sum_{i=1}^{N} [((i-1)\frac{d}{c}\sin\theta - \frac{(N-1)}{2}\frac{d}{c}\sin\theta)^2/2] \; X \; e^{j2\pi f_0[(i-1)\frac{d}{c}\sin\theta - \frac{(N-1)}{2}\frac{d}{c}\sin\theta]} \tag{91}$$

The results are summarized graphically in the following figures. The parameters used were for a four element array (N=4) with half wavelength spacing between elements ($d=\frac{1}{2}\lambda_0$). The frequency response of the array is shown in Figure 6 for several angles θ. All frequency responses in this paper are normalized by dividing the transfer function by NxT. As we approach array broadside the response becomes constant and distortion at the output is minimized. Figure 7 shows the phase response of $H_E(f,\theta)$. Note that this response varies linearly with frequency. The slope and intercept are a

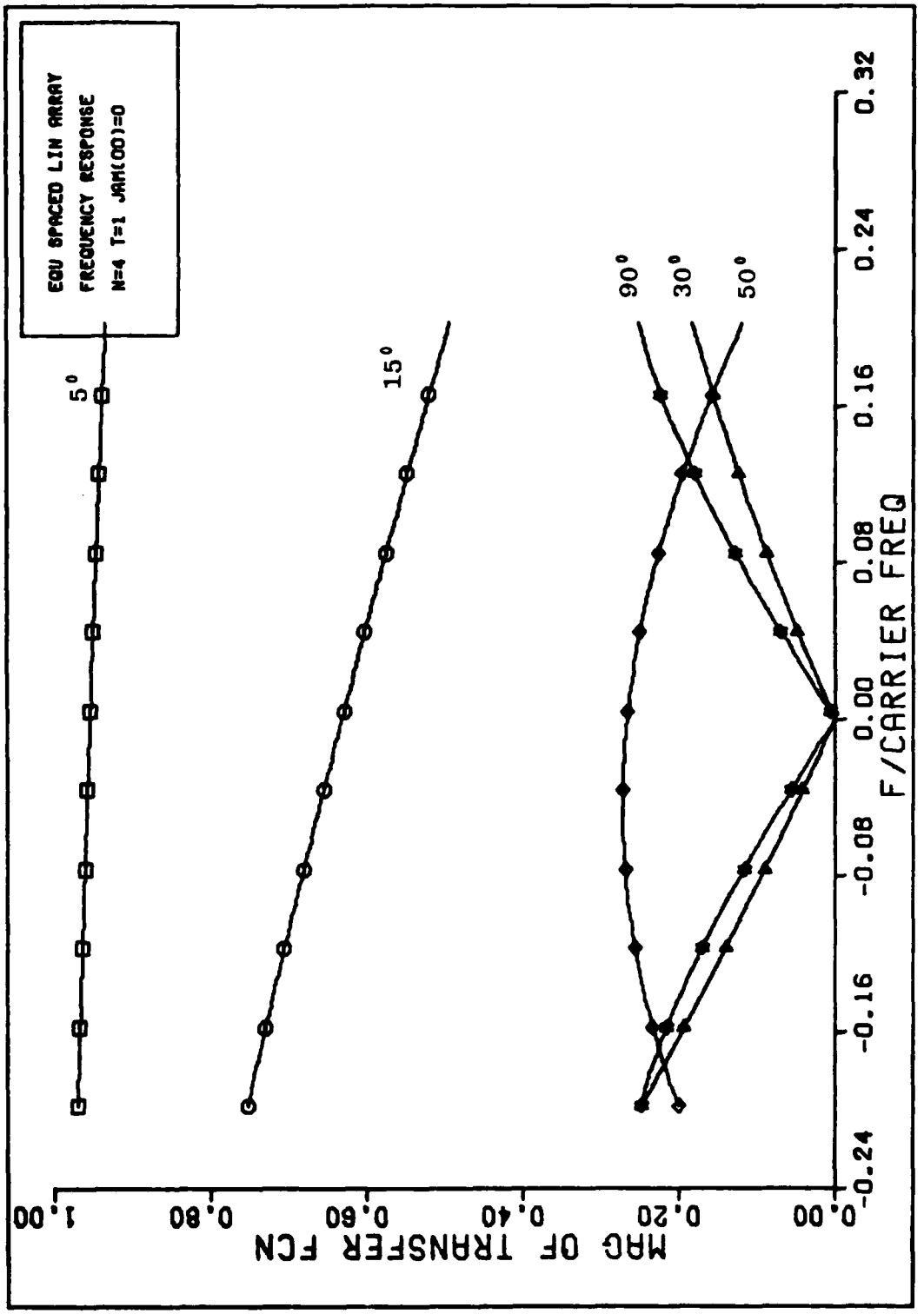

Figure 6. Frequency Response

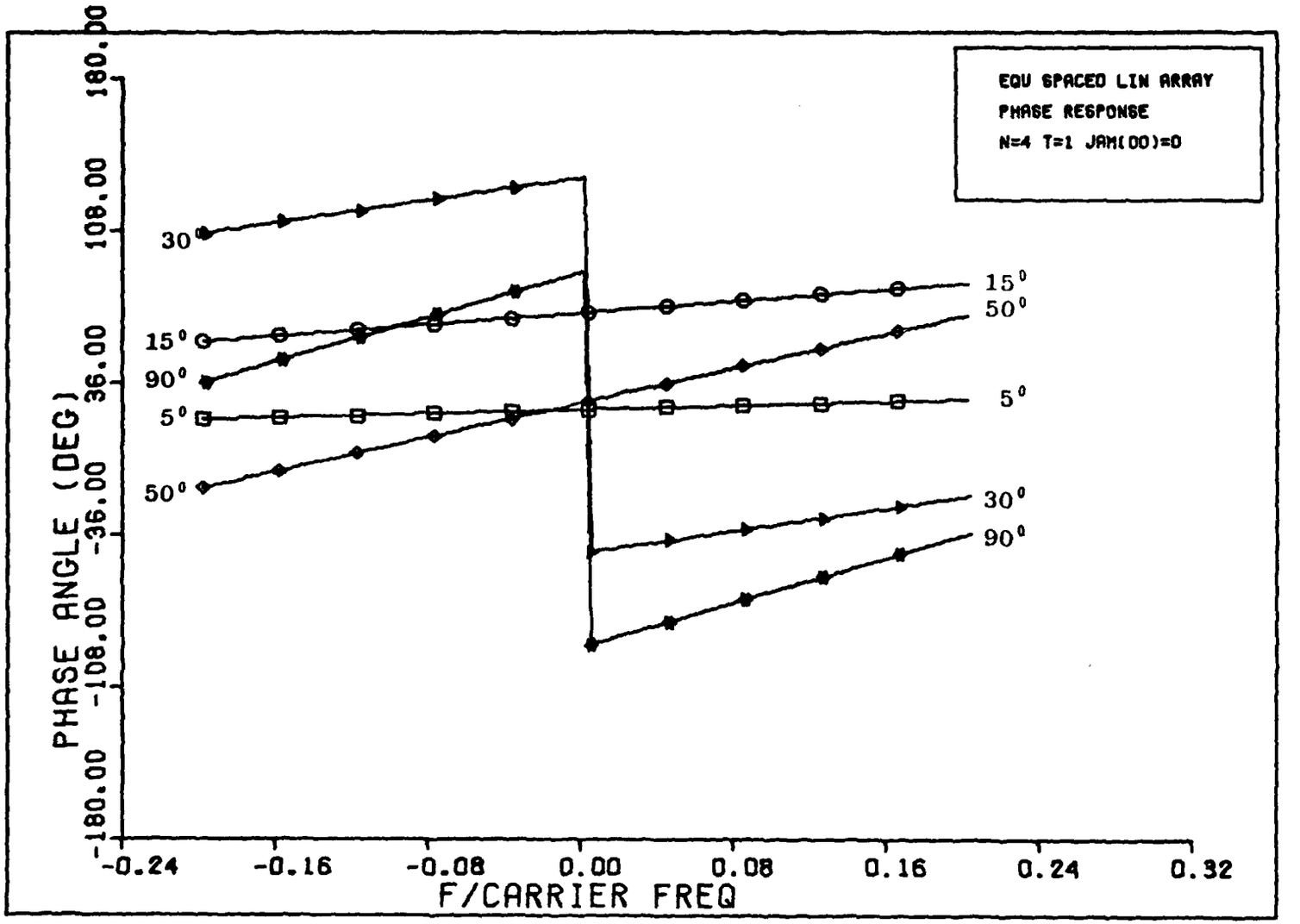

Figure 7. Phase Response

function of angle θ . For a given arrival angle θ , the phase response will not contribute to any signal distortion.

Figures 8, 9, and 10 are of the Taylor series coefficients $A(\theta)$, $B(\theta)$, and $C(\theta)$ respectively. For this particular array, $A(\theta)$, $B(\theta)$, and $C(\theta)$ are defined in Equations (89), (90) and (91). Several results are of particular interest. The array factor ($A(\theta)$) is purely real while $B(\theta)$ is purely imaginary. Since these terms are 90^0 out of phase with each other, the derivative term in the distorted output is added in phase quadrature to the undistorted correlation function ($r(\tau)$) . From Figures 8 and 9 we note that the antenna radiation pattern, $A(\theta)$, has an inverse relationship with the derivative radiation pattern, $B(\theta)$. In other words, the largest lobes in $A(\theta)$ correspond to the deepest nulls in $B(\theta)$ and vice versa. Using Figure 11 and the distortion threshold assumed in Eq(36) of Log $|A(\theta)/B(\theta)| \geq 6.7$, we see that the distortion term becomes significant at the nulls in the radiation pattern $A(\theta)$. This distortion persists for $\pm 2^0$ about the nulls. The third coefficient in the Taylor series, $C(\theta)$, has its strongest peak at $\theta=50^0$. This second derivative distortion term is apparent in Figure 6. The array frequency response has a noticeable curvature for the case of $\theta=50^0$. This curvature has a second order variation with frequency. Any second derivative distortion would not be significant in the array's output since the multiplying term $C(\theta)$ is so small, even at $\theta=50^0$.

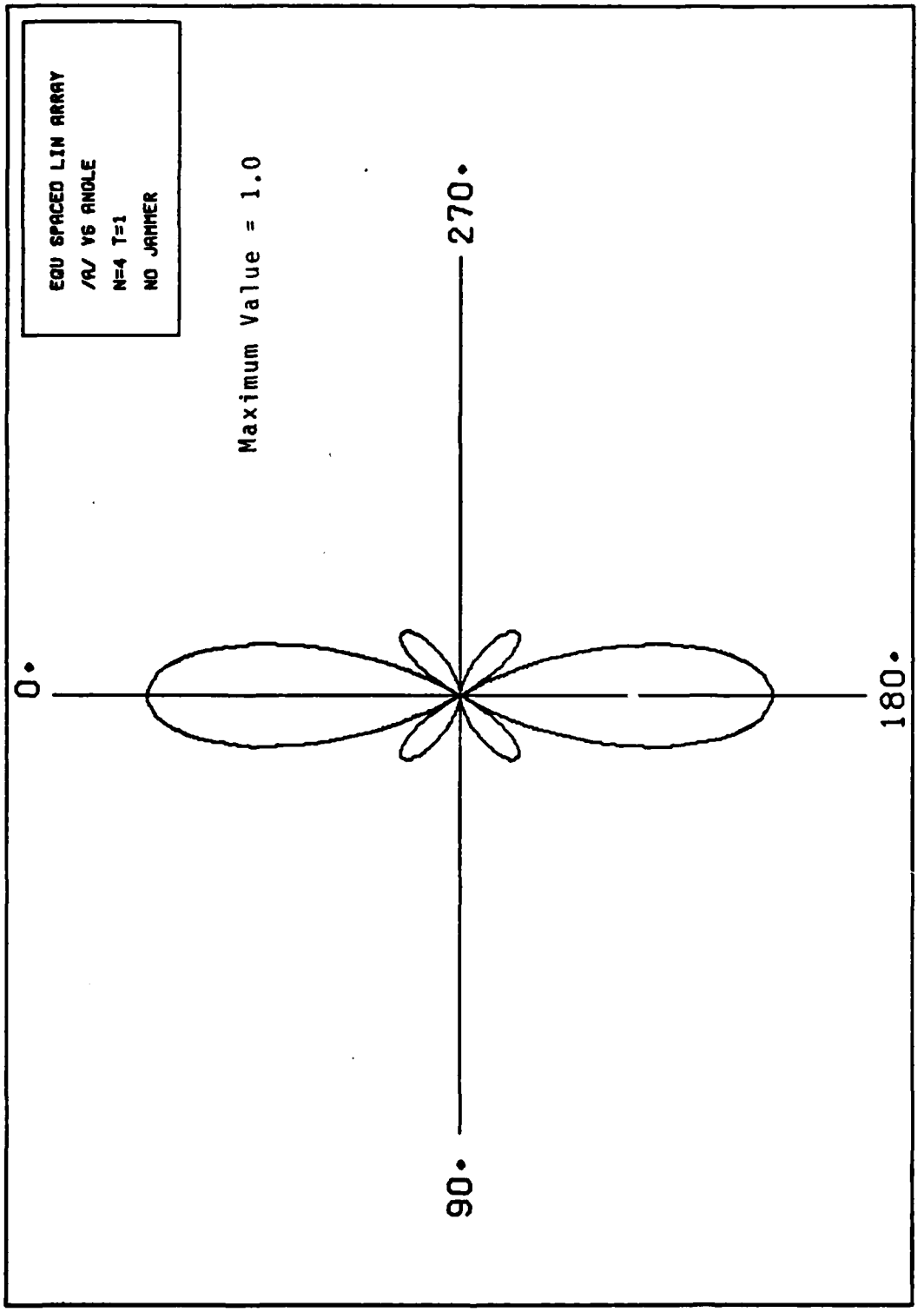

Figure 8. Polar Plot of $|A(\theta)|$

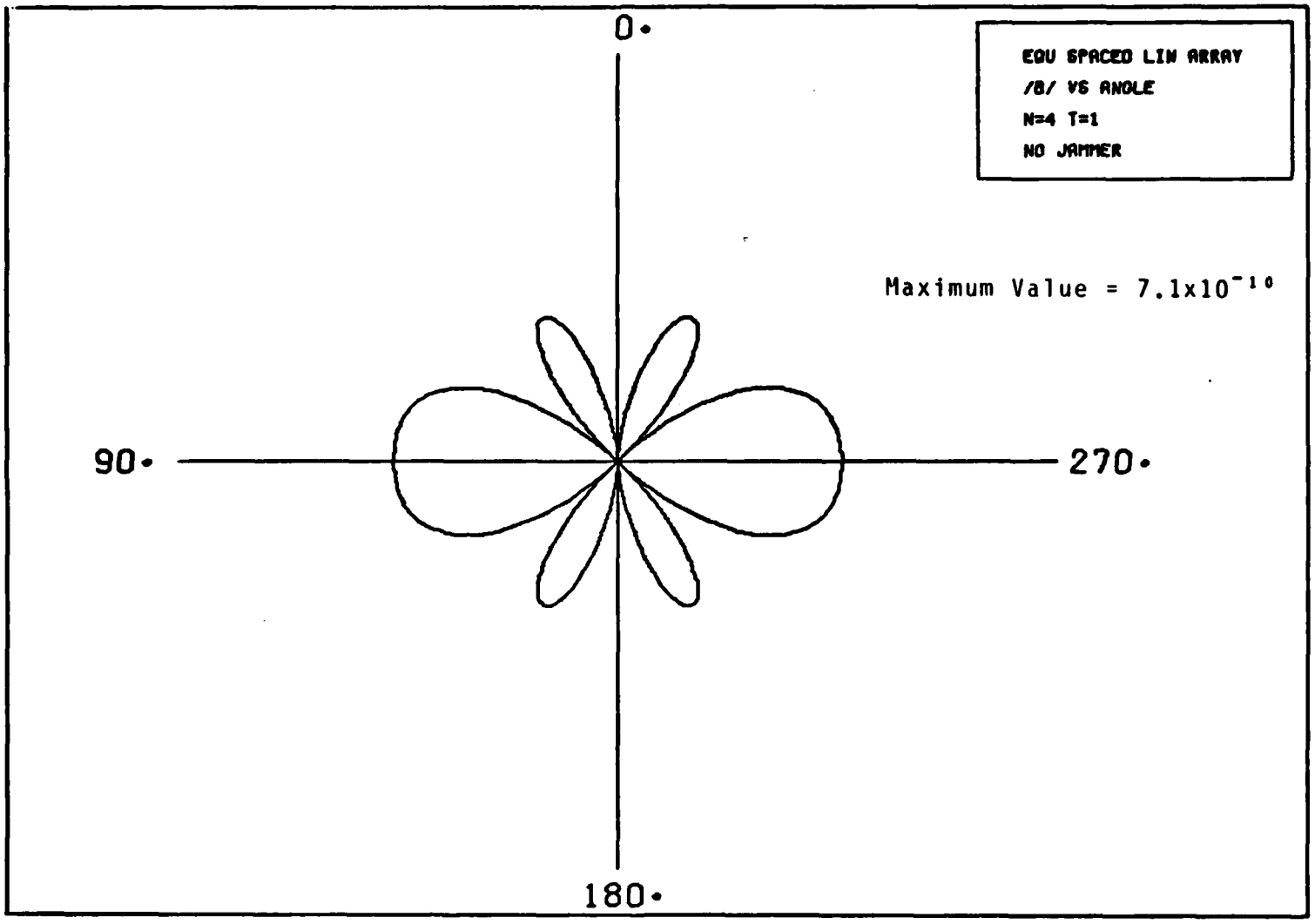

Figure 9. Polar Plot of |B(θ)|

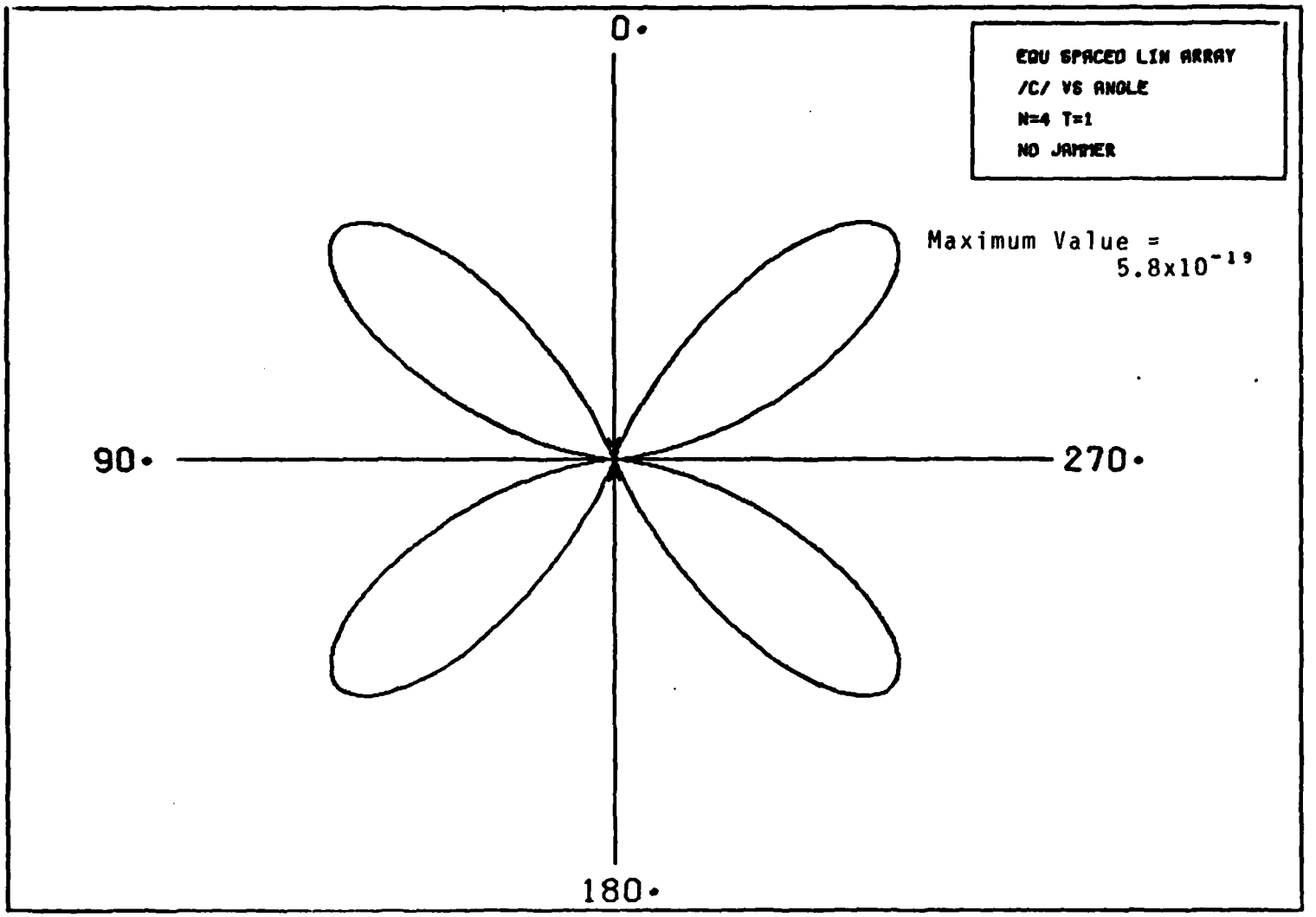

Figure 10. Polar Plot of |C(θ)|

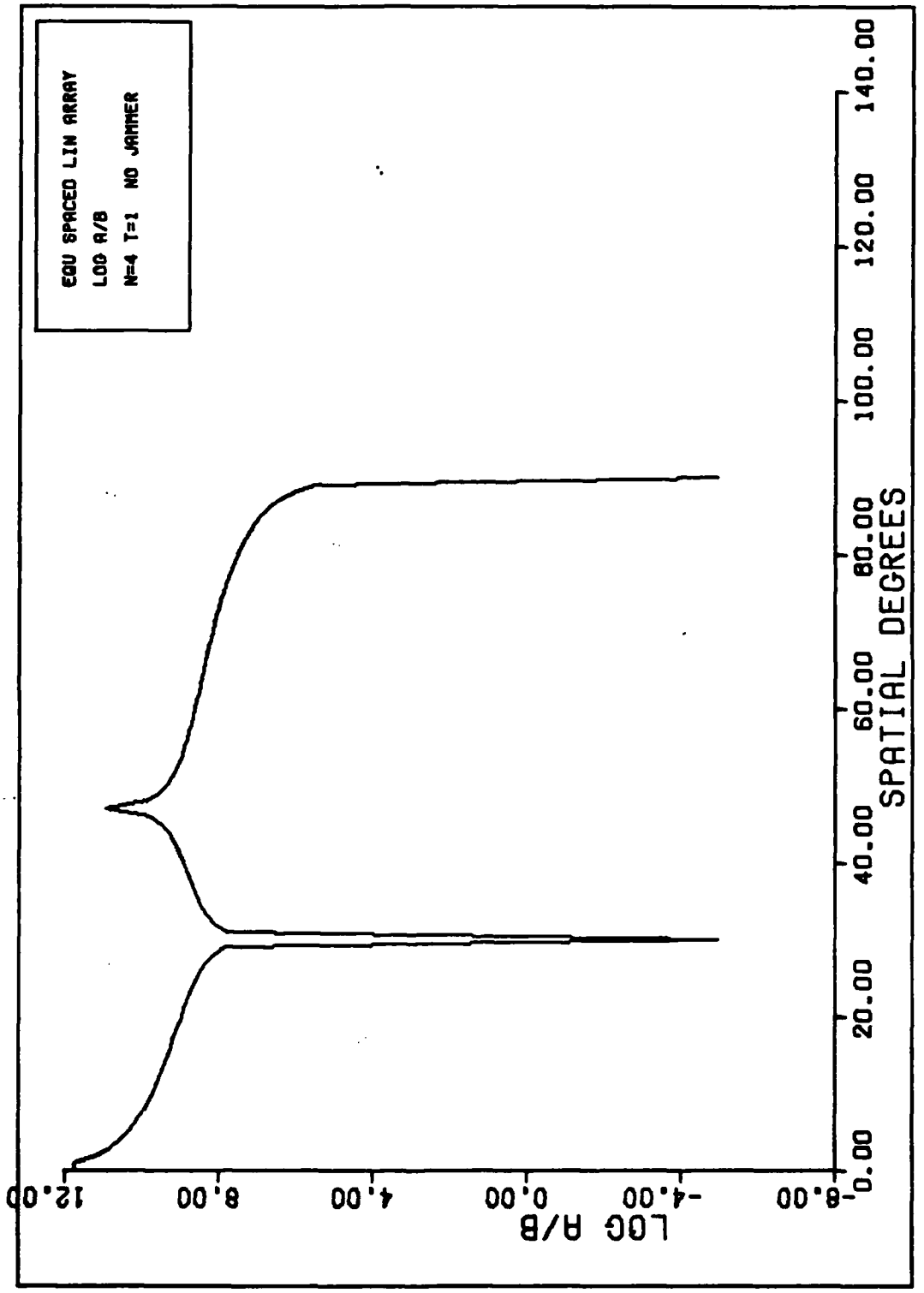

Figure 11. Plot of the Ratio $\left|\frac{A(\theta)}{B(\theta)}\right|$

The amplitude response of the array filter can be represented as a constant plus a term linear in frequency over a bandwidth of approximately 15% of the center frequency f_0($f/f_0=\pm.075$ in Figure 6). Both terms depend upon arrival angle θ. Thus, the first term in the Taylor series is sufficient to represent the array filter near broadside (see $\theta=5^0$ in Figure 6) while the second term in the series is strongly dominant in the vicinity of a null (see $\theta=30^0$ in Figure 6). In the next section we assess the impact of tapped delay lines on these results.

D. Transfer Function with Tapped Delay-Lines

The phase response of $H(f,\theta)$ has a greater phase offset and steeper slope due to the addition of delay-lines. This is apparent from the leading term in Eq.(83). As before this term is linear in frequency and therefore produces no distortion in the signal of interest.

The impact of $H_D(f)$ on overall frequency response of the array is analyzed by investigating the $\frac{\sin M(x)}{\sin(x)}$ form of the response which appears both in $H_D(f)$ and $H_E(f,\theta)$ (see Eq (87) and (88)). The modulus of $H_D(f)$ is centered at $f/f_0=0$ while the modulus of $H_E(f,\theta)$ is centered at $f/f_0=-1$. The generic forms of these functions are shown in Figure 12. Near the center frequency (i.e. $f/f_0=0$) the modulus of $H_D(f)$ is relatively constant. For bandwidths of $\pm 25\%$ of f_0, $|H_D(f)|$ drops only 5% below its peak value. These numbers are valid for $T=3^*$ and $\Delta=\frac{1}{2}\lambda_0$. As the ratio

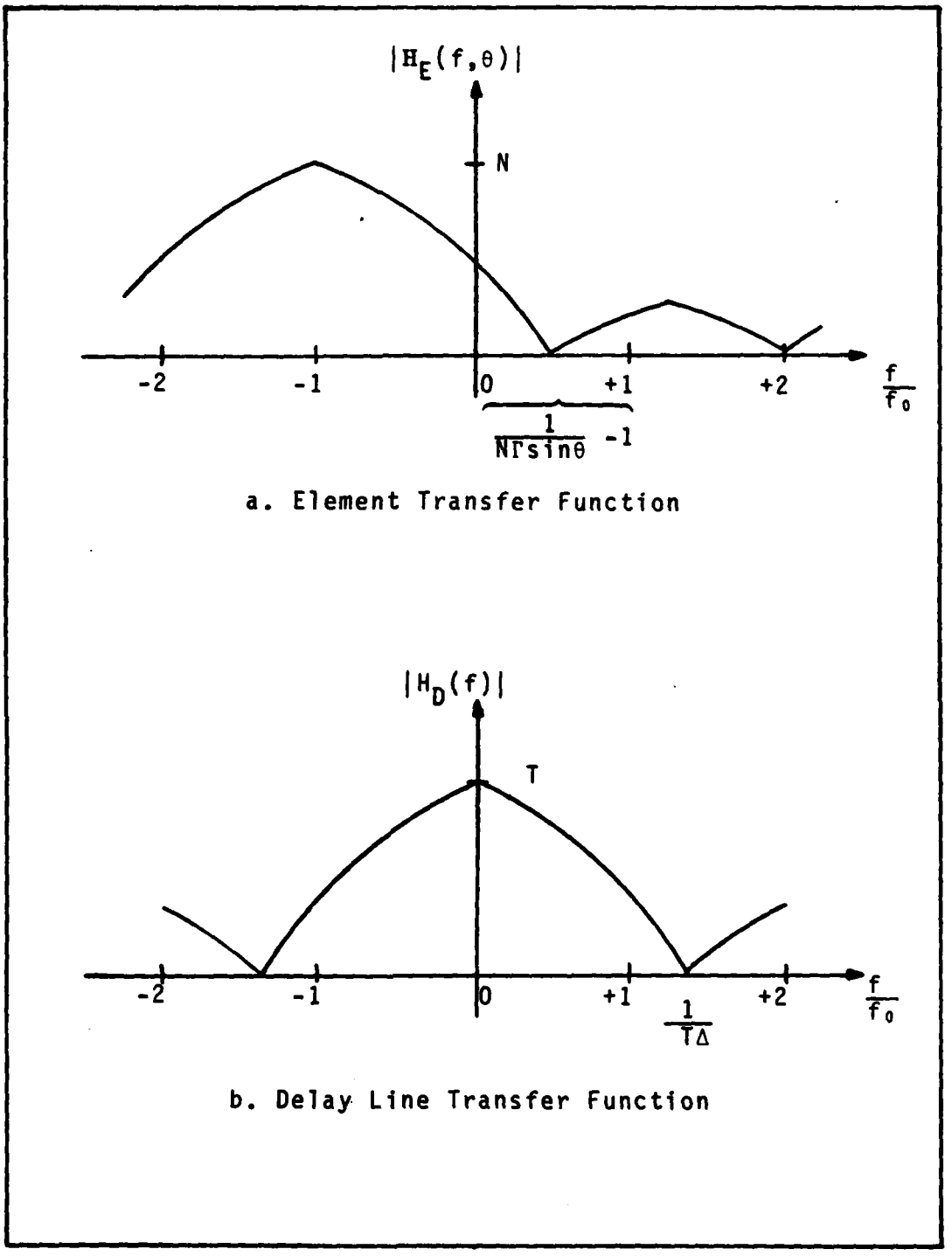

Figure 12. Generic Frequency Response of Transfer Functions

$1/T\Delta$ gets larger, the sidelobes in Figure 12b. move farther from the origin and the frequency response of $H_D(f)$ gets flatter. For the particular parameters used here, we would not expect the array's frequency response to change significantly due to the addition of tapped delay-lines. The following figures support this conclusion.

As before the parameters used are for a four element array (N=4) with half wavelength spacing between elements ($d=\frac{1}{2}\lambda_0$) . In addition, each element has a three-tap delay-line behind it (T=3) with quarter wavelength spacing between taps ($\Delta=\frac{1}{4}\lambda_0$) . The frequency response of the entire array is shown in Figure 13 for the same five angles used in Figure 6. The effect of tapped delay lines is most apparent as θ approaches broadside. At $\theta=0^0$, $H_E(f,\theta)$ reduces to unity and an array without taps has a constant frequency response. An array with taps will have a response determined by the tapped delay-line parameters (i.e. determined by $H_D(f)$). For $\theta=5^0$ in Figure 13 the curvature in the response due to a second order frequency dependence of $|H_D(f)|$ is readily apparent.

The phase response of this array with delay-lines is shown in Figure 14. As anticipated, it has a greater phase offset and steeper slope due to the tapped delay-lines (compare to Figure 7).

The similarity in frequency response of an array without delay lines versus an array with delay lines is reflected by

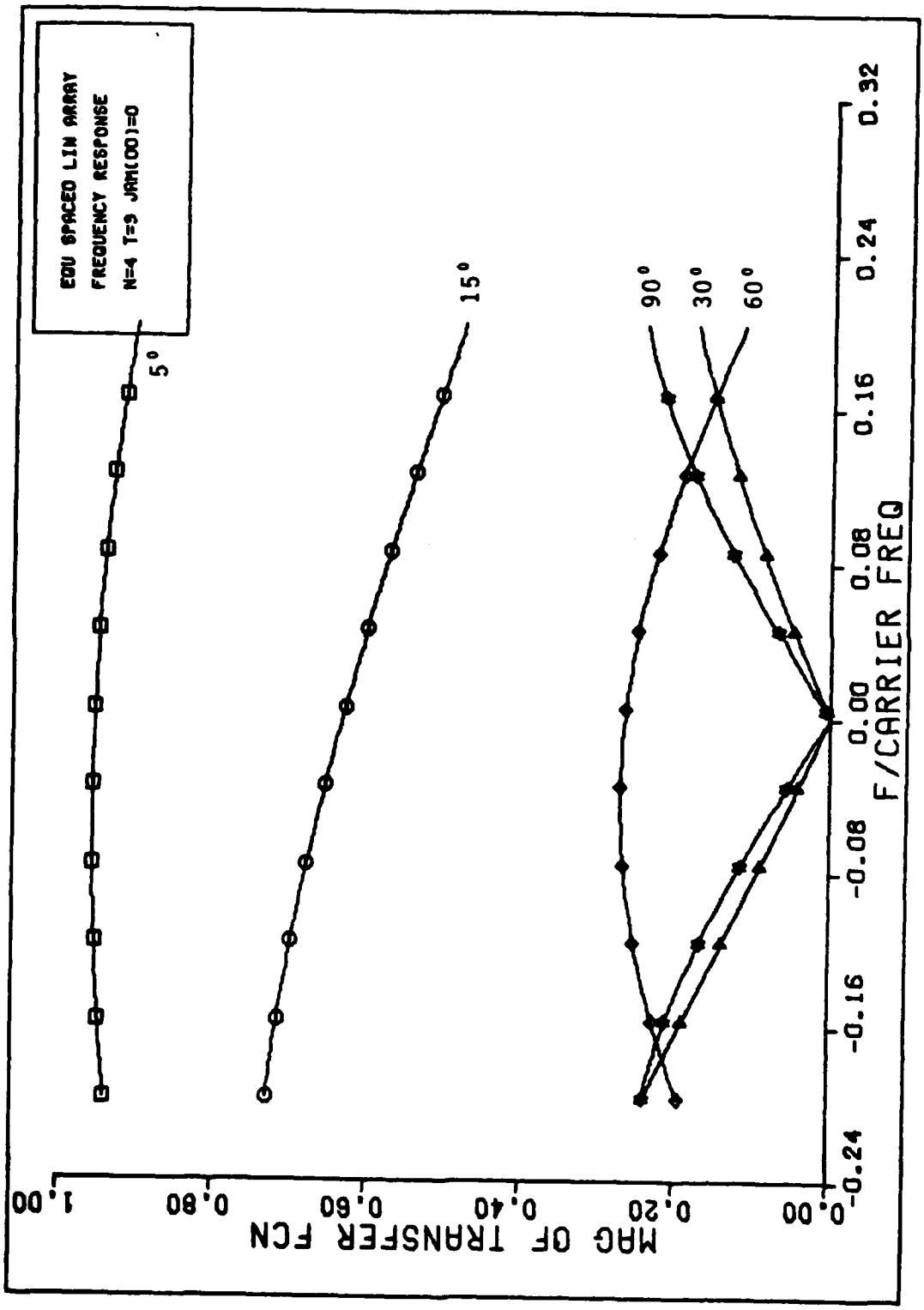

Figure 13. Frequency Response

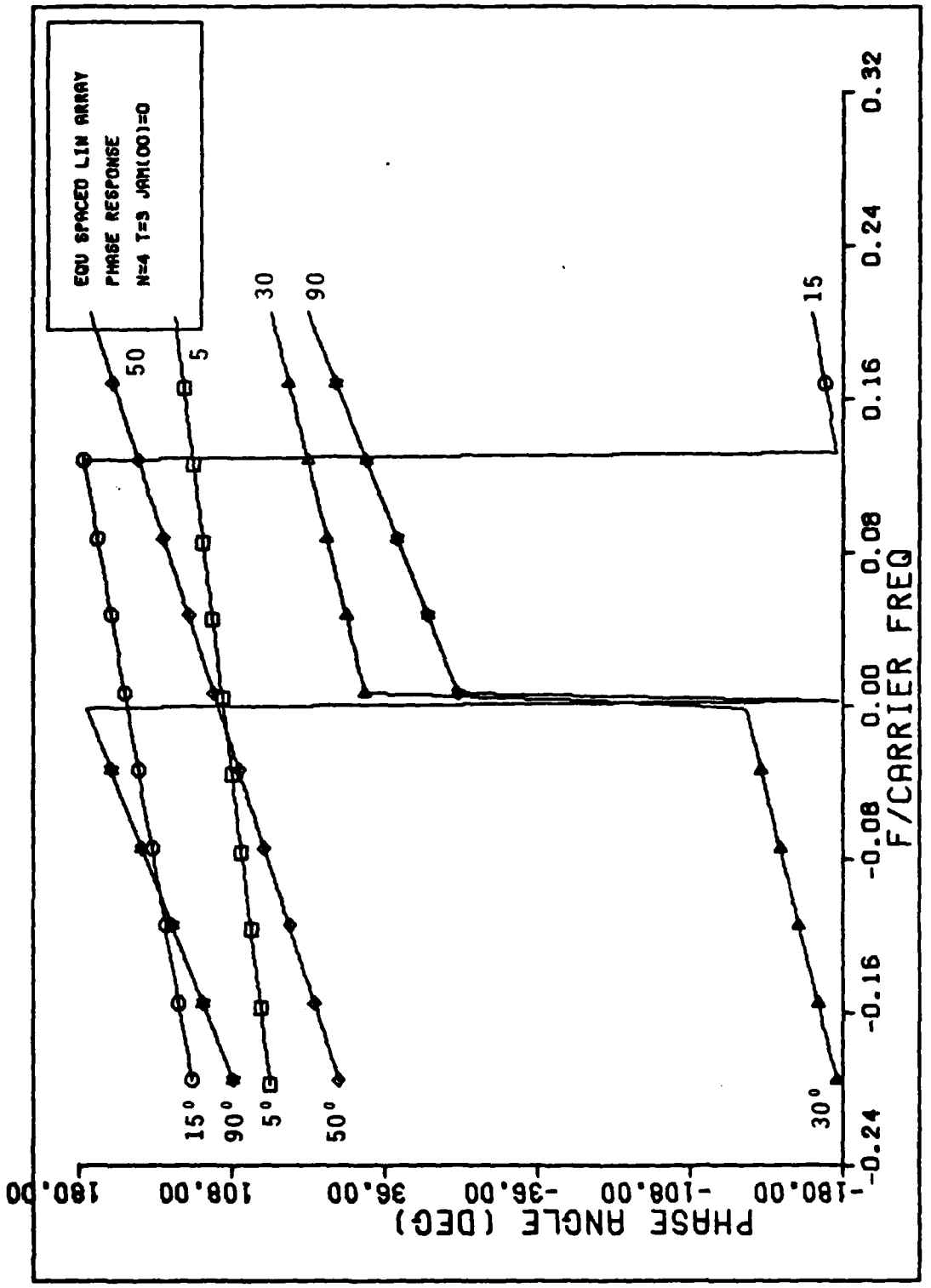

Figure 14. Phase Response

the Taylor series coefficients $A(\theta)$, $B(\theta)$, and $C(\theta)$ which quantify the arrays frequency dependence. Figures 15, 16, and 17 are polar plots of these coefficients for an array with tapped delay-lines. Comparison to Figures 8, 9, and 10 for the array without delay lines reveals little difference. Data for these six figures reveal no difference in values for $A(\theta)$ and $B(\theta)$ between the two arrays. The third term $C(\theta)$ is larger for the array with delay lines, as expected from the additional second order frequency dependence supported by Figure 13. Even so, $C(\theta)$ is on the order of 10^{-18} for all angles. This is insignificant in relation to signal distortion, based on the values of the second derivatives of signals appearing in Craddock's work (Ref 3).

For both arrays, $|A(\theta)|$ is much greater than $|B(\theta)|$ (on the order of 10^{8}) everywhere except at the antenna pattern nulls of 30^{0} and 90^{0}. This is consistent with the frequency response figures which show "V-shaped" nulls at $\theta=30^{0}$ and 90^{0} . The linearity in the array response, which is essentially unaffected by the addition of tapped delay-lines, leads to the conclusion identified by Raska, that the output of the array consists of the input signal and its first derivative (Ref 11:112-113). Figure 18 shows the "array filter bandwidth" versus angle as derived in Chapter II. By comparing this figure to Figure 11 we see that there is no difference. The location of significant first derivative distortion, based on a threshold of 6.7 as before, persists for 2^{0} about

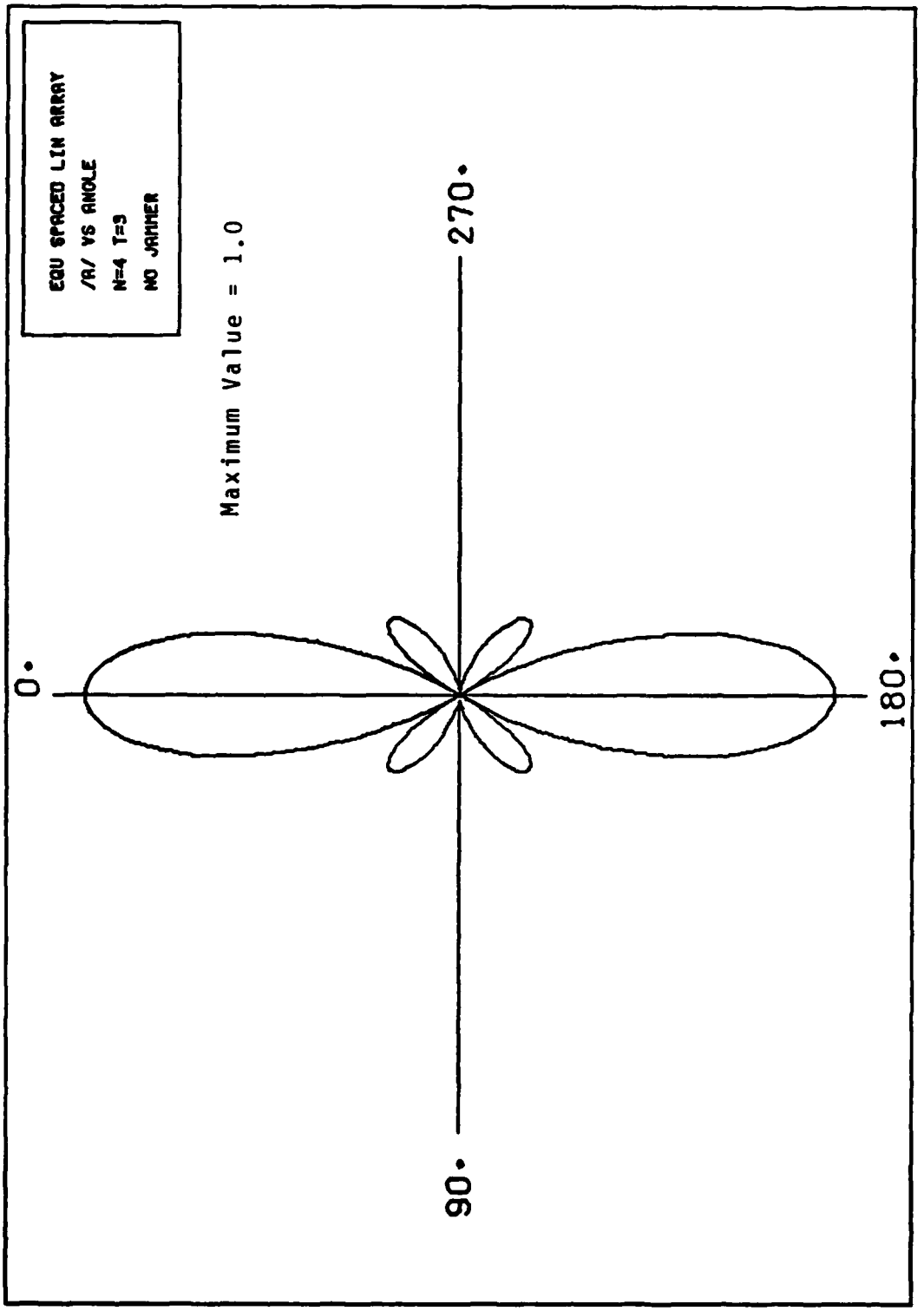

Figure 15. Polar Plot of $|A(\theta)|$

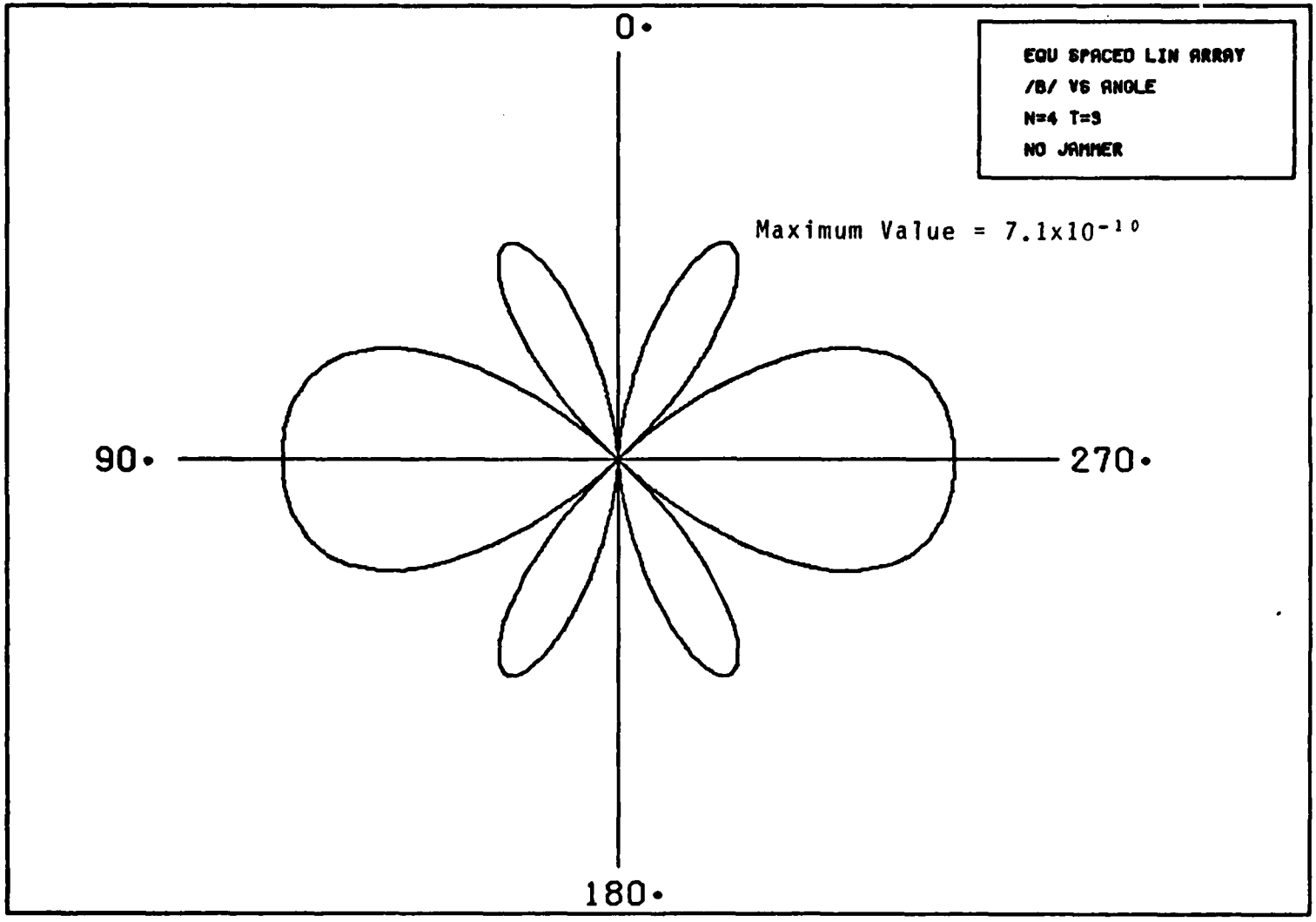

Figure 16. Polar Plot of $|B(\theta)|$

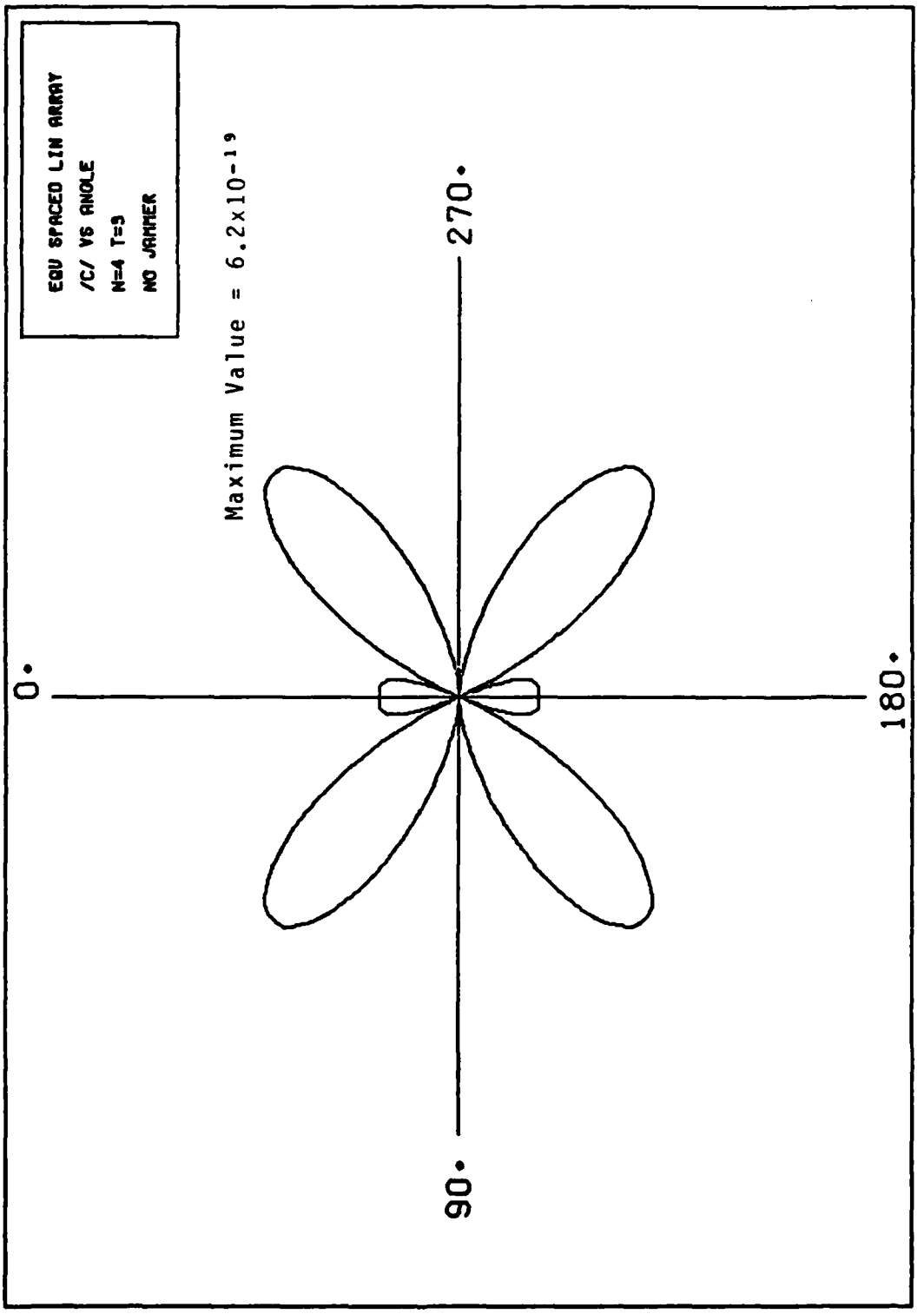

Figure 17. Polar Plot of |C(θ)|

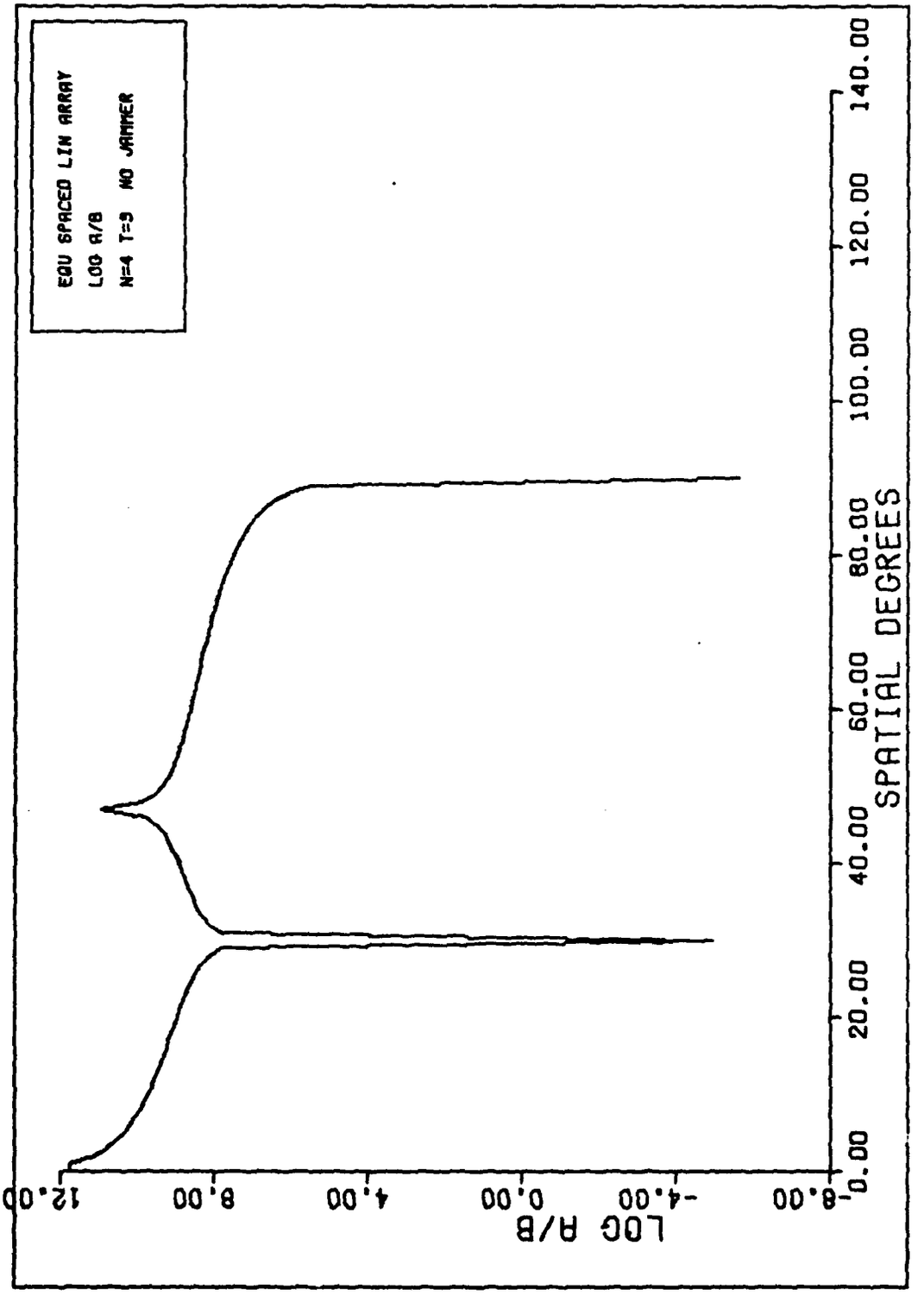

Figure 18. Plot of the Ratio $\left|\frac{A(\theta)}{B(\theta)}\right|$

each antenna pattern null.

In conclusion, the addition of tapped delay-lines to phase steered arrays does not change the frequency response of the array for moderately wideband signals in the UHF range. This bandwidth is on the order of $f/f_0=\pm 5\%$ or 10% bandwidth. Though the phase respone changes, it remains linear with frequency. Therefore the distortion of the array output is uneffected by the addition of tapped delay-lines for an array with fixed weights which implement phase steering at center frequency. It should be noted however that real systems may still perform differently with tapped delay-lines because actual phase shifters are dispersive in frequency. The following Chapter looks at the frequency response of an array whose weights are adapted to noise sources in the environment.

V Antenna Arrays with Adaptive Weights

This chapter addresses the transfer function of an antenna array with weighting coefficients. The weights are computed from assumed jammer parameters (power, angle of arrival, and bandwidth) using the weight equation discussed in Chapter III. The weights are then used to compute array transfer functions. In Chapter IV it was shown that for phase steered arrays, the signal output consists of the original signal plus its first time derivative (Ref 11:112-113). The purpose of this chapter is to determine if adaptive arrays lead to outputs with significant higher order time derivative signal distortion. To limit the scope of this analysis, several constraints are applied. First, for all cases the arrays are steered broadside. Second, the input thermal noise power to the array element is one watt.

A. Linear Array Adapted to Narrowband Jammers

In Chapter IV it was possible to derive a closed form solution for the antenna array's transfer function. That is not possible in this chapter because of the adaptive algorithm used to determine the weighting coefficients. For each scenario, the assumed jammer parameters and broadside steering constraint are used to calculate the covariance matrix $\vec{\Phi}$ (see Eqs(44) and (64) and the quiescent weights $\vec{W}_q$ (see Eqs (75) and (78)). The array weights are computed from Eq.(39) then used to compute the

transfer function with Eq.(16).

In addition, the coefficients of the Taylor series expansion are calculated using Eqs.(17) through (21). These coefficients can be used to verify the transfer function and identify the order of frequency dependence inherent in it.

The four separate scenarios to be evaluated are for a single jammer of 10 watts at 10^0 and 50^0 and of 1000 watts at 10^0 and 50^0 . These jammer locations are measured with respect to array broadside. In each case the transfer function is evaluated for an array without tapped delay lines (T=1) and for an array with tapped delay lines (T=3) . The choice of jammer locations is based on analyses of results from Chapter IV. With the adaptive algorithm used here, a null can be produced at the location of a sufficiently powerful jammer. In this analyses a jammer of 1000 watts is adequate to produce a null. Though the transfer function is dependent upon angle, the angle of interest is the location of the jammer. At this location the value of $A(\theta)$ is reduced sufficiently so that higher order terms in the Taylor series may become significant.

The antenna pattern for $A(\theta)$ is shown in Figure 8 for a particular unadapted array geometry. In this figure there are nulls at $\theta=30^0$ and 90^0 . It is expected and was verified that a jammer at either of these locations would not result in adaptive weights which would produce a more optimum pattern for nulling the jammer. Figure 9 shows the pattern

associated with the next Taylor series coefficient, $B(\theta)$. The magnitude of $B(\theta)$ is sufficient at almost all angles to represent the linear variation with frequency of the associated transfer function (see Figure 6). It is anticipated that any jammer location would lead to a frequency response which has at least a linear dependence on frequency, as quantified by $B(\theta)$.

The distortion pattern associated with $C(\theta)$ is shown in Figure 10. The second order variation with frequency which is associated with $C(\theta)$ was not significant for phase steered arrays, and bandwidths on the order of 15% of f_0 . However this was true due to the dominance of $A(\theta)$ at most angles. If a jammer is placed at $\theta=50^0$, where $C(\theta)$ has its peak value, $A(\theta)$ may be reduced enough to lead to observable second order frequency variations in the transfer function of that adapted array. This research verified this conclusion.

Based on the above, the two jammer angles chosen to be reviewed here were $\theta=10^0$ and $\theta=50^0$. The first angle leads to results which do not vary significantly from the unadapted case. The second angle leads to different results.

1. Phase Response

For all cases investigated during this research effort, including those in this chapter, the phase response of the array was linear with frequency. The numerical results for

the cases of a jammer located at $\theta=10^0$ will be used to illustrate this conclusion; the phase response of other cases will not be discussed. Phase response plots for most cases can be found in Appendix B.

Table II contains the modulus and phase values for the Taylor series coefficients produced by jammers located at $\theta=10^0$. Three cases are addressed. First, the unadapted array whose values are listed here for reference. Second, the adapted array for a low power jammer of 10 watts. Last, the case of a higher power jammer of 1000 watts. Note that all coefficients are either purely real or purely imaginary. The multiplying factor associated with each coefficient always results in a product which is purely real. These multiply factors are those shown in Eq.(18), repeated here for convenience

$$H(f,\theta) \triangleq e^{[j2\pi(f+f_0)t_c]}\{A(\theta)+(j2\pi f)B(\theta)+(j2\pi f)^2C(\theta)+...\} \quad (18)$$

The significance of this result is first that the complex number defined by the summation of terms in Eq.(18) is purely real. Second, the output signal and its first derivative are separated in phase by 90^0 due to the phase of $A(\theta)$ and $B(\theta)$ shown. The phase response of the transfer function is due to the sign of this summation and the leading exponential term in Eq(18). Therefore the phase response is linear with frequency.

Table II. Taylor Series Coefficients for Narrowband Jammer at 10^0.

Jammer Power (Watts)	N,T	Normalized Amplitude and Phase at 10^0		
		A(θ)	B(θ)	C(θ)
0	4,1	8.233×10^{-1} 0^0	1.525×10^{-10} 90^0	2.736×10^{-20} 0^0
0	4,3	8.233×10^{-1} 0^0	1.525×10^{-10} 90^0	1.674×10^{-19} 0^0
10	4,1	2.008×10^{-2} 0^0	1.525×10^{-10} 90^0	3.529×10^{-21} 180^0
10	4,3	6.804×10^{-3} 0^0	1.525×10^{-10} 90^0	2.882×10^{-21} 180^0
1000	4,1	2.058×10^{-4} 0^0	1.525×10^{-10} 90^0	8.586×10^{-21} 180^0
1000	4,3	6.860×10^{-5} 0^0	1.525×10^{-10} 90^0	4.287×10^{-21} 180^0

Thermal Noise Power = 1 Watt

Jammer Bandwidth = 0% f_0

$d = \lambda_0/2$

$\Delta = \lambda_0/4$

2. Frequency Response for a Jammer at $\theta=10^0$

The two jammer cases associated with Table II are discussed next for the T=1 geometry. Figures for the T=3 geometry can be found in Appendix C. Figure 19 is the frequency response resulting from a jammer with 10 Watts power.

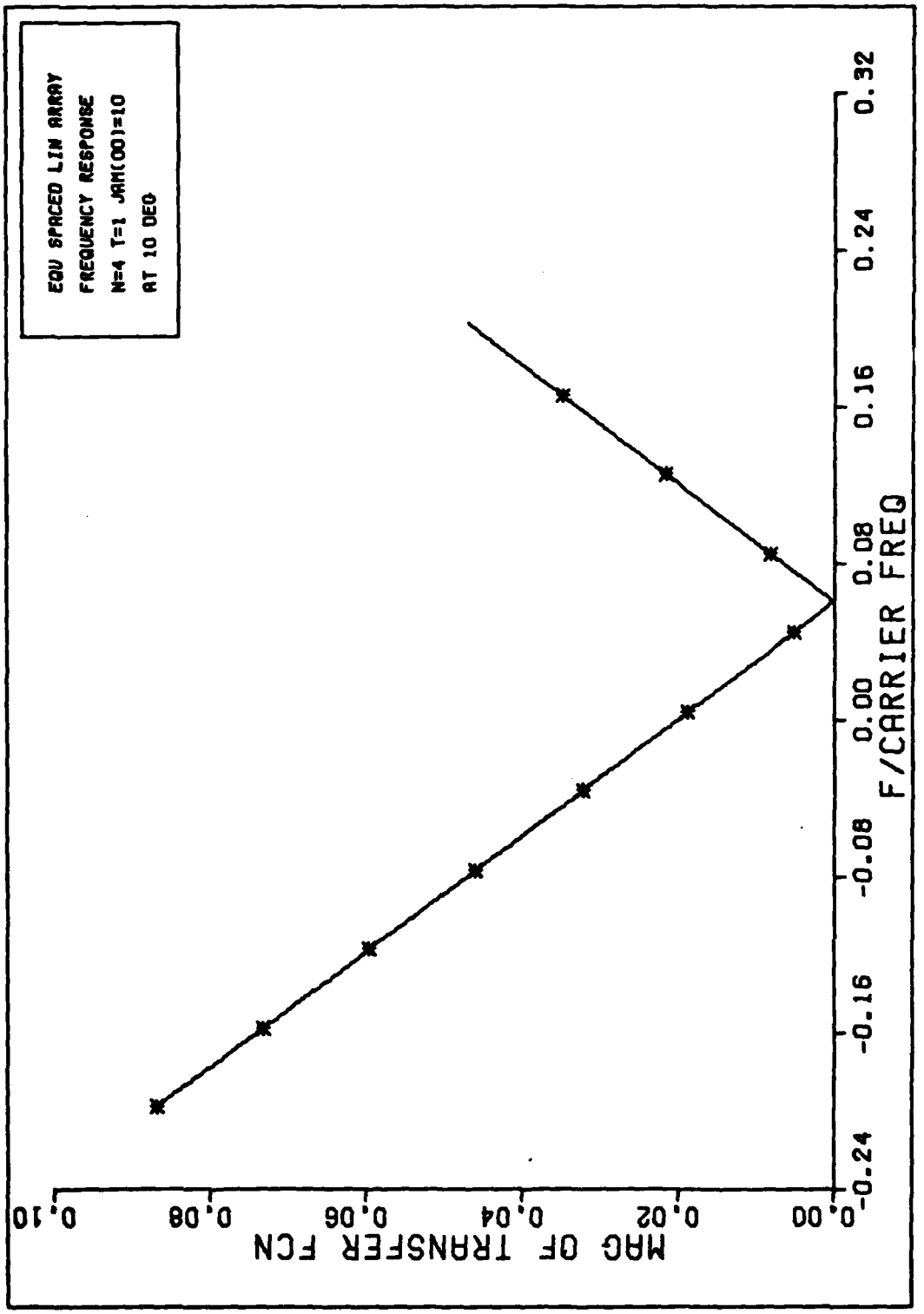

Figure 19. Frequency Response

The corresponding Taylor series coefficients are in line three of Table II. The question to be addressed for this case and subsequent cases is what order frequency dependence does this response have? It is concluded from Figure 19 that the dependence is linear with frequency. Therefore only the first two coefficients are required to adequately represent $|H(f,\theta)|$. This is denoted by using a subscript 2 as shown

$$|H(f,\theta)| \simeq |H_2(f,\theta)| \triangleq |A(\theta)+(j2\pi f)B(\theta)| \qquad (92)$$

This approximation is verified by noting that the value for $A(\theta)$ listed in Table II corresponds well with the value of $|H(f,\theta)|$ at $f/f_0=0$ in Figure 19. Also, the slope of the curve in Figure 19 is equal to $2\pi f_0 B(\theta)$ at $\theta=10^0$. The jammer power in this case is insufficient to produce a null in the transfer function.

Figure 20 is the frequency response for an array adapted to a jammer with 1000 Watts of power. The value of $B(\theta)$, both in the figure and Table II line four, is unchanged. However $A(\theta)$ has a well defined null at $\theta=10^0$. These response curves are typical of results produced by a jammer located at least 10^0 away from $\theta=50^0$. For bandwidths on the order of 15% of f_0 , the output of an array, either with or without delay lines, consists of the input signal and its first time derivative.

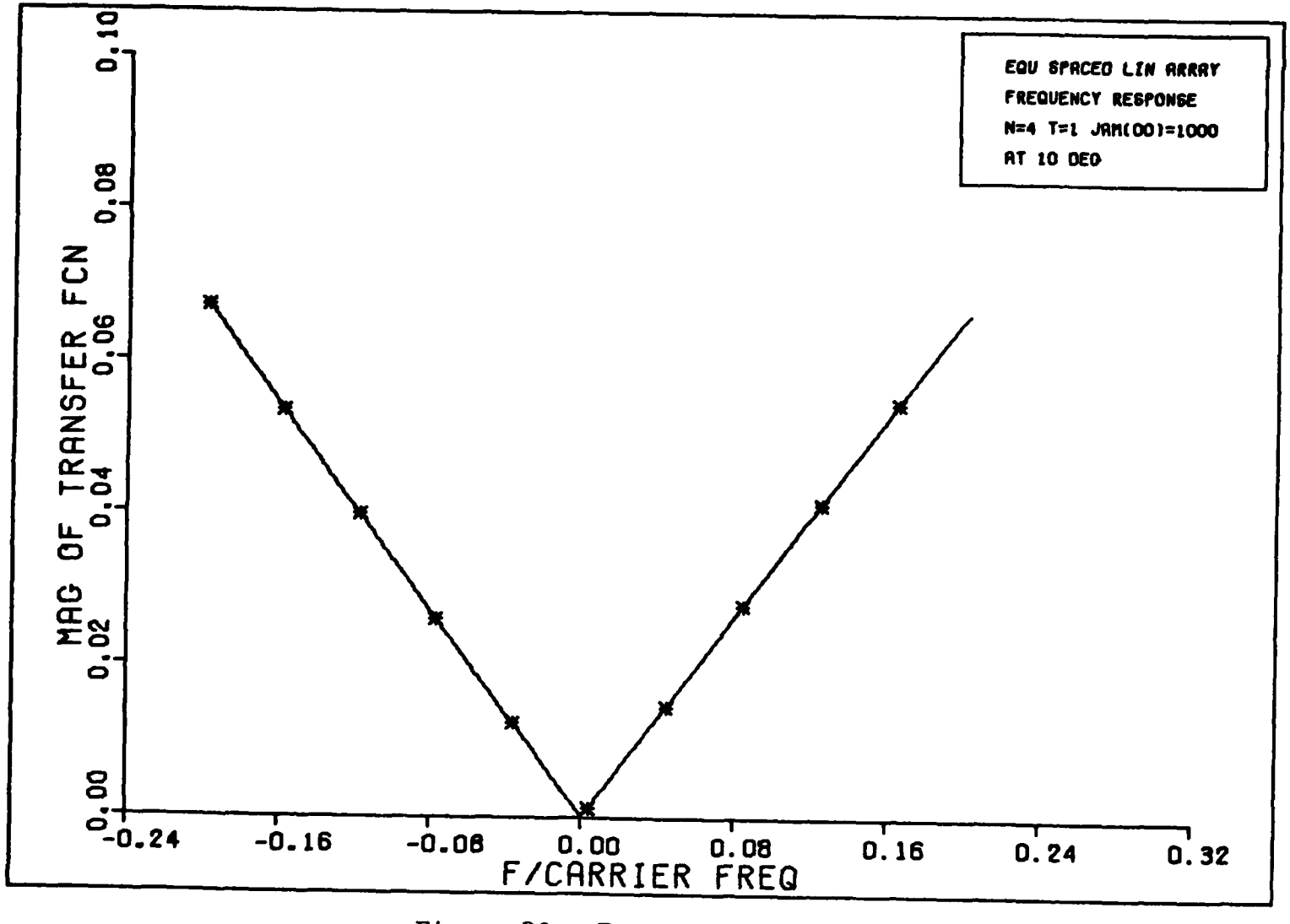

Figure 20. Frequency Response

3. Frequency Response for a Jammer at $\theta=50^0$

For this particular array geometry, a jammer located at $\theta=50^0$ produces second time derivative distortion in the array output. Other angles are not effected in this manner as seen in Figure 21. This figure shows the frequency response for several angles given an array adapted to a jammer at $\theta=50^0$ with 1000 watts power. Except for $\theta=50^0$, all frequency responses at other angles are linear in frequency for the bandwidth of interest. The numerical values of the first three Taylor series coefficients are in Table III for this case and the case where jammer power is 10 watts. Also listed for reference are the values for an unadapted array. Figure 22 is an expanded view for the case where the jammer power is 1000 watts and the array does not have delay lines. Two related observations are of interest. First, the null is asymmetrical about $f/f_0=0$. Second, the curve is not linear with frequency. The second order variation with frequency which leads to the asymmetrical response curve will be investigated first.

Using the subscript notation described earlier, the frequency response can be approximated by

$$|H(f,\theta)| \simeq |H_3(f,\theta)| \triangleq |A(\theta)+(j2\pi f)B(\theta)+(j2\pi f)^2 C(\theta)| \quad (93)$$

Substituting the coefficient values from line five of Table III into this equation yields the data points which are

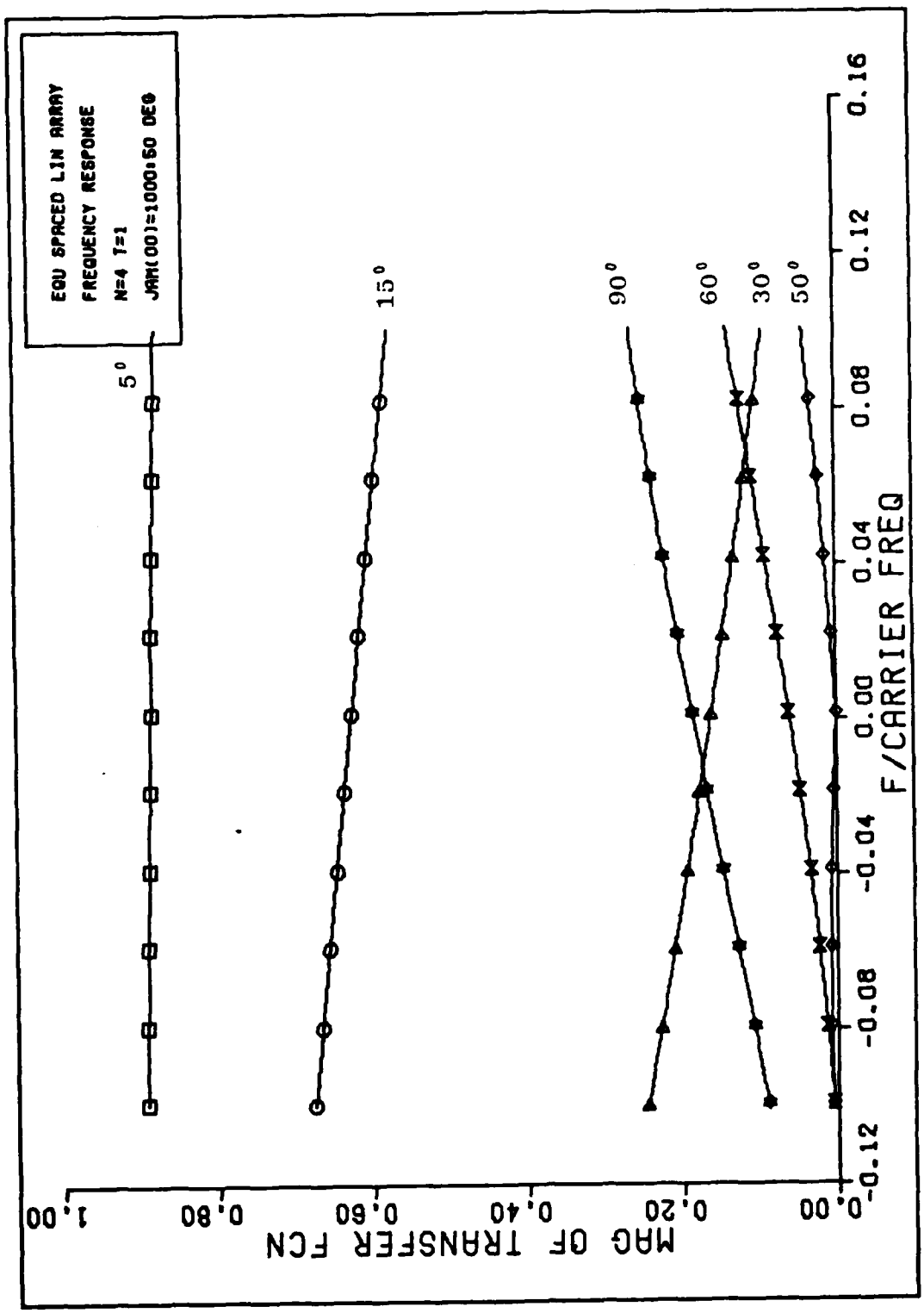

Figure 21. Frequency Response

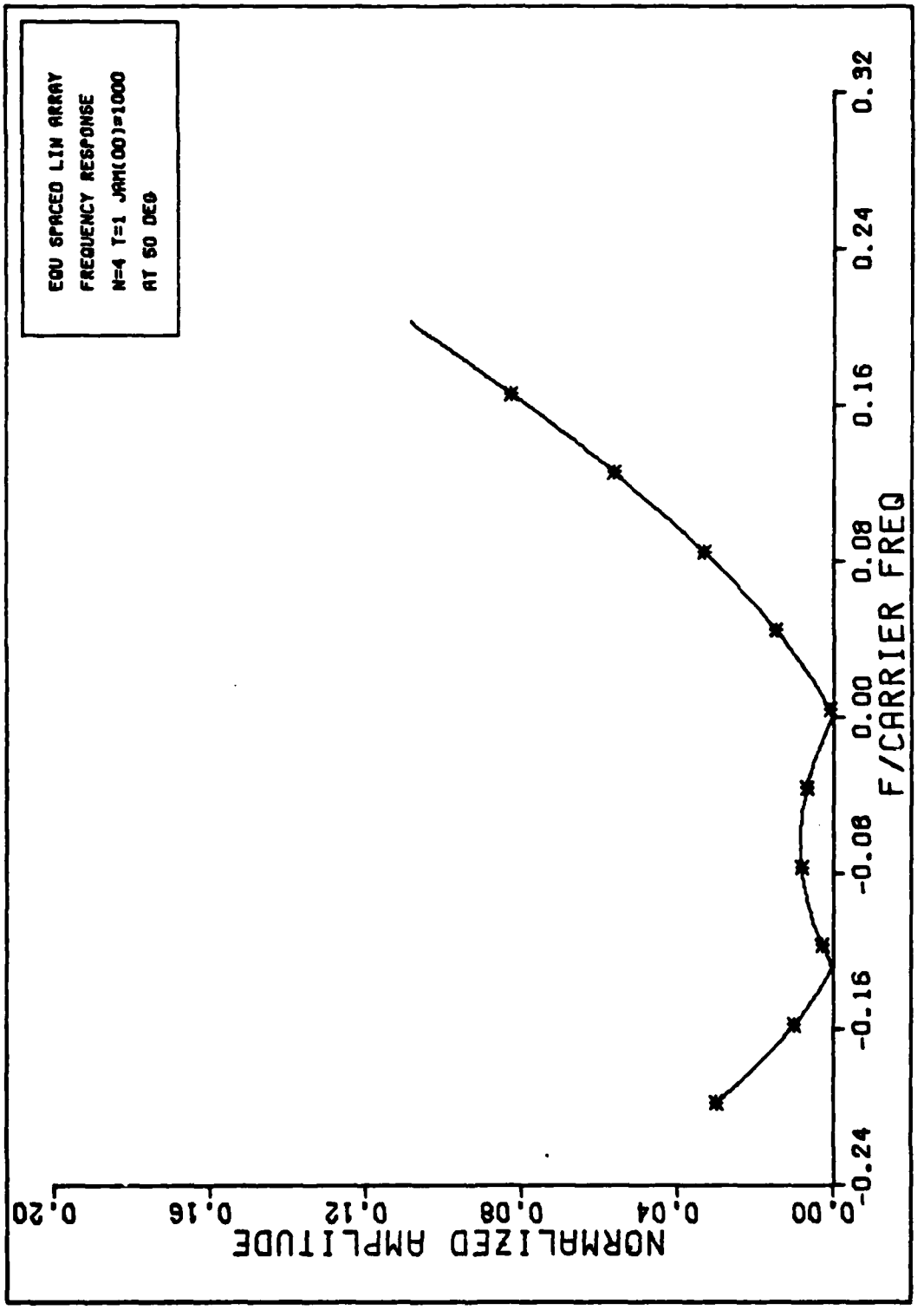

Figure 22. Frequency Response

Table III. Taylor Series Coefficients for Narrowband Jammer at 50^0

Jammer Power (Watts)	N,T	Normalized Amplitude and Phase at 50^0		
		A(θ)	B(θ)	C(θ)
0	4,1	2.665×10^{-1} 180^0	1.152×10^{-10} -90^0	5.742×10^{-19} -180^0
0	4,3	2.665×10^{-1} 180^0	1.152×10^{-10} -90^0	6.196×10^{-19} -180^0
10	4,1	$6.5\text{-}1 \times 10^{-3}$ 180^0	1.152×10^{-10} -90^0	3.796×10^{-19} -180^0
10	4,3	2.203×10^{-3} 180^0	1.152×10^{-10} -90^0	3.768×10^{-19} -180^0
1000	4,1	6.662×10^{-5} 180^0	1.152×10^{-10} -90^0	3.748×10^{-19} -180^0
1000	4,3	2.221×10^{-5} 180^0	1.152×10^{-10} -90^0	3.748×10^{-19} -180^0

Thermal Noise Power = 1 Watt

Jammer Bandwidth = 0% f_0

$d = \lambda_0/2$

$\Delta = \lambda_0/4$

contained in Table IV. Table IV lists these values, in column three, along with the actual value of the response, from Eq.(16). The error calculations in column four quantify the fact that this approximation is reasonable near $f/f_0=0$. For bandwidths of 12% of f_0 , $|H_3(f,\theta)|$ is accurate to within 4%.

Table IV. Frequency Response for Narrowband Jammer at 50^0

f/f_0	$\lvert H(f,\theta)\rvert$	$\lvert H_3(f,\theta)\rvert$	Percent error $\triangleq \left\lvert \frac{3-2}{2} \right\rvert$ x 100
-0.091	0.0070	0.0081	15.1%
-0.061	0.0084	0.0088	4.1%
-0.040	0.0072	0.0073	0.8%
-0.020	0.0044	0.0044	0.5%
0.000	0.0001	0.0001	0.0%
0.020	0.0058	0.0057	0.9%
0.040	0.0130	0.0130	0.4%
0.061	0.0216	0.0221	2.7%
0.091	0.0366	0.0380	3.9%
1	2	3	4

Thermal Noise Power = 1 Watt

Jammer Bandwidth = 0% f_0

Jammer Power = 1000 Watts

N=4 T=1 $d=\frac{\lambda_0}{2}$ $\Delta=\frac{\lambda_0}{4}$

Therefore, the output of this adapted array will be the input signal and its first time derivative as before. In addition, the signal's second time derivative could contribute to the distorted output.

The lack of symmetry of the null in Figure 22 is due to the dependence of this response on an odd function of frequency. The odd function is defined by $j2\pi fB(\theta)$ while the

AD-A085 708 AIR FORCE INST OF TECH WRIGHT-PATTERSON AFB OH SCHOO--ETC F/G 9/5
EFFECTS OF ADAPTIVE ANTENNA ARRAYS ON BROADBAND SIGNALS.(U)
JUN 80 W A RISKI

UNCLASSIFIED AFIT/GE/EE/80-4 NL

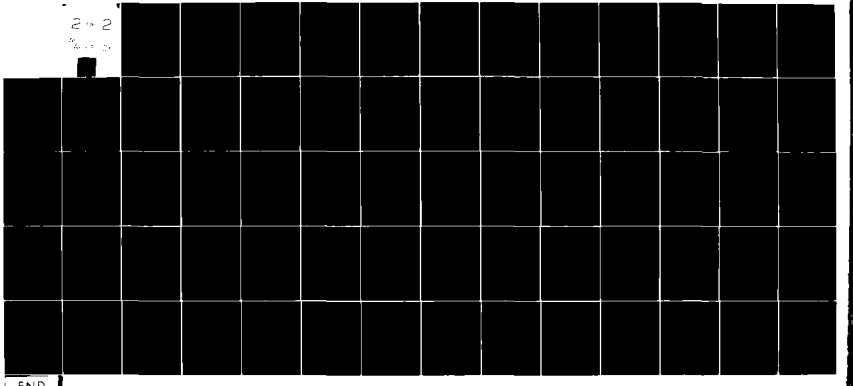

END
DATE FILMED
7-80
DTIC

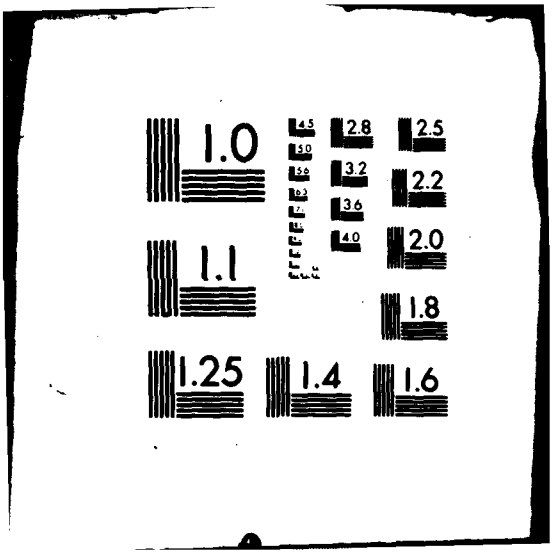
1.0
1.1
1.25
1.4
1.6
1.8
2.0
2.2
2.5
2.8
3.2
3.6
4.0
4.5
5.0
5.6
6.3

even function is $(j2\pi f)^2 C(\theta)$. The null at $f/f_0=0$ is defined by the value of $A(\theta)$. The other null is due to the 180^0 phase difference between the above functions for negative frequency offsets. As the jammer power is reduced, the value of $A(\theta)$ increases and the response curve is shifted by an associated amount.

Figure 23 is the transfer function for an array adapted to a jammer with 10 Watts, still located at $\theta=50^0$. Note that it has the same first and second order dependence on frequency. This figure is the same as Figure 22 with a constant negative offset, defined by $A(\theta)$. This value is in line three of Table III. It can be concluded, from the values in Table II and Table III, that $A(\theta)$ is a function of jammer power for a given angle. Also, $B(\theta)$ and $C(\theta)$ are not a function of jammer power. For unadapted arrays it was noted that $A(\theta)$ and $B(\theta)$ have an inverse relationship i.e. peaks in $A(\theta)$ are nulls in $B(\theta)$ and vice versa. This is not necessarily true for adapted arrays. A null in $A(\theta)$ produced by a jammer does not lead to a peak in $B(\theta)$ at that same location. Figures 24, 25, and 26 are polar plots of $A(\theta)$, $B(\theta)$, and $C(\theta)$ for an array adapted to a jammer of 1000 Watts at $\theta=50^0$. By comparing these figures to equivalent figures for the unadapted array (Figures 8 and 9) this observation can be verified.

Phase response curves for adapted arrays with delay lines (T=3) are in Appendix B. Appendix C contains frequency

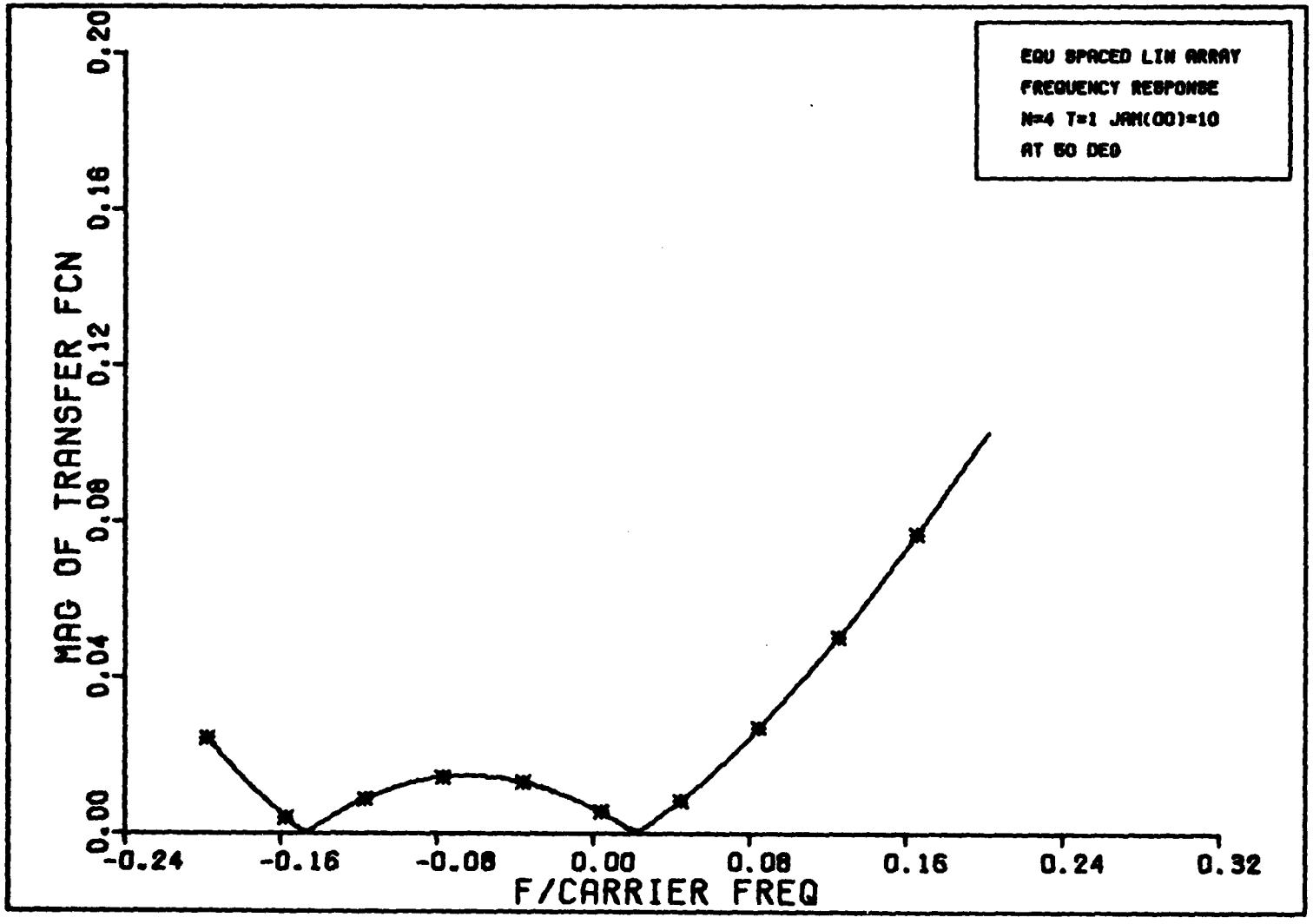

Figure 23. Frequency Response

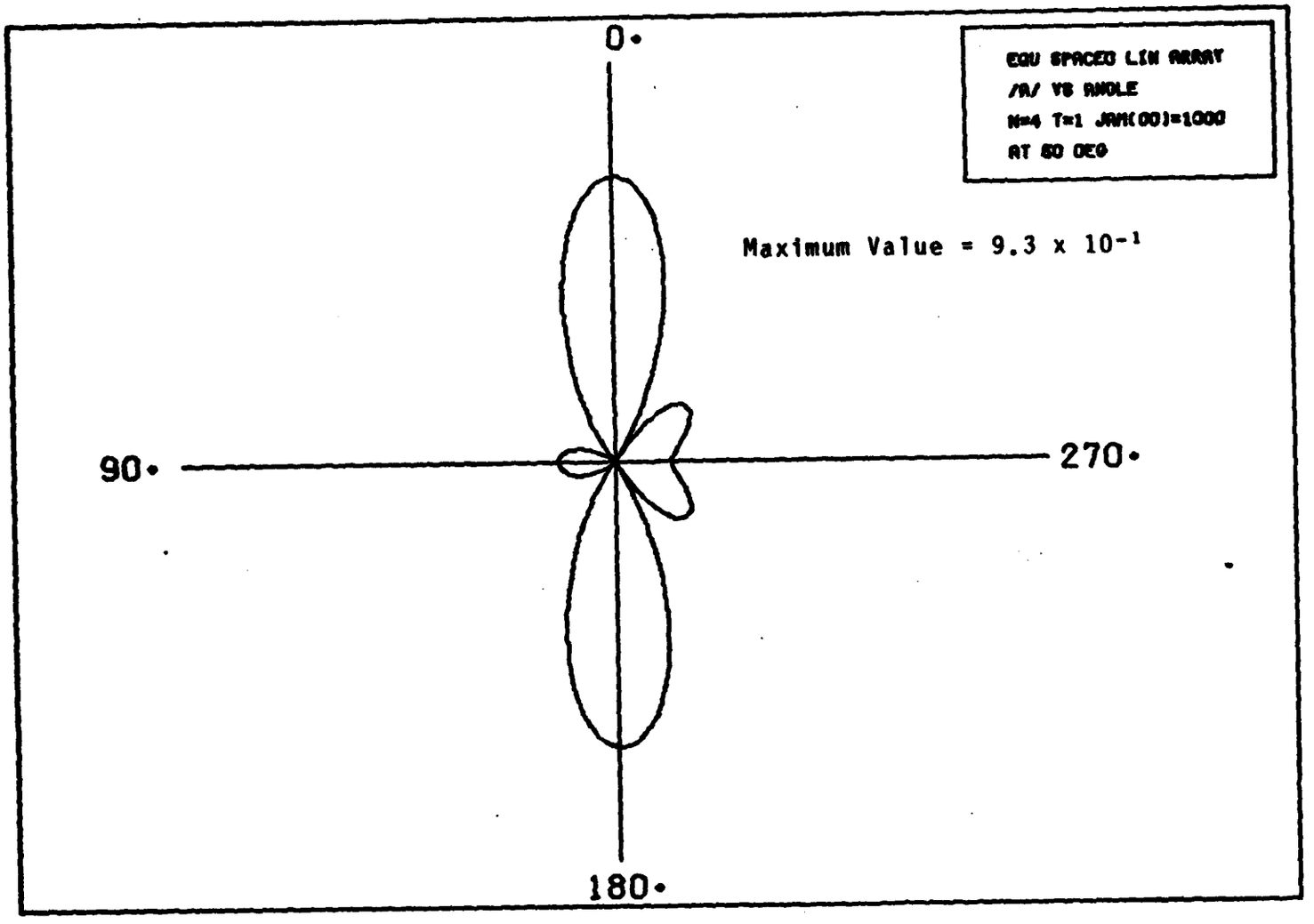

Figure 24. Polar Plot of |A(θ)|

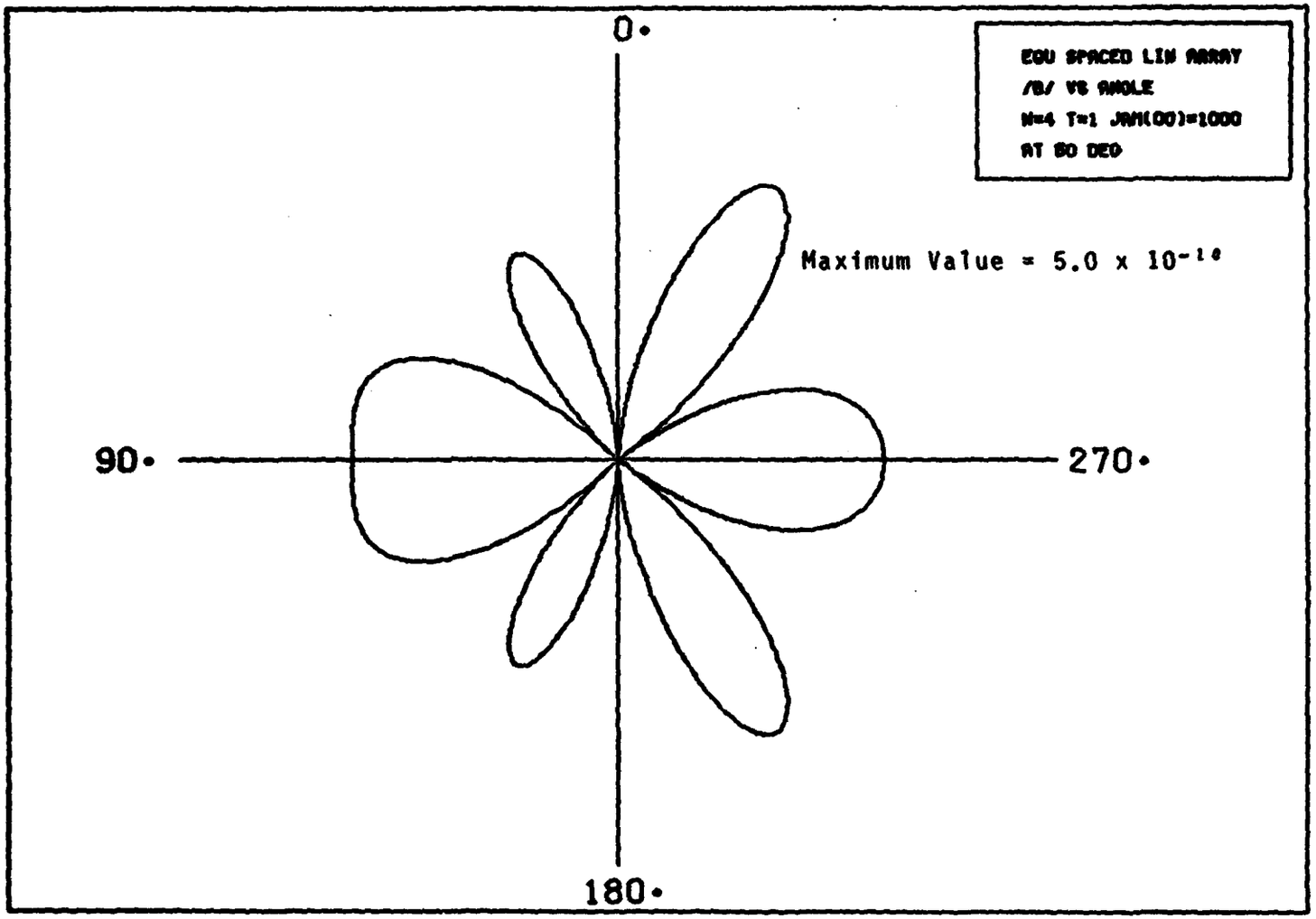

Figure 25. Polar Plot of |B(θ)|

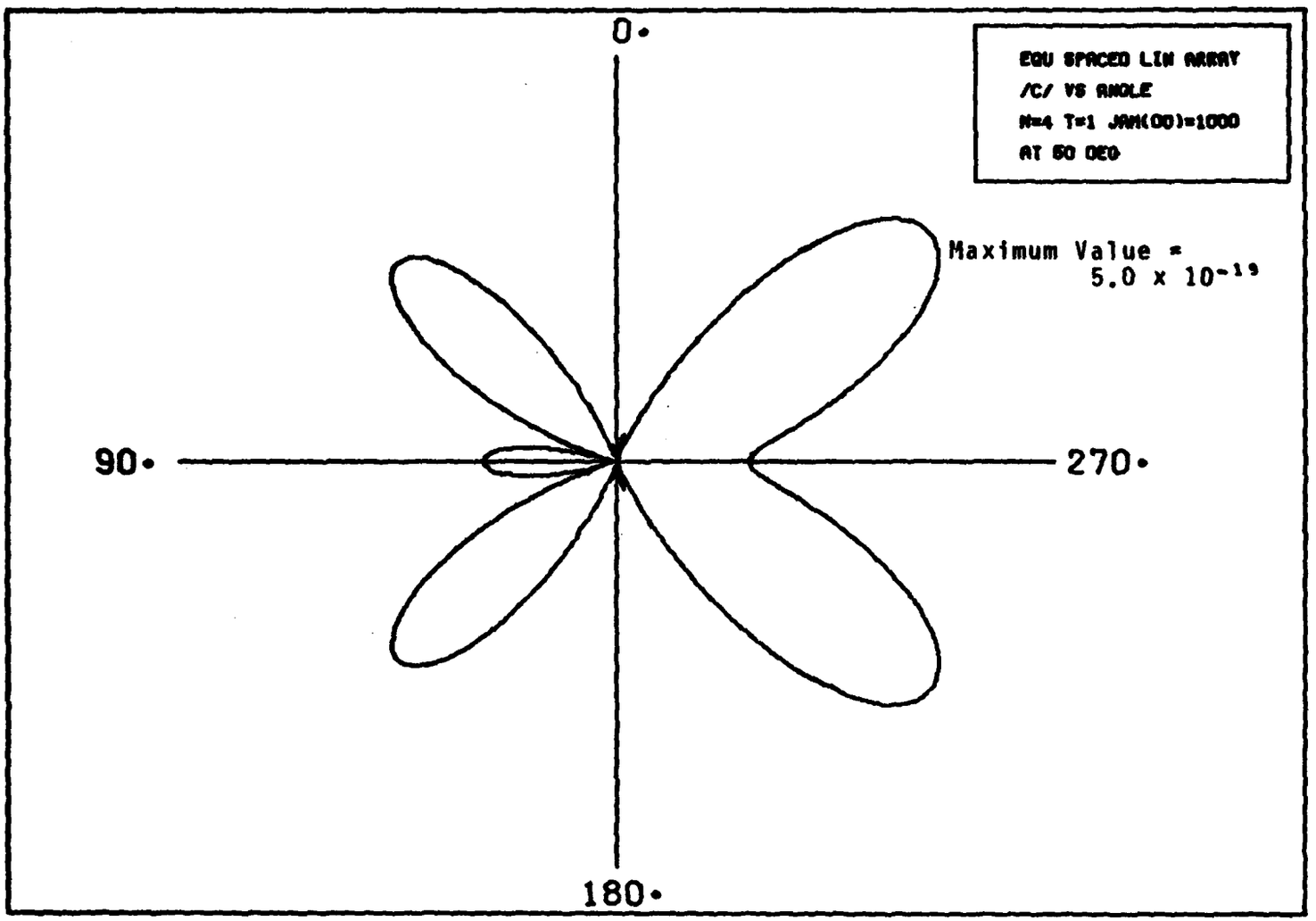

Figure 26. Polar Plot of $|C(\theta)|$

response curves and polar plots of coefficients. The addition of delay lines has no impact on these results.

In summary, narrowband jammers do not lead to adapted arrays with output distortion significantly different than that for unadapted arrays. For jammers located at $50^0 \pm 10^0$, second order derivative distortion is possible if such signals had a magnitude sufficient to offset the value of $C(\theta)$. However, existing work does not contain derivative signals with the necessary magnitudes (Ref 3). Therefore, even for a jammer at 50^0, the results do not vary substantially from the unadapted array case.

4. Frequency Response for Multiple Jammers

The frequency responses for several multiple jammer cases are reviewed in this section. The first case is defined by two jammers located one degree apart, each transmitting 1000 Watts of power. Figure 27 contains the frequency response curves, for the associated adapted array, at location $\theta=10^0$ and $\theta=11^0$ i.e. in the direction of the jammers. Though the array geometry would support a null on each jammer, only one degree of freedom was used. The weights calculated by the algorithm result in a null located between the jammers at $\theta=10.5^0$. The values of $A(\theta)$ at 10^0 and 11^0 are non-zero and nearly equal, due to the symmetry of jammer powers. The transfer functions in Figure 27 are approximated by the first two terms in the Taylor series expansion. The

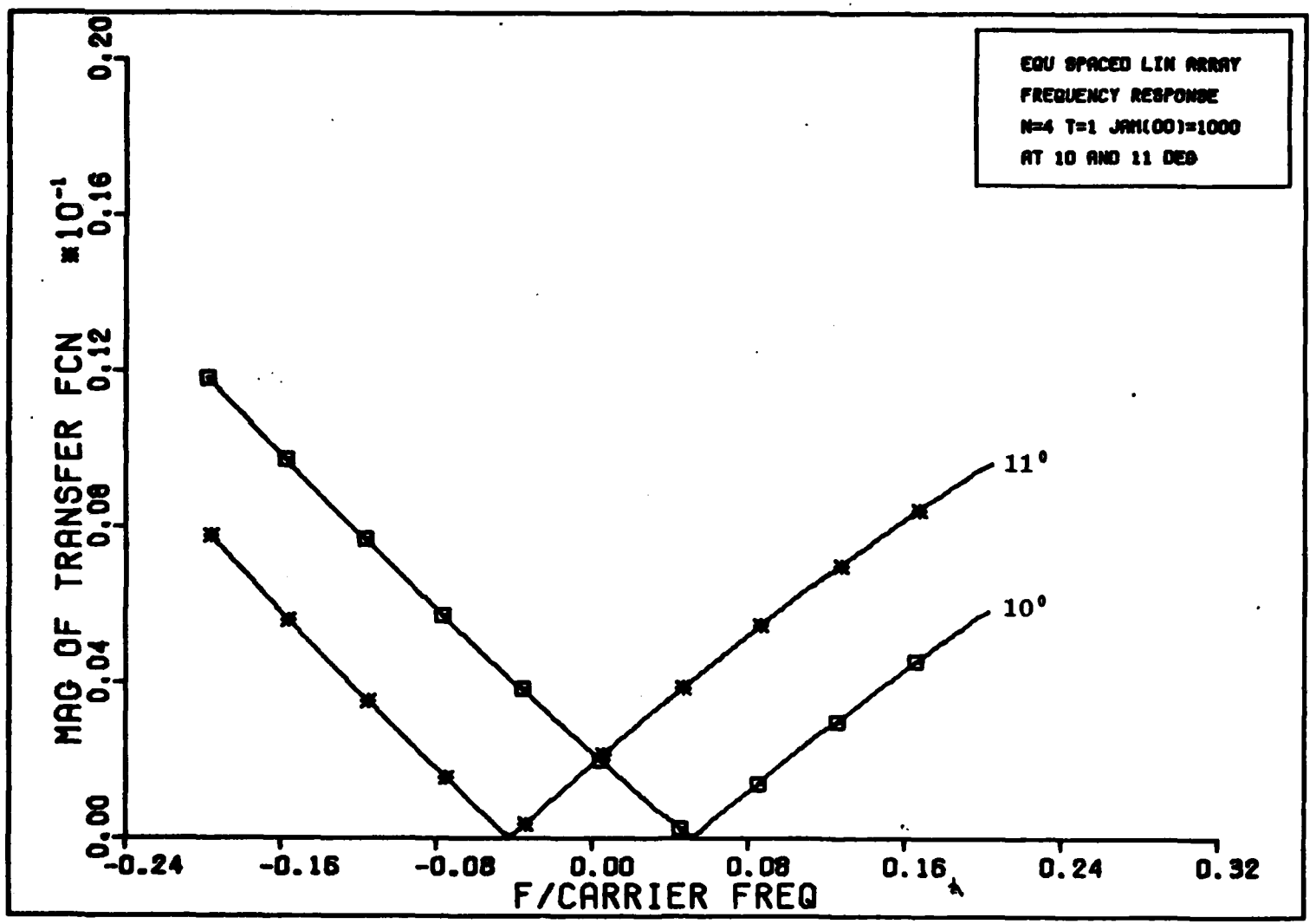

Figure 27. Frequency Response

single nulls shown on each side of the carrier frequency occur due to the 180^0 phase shift in $A(\theta)$ at 10.5 . The null frequencies are defined by the points at which the magnitude of the first and second Taylor series terms are equal. That is

$$\left.\frac{A(\theta)}{2\pi f_0 B(\theta)}\right|_{\theta=10^0,11^0} = \frac{f}{f_0} \qquad (94)$$

Evaluating this equation for the coefficient values at $\theta=10^0$ and 11^0 produces null frequency ratios of .0492 and -.0452 respectively. Figure 27 verifies this calculation.

The second case investigated is defined by two jammers of equal power located 50 degrees apart. Figure 28 contains the frequency response curves for $\theta=10^0$ and 60^0 which is where the jammers are located. The adapted weights result in a spatial null being produced in the direction of each jammer. In general, an N element array has N-1 degrees of freedom and can produce N-1 nulls over its field of view (Ref 12:5). The four element array used in this research will support three nulls in the antenna pattern.

Figure 29 contains the response curves for the third multiple jammer scenario. Three equal power jammers are placed at $\theta=10^0$, 35^0 , and 60^0 . Note that a null has been placed on each jammer. The response curve in direction $\theta=60^0$ reveals a second order frequency dependence, as discussed for the scenarios involving jammers at $\theta=50^0$. This

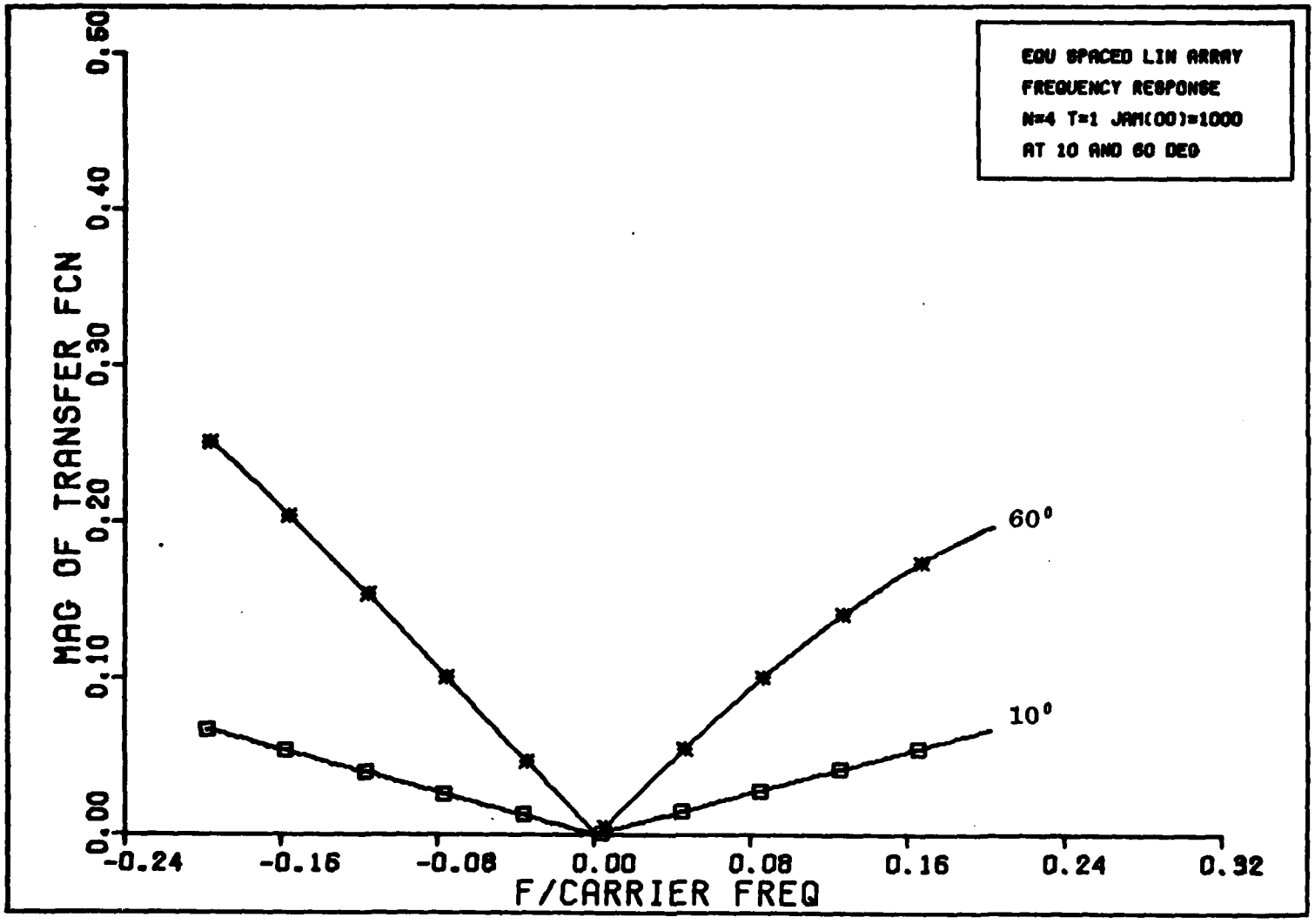

Figure 28. Frequency Response

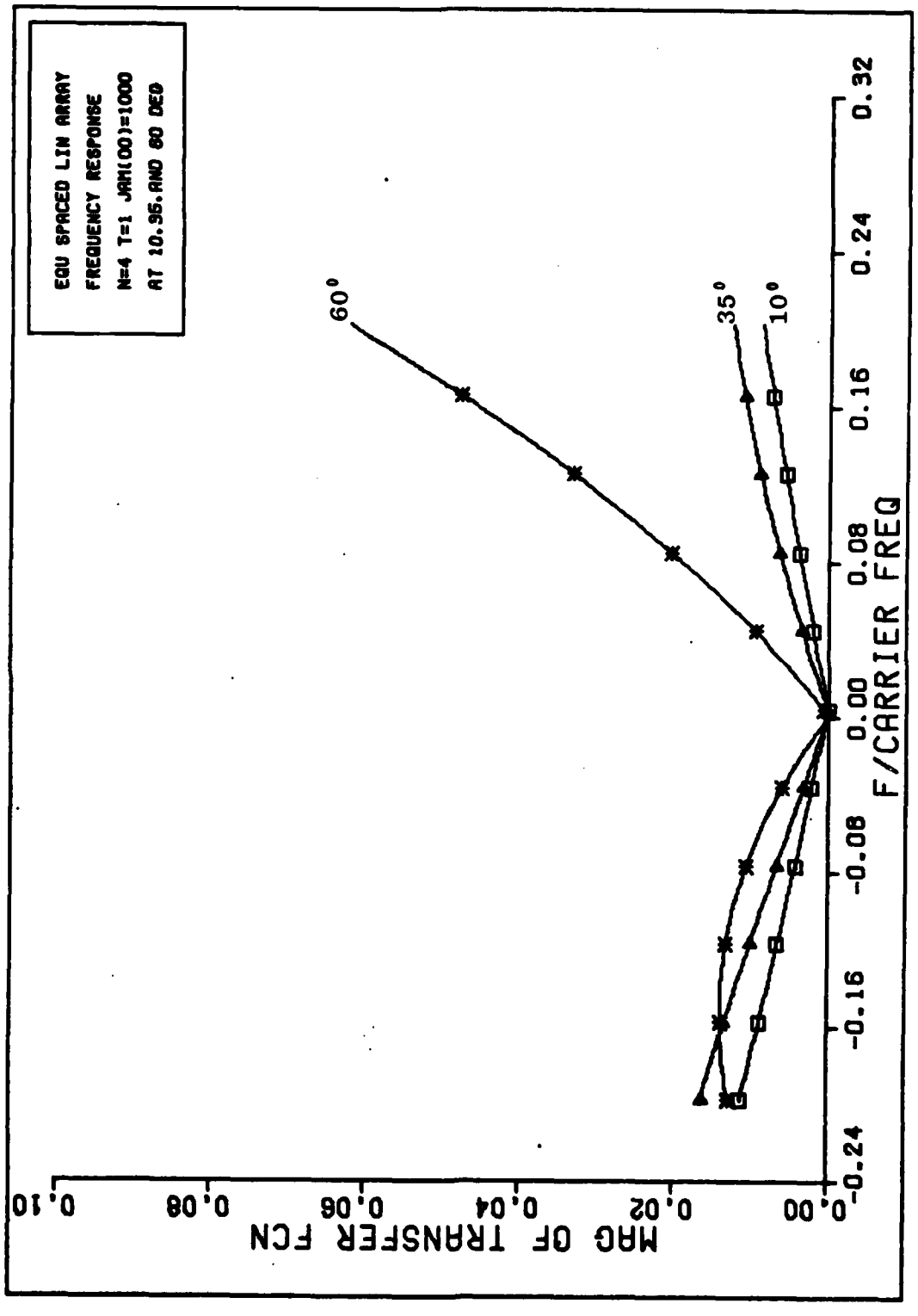

Figure 29. Frequency Response

illustrates the spatial breadth of this distortion. Though not quantified, this persists for $\theta=50^0\pm10^0$ for bandwidths on the order of 30% of f_0 .

If a fourth jammer is added to this scenario, the adaptive algorithm would be overconstrained. There would be more interference sources present than spatial degrees of freedom.

Figure 30 shows the response curves for an overconstrained array. A fourth jammer has been added at $\theta=85^0$. The adapted weights result in no nulls being placed in the direction of the jammers, though the unadapted array pattern null at $\theta=90^0$ tends to null the jammer located at $\theta=85^0$. This figure is for an array geometry including tapped delay lines. As shown in Chapter IV, the transfer function associated with delay lines is independent of spatial parameters. Therefore it is expected that they would not increase the spatial degrees of freedom associated with an array adapted to zero bandwidth jammers. Figure 30 verifies this since one additional degree of freedom would have resulted in a null being placed on each of the four jammers. Therefore delay lines can not be substituted for antenna elements to relieve the problem of an overconstrained array (Ref 12:14).

In summary, adding multiple narrowband jammers to the noise environment does not effect the distortion results.

B. Linear Array Adapted to Broadband Jammer

The transfer function of an array adapted to a broadband jammer is investigated in this section. The single broadband

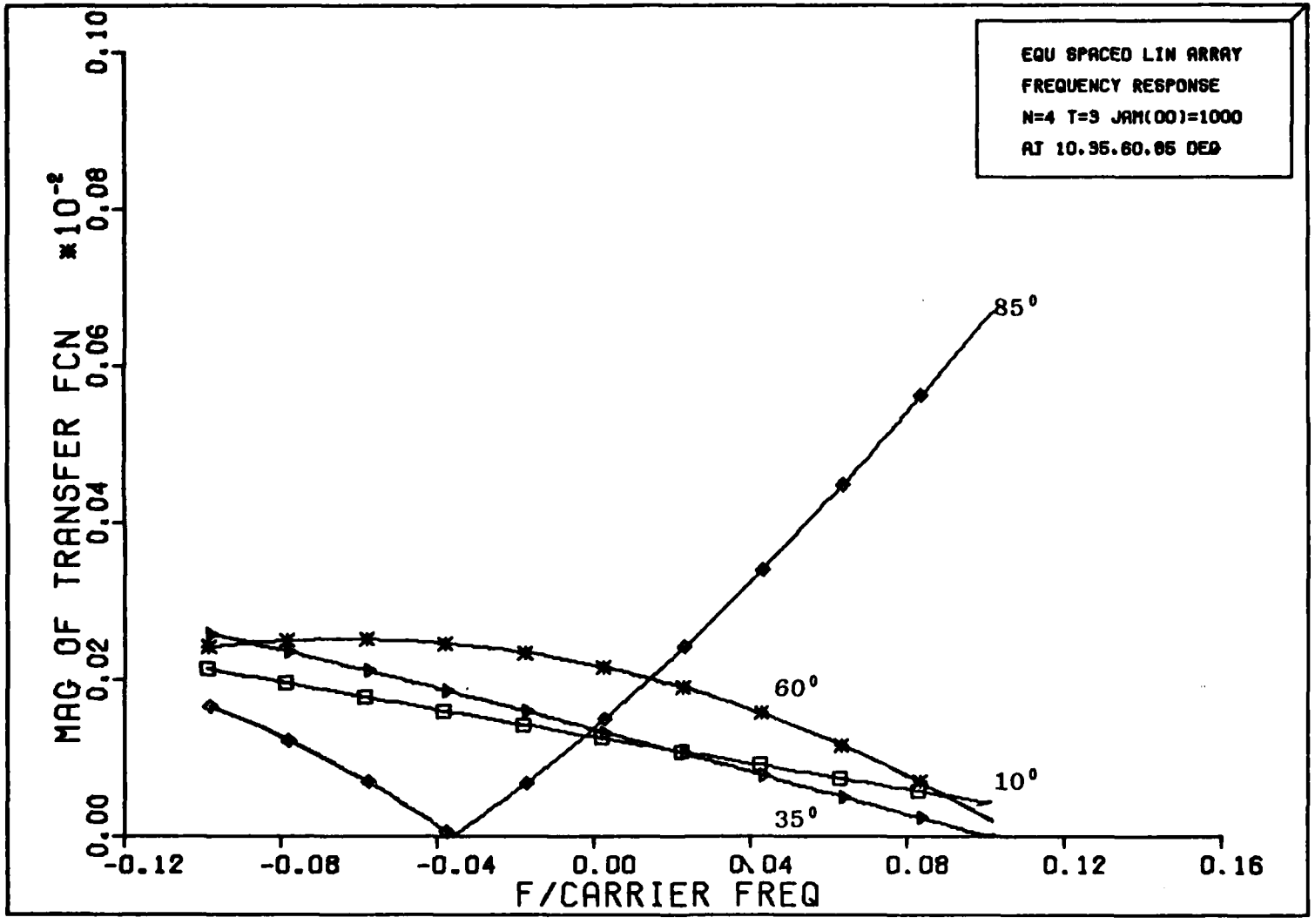

Figure 30. Frequency Response

jammers is represented as a sum of narrowband jammers each at a different frequency, but all at the same spatial location. Four scenarios are used to investigate the impact of delay lines and jammer bandwidth on the array's frequency response. The associated phase responses can be found in Appendix B. All scenarios use a jammer with a bandwidth which is 4% f_0 . The total transmitted power is 1000 Watts. This power is divided evenly between five uncorrelated, discrete spectral lines. These lines are spaced at constant frequency increments centered about f_0 . The factors which differentiate each case are jammer location and the presence, or absence, of tapped delay lines.

1. Frequency Response for a Jammer at $\theta=10^0$. Figure 31 is the frequency response for the adapted array without tapped delay lines. To evaluate the depth of the null, we define $f/f_0=\pm.02$ as the endpoints of the bandwidth of interest, since the jammer has this same bandwidth. At these points, the array without delay lines has a response which is down 23.0db relative to a normalized peak amplitude of 0db.

Figure 32 contains the response associated with an adapted array with delay lines. The null depth for the bandwidth of interest is 29.2db. The addition of delay lines leads to an increase of 6.2db in null depth. The result drawn from this comparison is that the addition of delay lines to an array improves the null bandwidth in the direction of a broadband jammer.

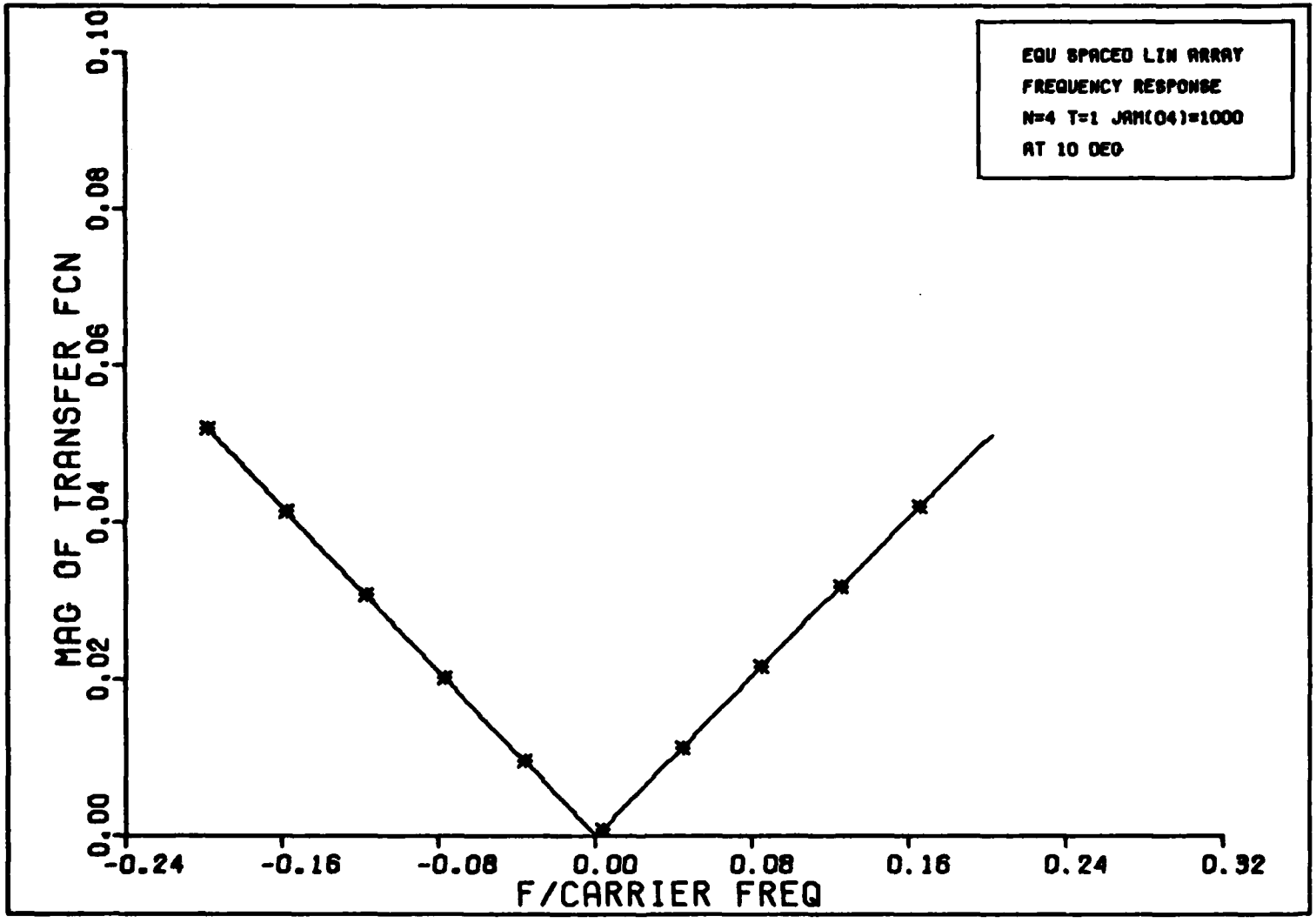

Figure 31. Frequency Response

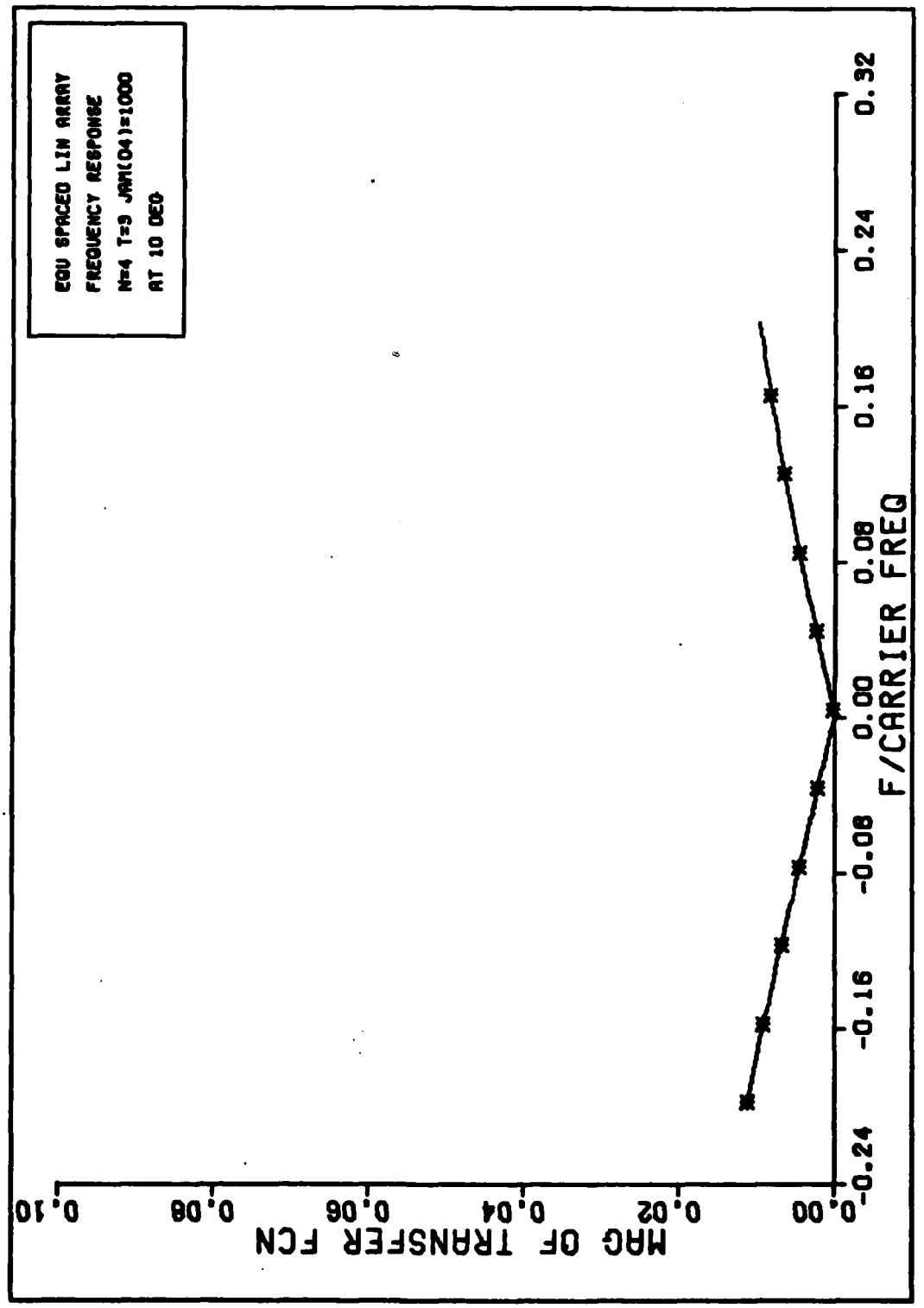

Figure 32. Frequency Response

Table V lists the Taylor series coefficients associated with Figures 31 and 32. The slope of the response curves is determined by $2\pi B(\theta)$. Looking at Table V, the values for $B(\theta)$ do decrease, consistent with Figures 31 and 32. The adapted array with delay lines has the smallest value for $B(\theta)$. This is consistent with the broader nuller seen in the response curve for that array. For this broadband case, the first two Taylor series expansion terms are necessary to approximate $|H(f,\theta)|$. This was verified using the values in Table V.

2. Frequency Response for a Jammer at $\theta=50^0$. Figures 33 and 34 show the frequency responses of an array without and with tapped delay lines for a broadband jammer located at $\theta=50^0$. For endpoints still defined by the bandwidth of the jammer, the improvement in null depth is 2.5db. This can be verified by comparing Figures 35 and 36 which are an expanded view of the response curves for the same cases as above. The figures also show the improvement in frequency response symmetry about f_0 as delay lines are added. This change is reflected in the Taylor series coefficient associated with first order frequency coefficient, $B(\theta)$. Table VI contains the coefficient values for these two cases. These scenarios support the observation that the first three terms in the Taylor series are necessary to approximate $H(f,\theta)$. It can be expected from looking at Figure 34 and Table VI that as an arrays frequency response becomes more symmetrical about f_0

Table V. Taylor Series Coefficients for Broadband Jammer at 10^0

N,T	Normalized Amplitudes and Phase at 10^0		
	A(θ)	B(θ)	C(θ)
4,1	2.016×10^{-4} 0^0	1.175×10^{-10} 90^0	4.293×10^{-21} 180^0
4,3	6.450×10^{-5} 0^0	2.614×10^{-11} 90^0	4.253×10^{-21} 180^0

Thermal Noise Power = 1 Watt

Jammer Bandwidth = 4% f_0

Jammer Power = 1000 Watts

$d = \lambda_0/2$

$\Delta = \lambda_0/4$

Table VI. Taylor Series Coefficients for Broadband Jammer at 50^0

N,T	Normalized Amplitude and Phase at 50^0		
	A(θ)	B(θ)	C(θ)
4,1	4.288×10^{-4} 180^0	1.712×10^{-11} -90^0	3.748×10^{-19} 180^0
4,3	3.822×10^{-4} 180^0	5.328×10^{-12} -90^0	3.727×10^{-19} -180^0

Thermal Noise Power = 1 Watt

Jammer Bandwidth = 4% f_0

Jammer Power = 1000 Watts

$d = \lambda_0/2 \quad \Delta = \lambda_0/4$

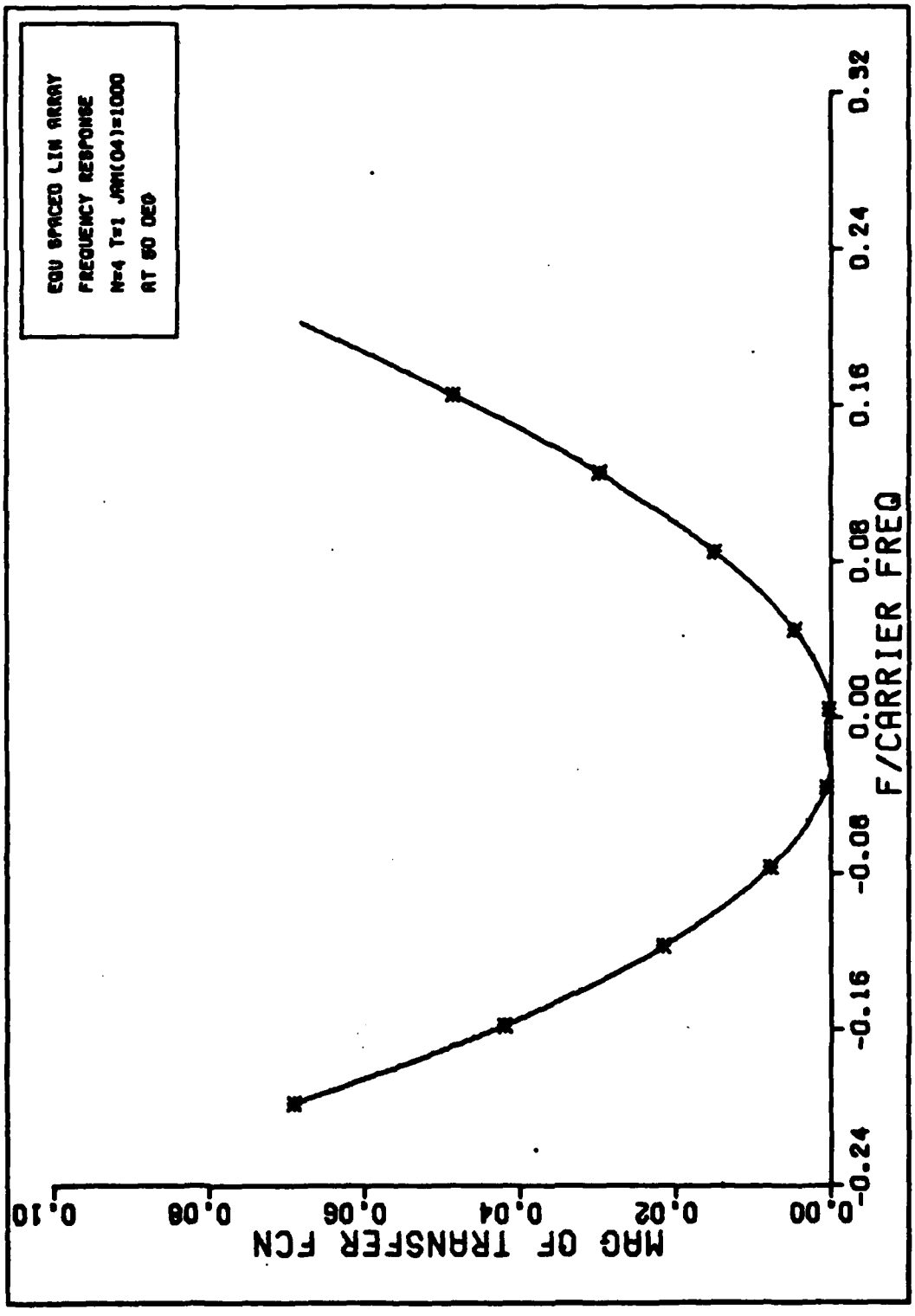

Figure 33. Frequency Response

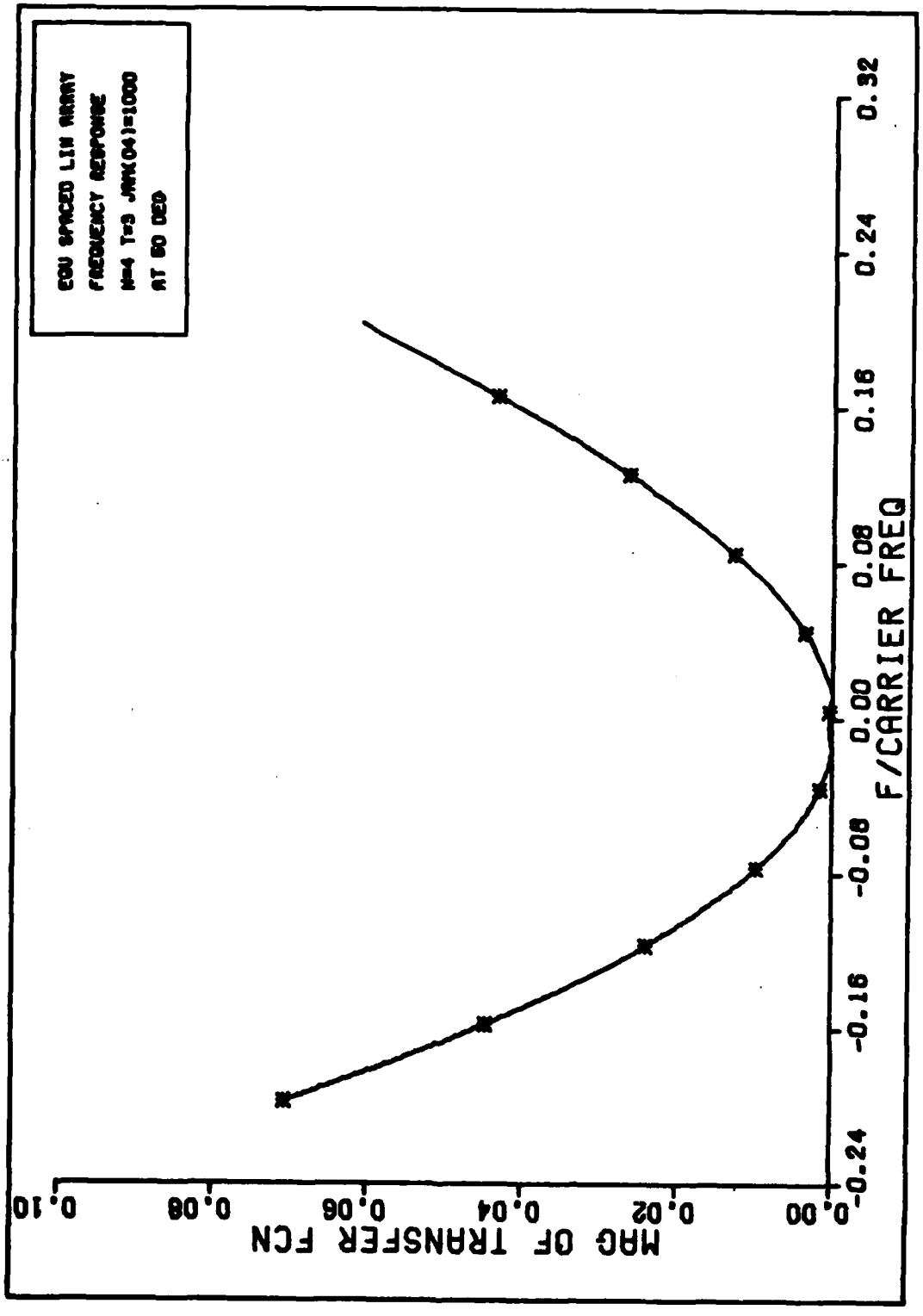

Figure 34. Frequency Response

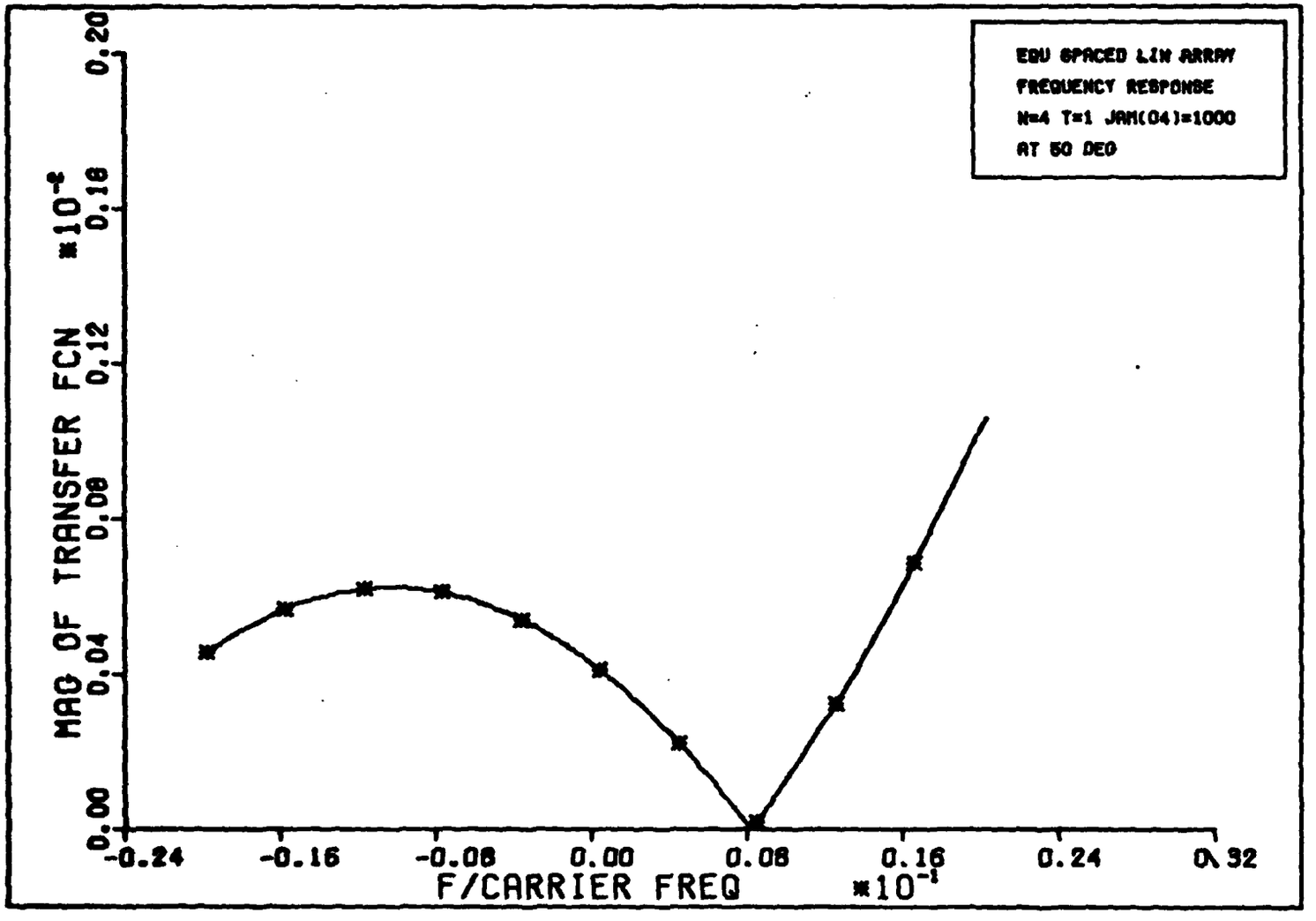

Figure 35. Frequency Response

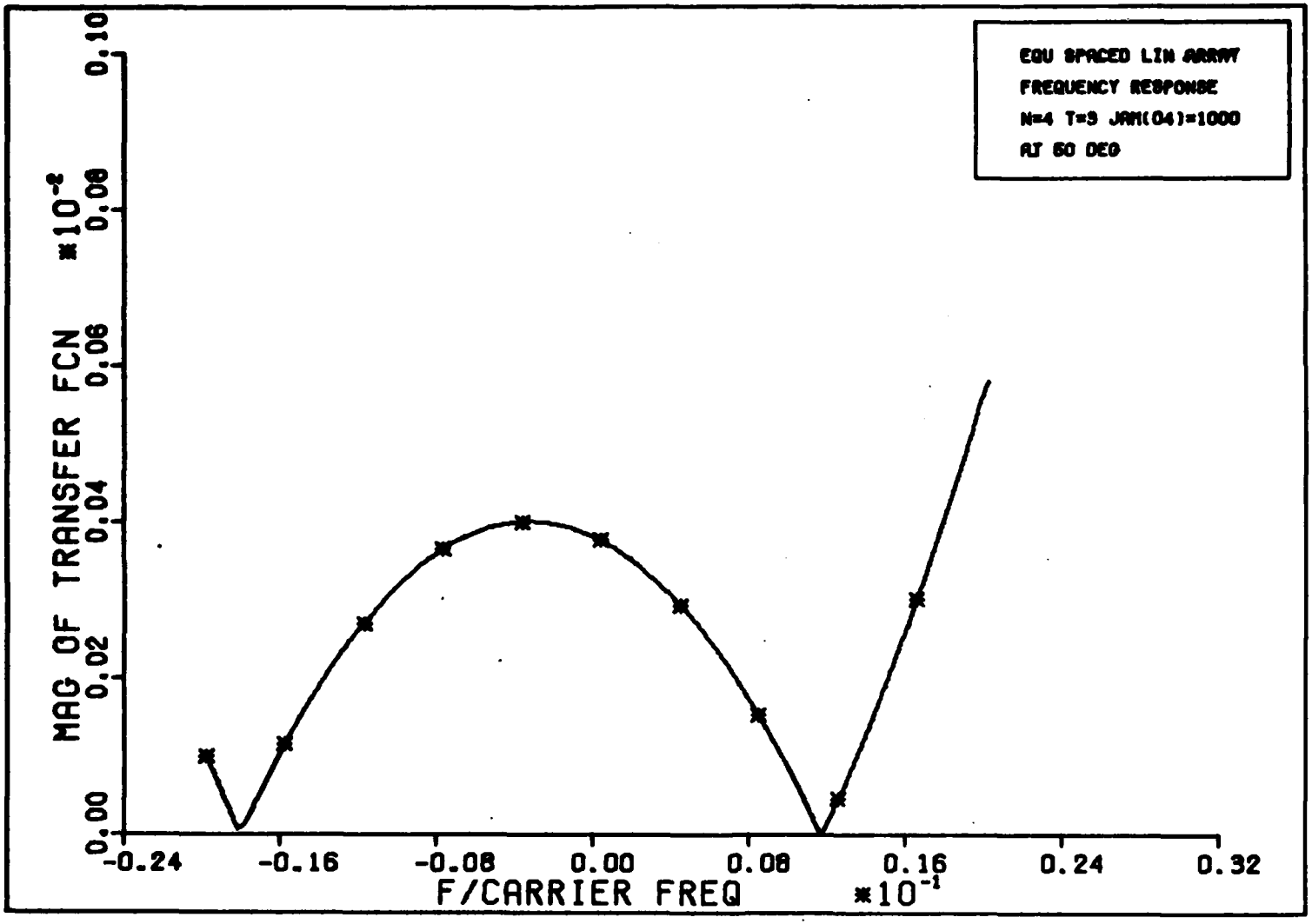

Figure 36. Frequency Response

and its second order frequency dependence dominates the response, the output of the array may contain no distorted signal. This is true for those desired signals whose second time derivative is insignificant, since it is that derivative term which is scaled by $C(\theta)$. The shift towards symmetry for these cases indicates the decreasing magnitude of $B(\theta)$.

It is of interest to know whether the bandwidth of the null could be due to the transfer function of a delay line behind an antenna element. To investigate this, the transfer function of the delay line behind the first element of the array was analyzed. The particular array used was the one associated with Figure 36. The weights for the three ports of element one are listed in Table VII. The associated transfer function is calculated for several frequency values in Table VIII. The transfer function for the delay line is defined by Eq.(16) using $N=1$. It can be concluded from the frequency response data points in the second column of Table VIII that the null breadth is not due to the delay line alone. This is expected since this response is independent of spatial location of the signal of interest.

In the course of this research, results were compared to other reference works to verify the validity of the computer program used to produce frequency response curves. Results from adapted array geometries without delay lines were checked versus Gabriel and verified as correct (Ref 6). Results from

Table VII. Weights for Broadband Jammer at 50°

Weight	Modulus	Phase (Degrees)
$w_{1,1}$	.69456	90.27
$w_{1,2}$	.71794	-2.64
$w_{1,3}$	.74195	-95.42

Thermal Noise Power = 1 Watt

Jammer Bandwidth = 4% f_0

Jammer Power = 1000 Watts

N=4 T=3 $d=\lambda_0/2$ $\Delta=\lambda_0/4$

Table VIII. Transfer Function of Delay Line for Broadband Jammer at 50°

f/f_0	Normalized Modulus	Phase (Degrees)
-.05	0.179	-68.3
-.04	0.178	-68.9
-.03	0.179	-69.6
-.02	0.179	-70.3
-.01	0.179	-70.9
0.00	0.179	-71.6
0.01	0.179	-72.3
0.02	0.180	-72.9
0.03	0.180	-73.6
0.04	0.180	-74.3
0.05	0.179	-75.0

Thermal Noise Power = 1 Watt

Jammer Bandwidth = 4% f_0

Jammer Power = 1000 Watts

N=1 T=3 $d=\lambda_0/2$ $\Delta=\lambda_0/4$

adapted array geometries with delay lines, i.e. with frequency dependent weights, were checked versus Compton and discrepancies found (Ref 2). The null depths resulting from his research could not be duplicated. To illustrate the differences, Figure 37 should be compared to Compton's Figure 22 (Ref 2:34). Both scenarios involve a two element linear array with three tap delay-lines. The adapted weights are in response to a jammer at $\theta=50^0$ with 4% f_0 bandwidth. Compton's response curve has endpoints, at $f/f_0=\pm.02$, which are down 43db versus Figure 37 which is down 22db. His null at $f/f_0=0$ is down 73db versus Figure 37 which is down 42 db. Two areas were investigated to explain these discrepancies. First, the adapted weights associated with jammers having non-zero bandwidth were compared to weights resulting from jammers into zero bandwidth. Second, the covariance matrices were compared.

Table IX contains the weights associated with an array adapted to a zero bandwidth jammer. Only the weights of element one are listed here . It should be noted that the weights have phases which are 90^0 apart. This is consistent with the delay line spacing of $\lambda_0/4$. Comparing this to Table VII, it is apparent that the weights associated with a 4% f_0 bandwidth jammer are dependent on the jammer bandwidth. They are not 90^0 apart as above. The conclusion is that the adaptive algorithm implemented for this research does produce weights which are dependent on jammer bandwidth. Since numerical date, such as

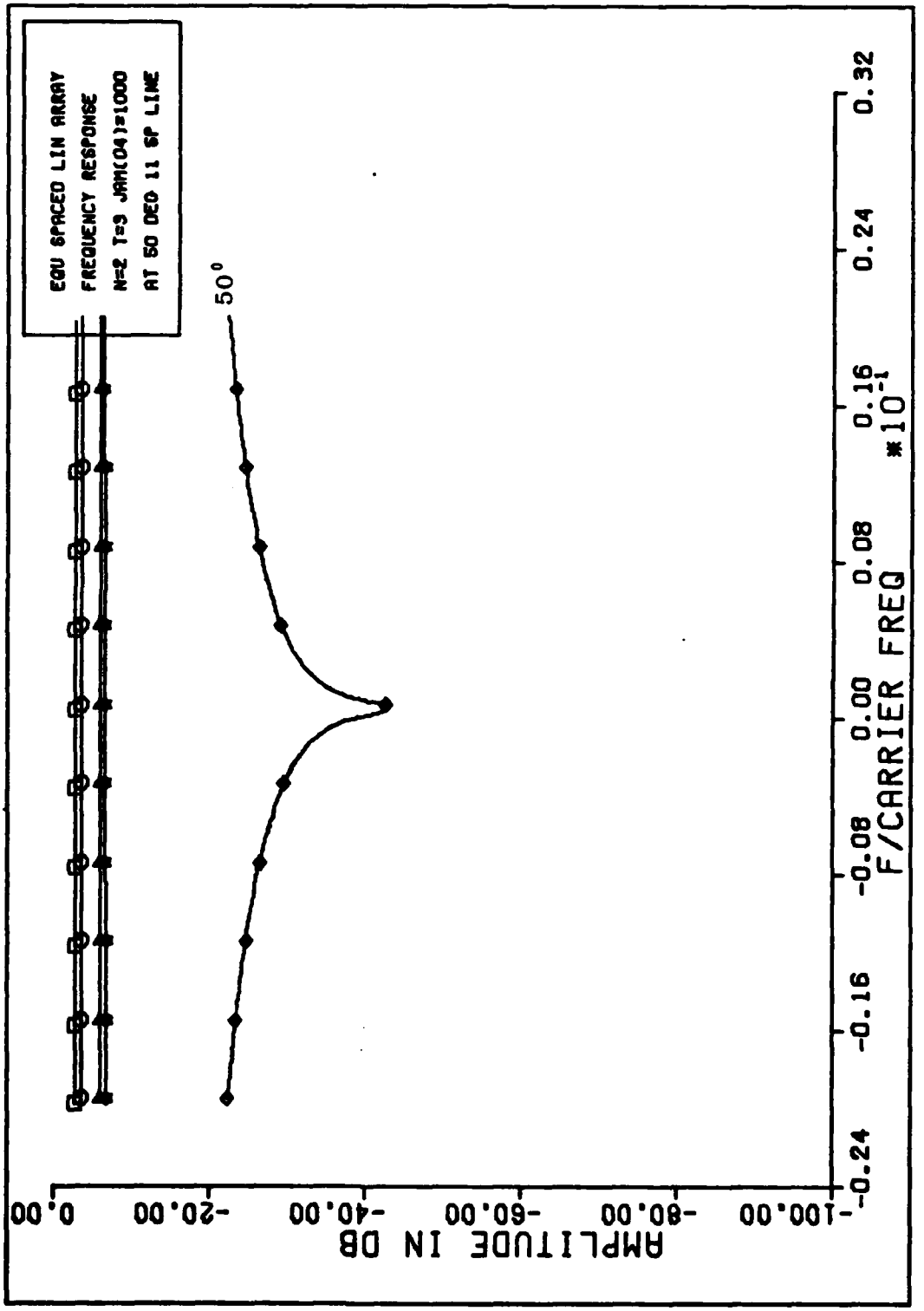

Figure 37. Frequency Response

Table IX. Weights for Narrowband Jammer at 50^0

Weight	Modulus	Phase (Degrees)
$W_{1,1}$	.772	81.03
$W_{1,2}$	.772	-8.97
$W_{1,3}$	.772	-98.97

Thermal Noise Power = 1 Watt

Jammer Bandwidth = 0% f_0

Jammer Power = 1000 Watts

N=4 T=3 $d=\lambda_0/2$ $\Delta=\lambda_0/4$

values of the weights, are not presented in Compton's work, the weights associated with Figure 37 can not be quantitatively compared to see if a difference exists. However, it can be assumed from the response curves that this is true. The important point is that the computer program used here produces correct results based on the covariance matrix used here. The discrepancy in results can be attributed to that matrix.

The program used here calculates a covariance matrix defined by Eqs.(44) and (47). From these equations it should be noted that the information used in this matrix comes only from the interference and thermal noise sources. Compton makes use of the desired signal's correlation function in addition to the above. The point to be made is that the a priori knowledge of the desired signal is exploited more fully in Compton's research than in the research presented here. The only a priori knowledge of the desired signal

assumed here is its location, which is used to determine the quiescent weights in Eq.(78). It is this difference which is assumed to produce different adapted weights and therefore different frequency response curves.

In this chapter several array transfer functions were analyzed. The array weighting coefficients were determined by an algorithm using given noise information. The conclusion to be drawn is that, for some locations within an adapted array's field of view, the associated transfer function requires the first three Taylor series terms to be adequately represented. Also, the presence of tapped delay-lines does not significantly improve the array's performance for scenarios involving zero bandwidth jammers. They do improve performance when non-zero bandwidth jammers are involved. For the particular cases investigated here, the improvement was 6.2db and 2.5db for a jammer located at 10^0 and 50^0 respectively.

VI Conclusions and Recommendations

This thesis has investigated the effects of adaptive antenna arrays with tapped delay-lines on wideband signals. The array was analyzed as a filter and its transfer function derived. The properties of the output waveform were determined by expanding the transfer function in a Taylor series. The conclusions drawn from Chapter II follow.

(1) The output of an array contains an infinite sum of components consisting of the input signal and all the n^{th} order time derivatives of the signal.

(2) Each component is weighted by a complex number (Taylor series coefficient) that adjusts its phase and amplitude before the components are added together.

In Chapter III we looked at the optimum weights to produce maximum signal power and minimum noise power at the array output. The emphasis was on the adaption algorithm and the noise covariance matrix in particular. The conclusion follows.

(3) For purposes of adapting the array weights, a broadband noise source can be modelled very well by a group of narrowband noise sources of appropriate power and frequency.

In Chapter IV we investigated the transfer functions for arrays using phase steering of the main beam. The beam was steered broadside and the frequency and phase response analyzed for various signal arrival angles.

(4) The signal term dominates the output except in the vicinity of nulls, where the first Taylor series coefficient vanishes. Then the first derivative term becomes the main output of the array.

(5) The addition of tapped delay-lines to phase steered arrays does not change their frequency response for moderately wideband signals (f/f_0=10%) .

In Chapter V we analyzed the transfer functions of arrays adapted to reduce interference from narrowband then broadband jammers. The conclusions follow.

(6) For both phase steered and adapted linear arrays the signal and its derivative are separated in phase by 90^0.

(7) One jammer location resulted in the frequency response having a strong second order variation with frequency. Therefore, three, rather than two, Taylor series terms were required to represent this response accurately. However, for the modulation techniques reviewed in Craddock's work, none had a second derivative term of sufficient magnitude to be present at the output (Ref 3). Therefore, for all cases investigated the array output consists of the signal and its first time derivative only.

(8) Increasing jammer bandwidth reduced the Taylor series coefficient associated with a first derivative signal at the array output (assuming an array with tapped delay-lines). This results in broader nulls and less first derivative signal distortion.

(9) The addition of tapped delay-lines improves array performance when the noise environment contains broadband jammers. For the particular array geometry and noise environment investigated, the improvement in null depth, for the 4% f_0 bandwidth of the jammer, was 6.2db with a noise source at 10^0 and 2.5db with a noise source at 50^0.

(10) The addition of tapped-delay lines does not increase the spatial degrees of freedom which an array has.

(11) The inverse relationship between the first and second Taylor series coefficients ($A(\theta)$ and $B(\theta)$) does not hold true in general. A null produced in the direction of a jammer does not lead to a corresponding peak in $B(\theta)$.

The analysis performed in this thesis indicates areas whether farther research is warranted. The following are recommended.

(1) The results of this research are based on broadside steering of the array's main beam. In Chapter IV, the transfer function of an array is shown to be dependent upon steering angle (see Eq.(86)). Research should be done to verify whether these results are valid for any choice of steering angle.

(2) The signal distortion derived here is based on a steady state analysis. Research should be done to analyze the transient response of the array. Particular emphasis should be placed on how various transient conditions alter the desired signal at the array's output.

(3) The results presented here could be analyzed from an adversary role. It is apparent that jamming signals with high power in the derivative term would be difficult to null. Research could be done to identify signals whose correlation function has a first derivative signal with particularly high power.

(4) A quantitative analysis should be done to investigate further the discrepancy identified between results presented here and Compton's work.

Bibliography

1. Compton, Jr., R.T. "An Adaptive Array in a Spread-Spectrum Communication System," Proceedings of the IEEE,Vol. 66,No.3:289-298 (March 1978).

2. Compton, Jr., R.T. and W.E. Rodgers. Adaptive Array Bandwidth with Tapped Delay-Line Processing. Report 3832-3, The Ohio State University ElectroScience Laboratory, Department of Electrical Engineering; prepared under Contract N00019-74-C-0141 for Naval Air Systems Command, May 1975. (AD 015 098).

3. Craddock, Joseph L. "Analysis of Modern Digital Modulation Techniques." MS Thesis, Wright-Patterson AFB, Ohio: Air Force Institute of Technology, December 1978. (AD A064363).

4. Davenport, Jr., W.B. and W.L. Root. An Introduction to the Theory of Random Signals and Noise. New York: McGraw-Hill Book Company, 1958.

5. Dixon, R.C. Spread Spectrum Systems. New York: John Wiley and Sons, Inc., 1976.

6. Gabriel, William F. "Adaptive Arrays-An Introduction," Proceedings of the IEEE, Vol.64,No.2:239-272(February 1976).

7. Gagliardi, Robert M., and Karp, Sherman. Optical Communications. New York: John Wiley and Sons, Inc., 1976.

8. Hendrickson, Richard L. "Adaptive Array Antenna Technology," Technical Report MTR-5270. McLean, Va.: The MITRE Corporation, August 1976 (ADB017908)

9. Jordan, Edward C., and Balmain, Keith G. Electromagnetic Waves and Radiating Systems. New Jersey: Prentice-Hall, Inc., 1968.

10. Papoulis, A. Probability, Random Variables, and Stochastic Processes. New York: McGraw-Hill Book Company, 1965.

11. Raska, Jr., Edward "Effects of Antenna Arrays on Broadband Signals". MS Thesis. Wright-Patterson AFB, Ohio: Air Force Institute of Technology, September 1978. (AD A064679).

12. Ricardi, L.J. "A Summary of Methods for Producing Nulls in an Antenna Radiation Pattern," Technical Note 1976-38. Lexington, Mass. Lincoln Laboratory, 2 Sept76(ADA032340).

13. Schwartz, M., et al. Communication Systems and Techniques. New York: McGraw-Hill, Inc, 1966.

14. Steinberg, Bernard D. Principles of Aperture and Array System Design: Including Random and Adaptive Arrays. New York: John Wiley and Sons, Inc., 1976.

15. Thourel, L. The Antenna. New York: John Wiley and Sons, Inc., 1960.

16. Van Trees, Harry L. Detection, Estimation, and Modulation Theory, Part I. New York: John Wiley and Sons, Inc., 1968.

17. Widrow, B., et al. "Adaptive Antenna Systems," Proceedings of the IEEE, Vol.55,No.12:2143-2159 (December 1967).

Appendix A: Perturbation Analysis

It is generally accepted that there exists a duality between the frequency domain and spatial domain in the vicinity of an antenna pattern null. In the course of the research for this paper, this relationship often appeared when graphically looking at frequency response $|H(f,\theta)|$ versus frequency deviation f and antenna pattern $|A(\theta)|$ versus angle θ. To analytically investigate this duality relationship, two perturbation analyses were done. The first was done in the spatial domain by varying angular deviation $\partial\theta$ about null angle θ_N given that $f=0$. The second was done in the frequency domain by perturbing frequency deviation f about center frequency f_0 given that $\partial\theta=0$.

This analysis is done for an equally spaced linear array without tapped delay lines. From Eq.(88) the amplitude response of the transfer function for this case is given by

$$|H_E(f,\theta)| = \left| \frac{\sin N[\pi(f_0+f)\frac{d}{c}\sin\theta]}{\sin [\pi(f_0+f)\frac{d}{c}\sin\theta]} \right| \qquad \text{(A-1)}$$

Written more explicitly, in light of the variables to be perturbed, this can be written as

$$|H_E(f_0+f,\theta_N+\partial\theta)| = \left| \frac{\sin N[\pi(f_0+f)\frac{d}{c}\sin(\theta_N+\partial\theta)]}{\sin [(f_0+f)\frac{d}{c}\sin(\theta_N+\partial\theta)]} \right| \qquad \text{(A-2)}$$

Null angle θ_N is defined at center frequency. Using Eq.(A-2),

the null angles are given by

$$\theta_N = \sin^{-1}\left(\frac{i}{Nf_0 d/c}\right) , \quad i=1,2,\ldots,N-1 \qquad \text{(A-3)}$$

The analysis which follows is done assuming θ_N is defined as the first null angle (i.e. i=1). This choice does not effect the qualitative results.

First, performing the analysis in the spatial domain given f=0 and using small angle trigonometric approximations we have

$$|H_E(f_0,\theta_N+\partial\theta)| = \left|\frac{\sin N[\pi f_0 \frac{d}{c}\sin(\theta_N+\partial\theta)]}{\sin[\pi f_0 \frac{d}{c}\sin(\theta_N+\partial\theta)]}\right|$$

$$= \left|\frac{\sin N[\pi f_0 \frac{d}{c}(\sin\theta_N\cos\partial\theta+\cos\theta_N\sin\partial\theta)]}{\sin[\pi f_0 \frac{d}{c}(\sin\theta_N\cos\partial\theta+\cos\theta_N\sin\partial\theta)]}\right|$$

$$= \left|\frac{\sin N[\pi f_0 \frac{d}{c}(\sin\theta_N+\partial\theta\cos\theta_N)]}{\sin[\pi f_0 \frac{d}{c}(\sin\theta_N+\partial\theta\cos\theta_N)]}\right| \qquad \text{(A-4)}$$

Equation (A-4) is accurate to within 1% for $\partial\theta$ on the order of $\pm 6^0$. Substituting the expression for θ_N given by Eq. (A-3) for the first null angle into Eq.(A-4) yields

$$|H_E(f_0,\theta_N+\partial\theta)| = \left|\frac{\sin\pi(\varepsilon\partial\theta+1)}{\sin\frac{\pi}{N}(\varepsilon\partial\theta+1)}\right| \qquad \text{(A-5)}$$

where

$$\epsilon \triangleq Nf_0\frac{d}{c}\sqrt{1-\left(\frac{1}{Nf_0\frac{d}{c}}\right)^2} \qquad \text{(A-6)}$$

Note the ϵ is a constant whose value is determined by the antenna array geometry. Equation (A-5) is the general form of the solution in the spatial domain.

Performing the analysis in the frequency domain given $\partial\theta=0$ and the same value for θ_N leads to

$$|H_E(f+f_0,\theta_N)| = \left|\frac{\sin N[\pi(f+f_0)\frac{d}{c}\sin\theta_N]}{\sin[\pi(f+f_0)\frac{d}{c}\sin\theta_N]}\right|$$

$$= \left|\frac{\sin N\left[\pi(f+f_0)\frac{d}{c}\sin(\sin^{-1}\frac{1}{Nf_0\frac{d}{c}})\right]}{\sin\left[\pi(f+f_0)\frac{d}{c}\sin(\sin^{-1}\frac{1}{Nf_0\frac{d}{c}})\right]}\right|$$

$$= \left|\frac{\sin\pi(\frac{f}{f_0}+1)}{\sin\frac{\pi}{N}(\frac{f}{f_0}+1)}\right| \qquad \text{(A-7)}$$

Equation (A-7) is the general form of the solution in the frequency domain.

Conclusions can be drawn by comparing Eqs (A-5) and (A-7). The antenna pattern defined in Eq.(A-5) and the frequency response defined in Eq.(A-7) have the same generic form. Plotting these functions versus independent variables $\partial\theta$ and f/f_0 respectively will yield identical curves if f/f_0 is scaled by the constant ϵ given in Eq.(A-6). These results are valid in the vicinity of an antenna pattern null ($\partial\theta=\pm6^0$) for any given linear, equally spaced array.

Appendix B: Phase Response Figures

This appendix contains the phase response plots associated with the frequency response figures in Chapter IV, V and Appendix C. As noted in the body of this report, all response curves here show a linear variation with frequency. The abrupt change of phase in these figures is associated with the change in sign of the modulus of the transfer functions.

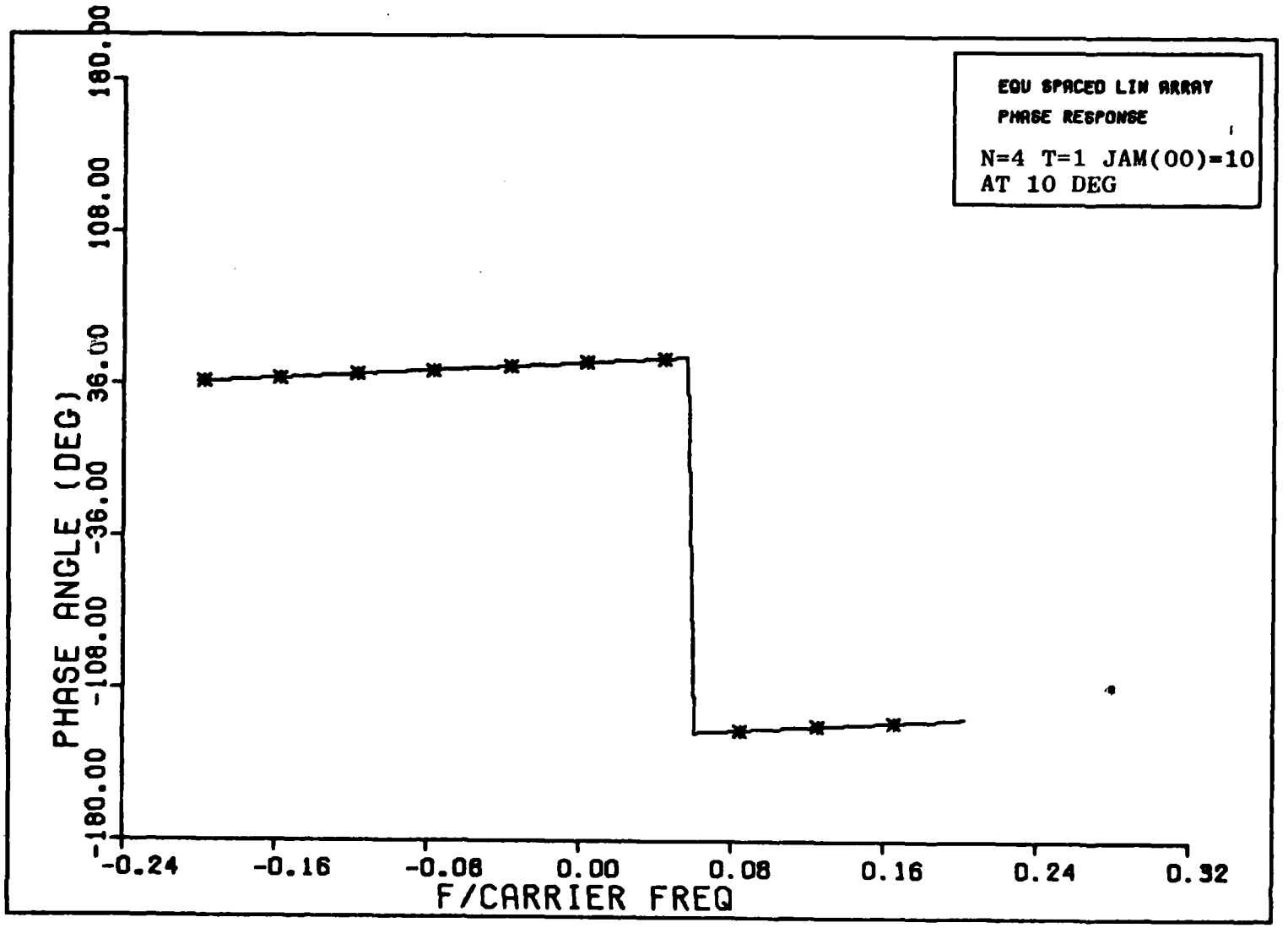

Figure B-1. Phase Response

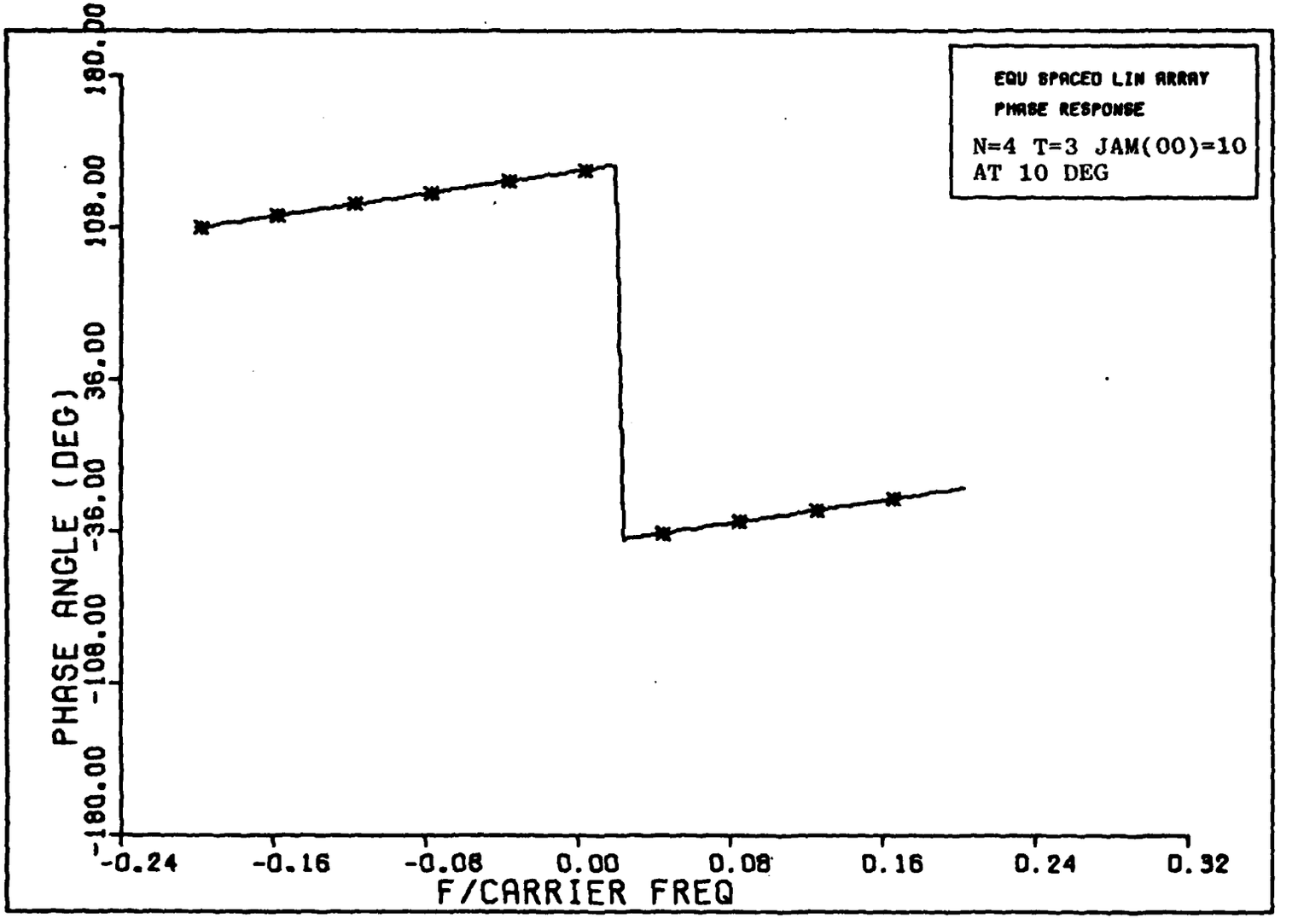

Figure B-2. Phase Response

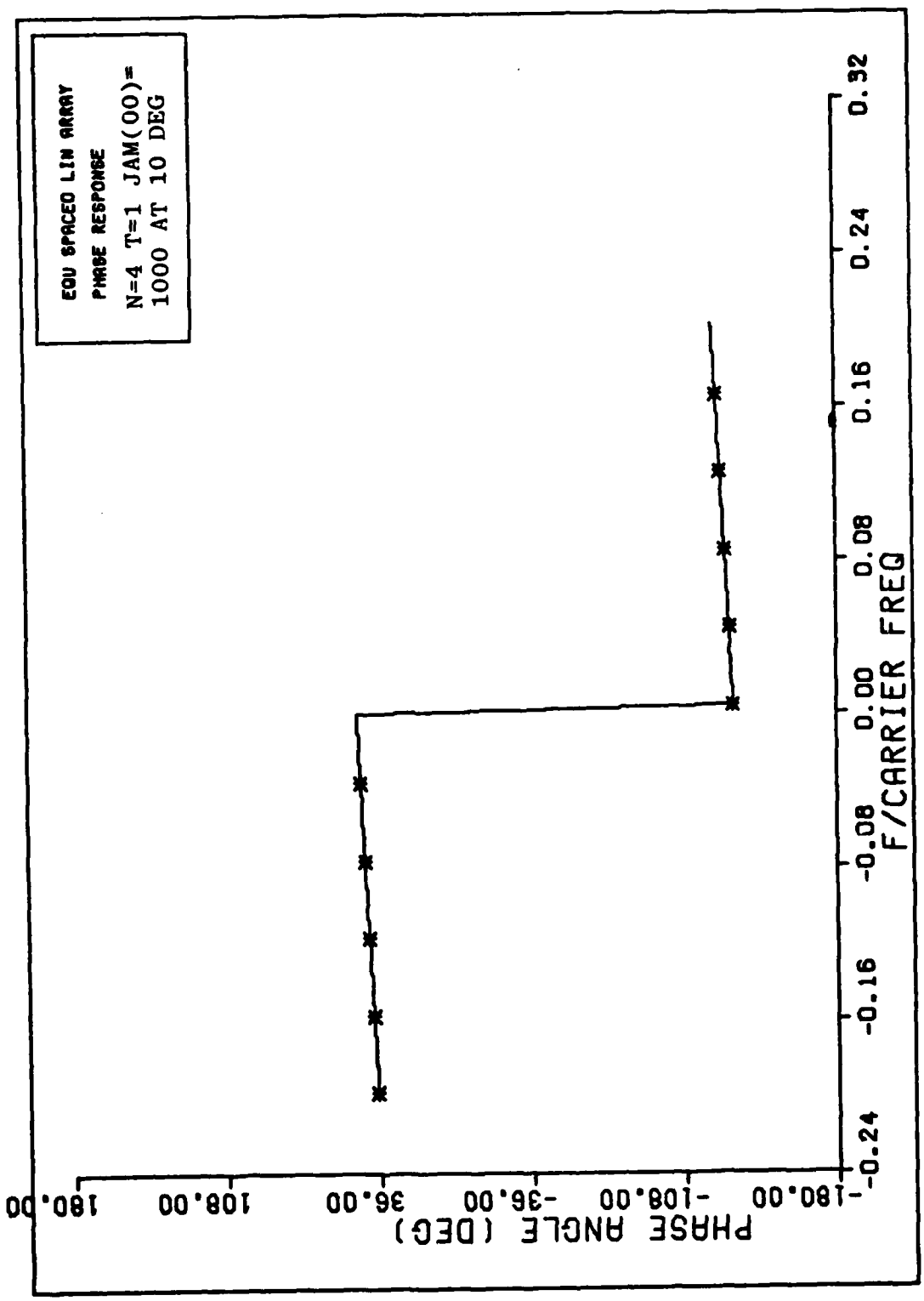

Figure B-3. Phase Response

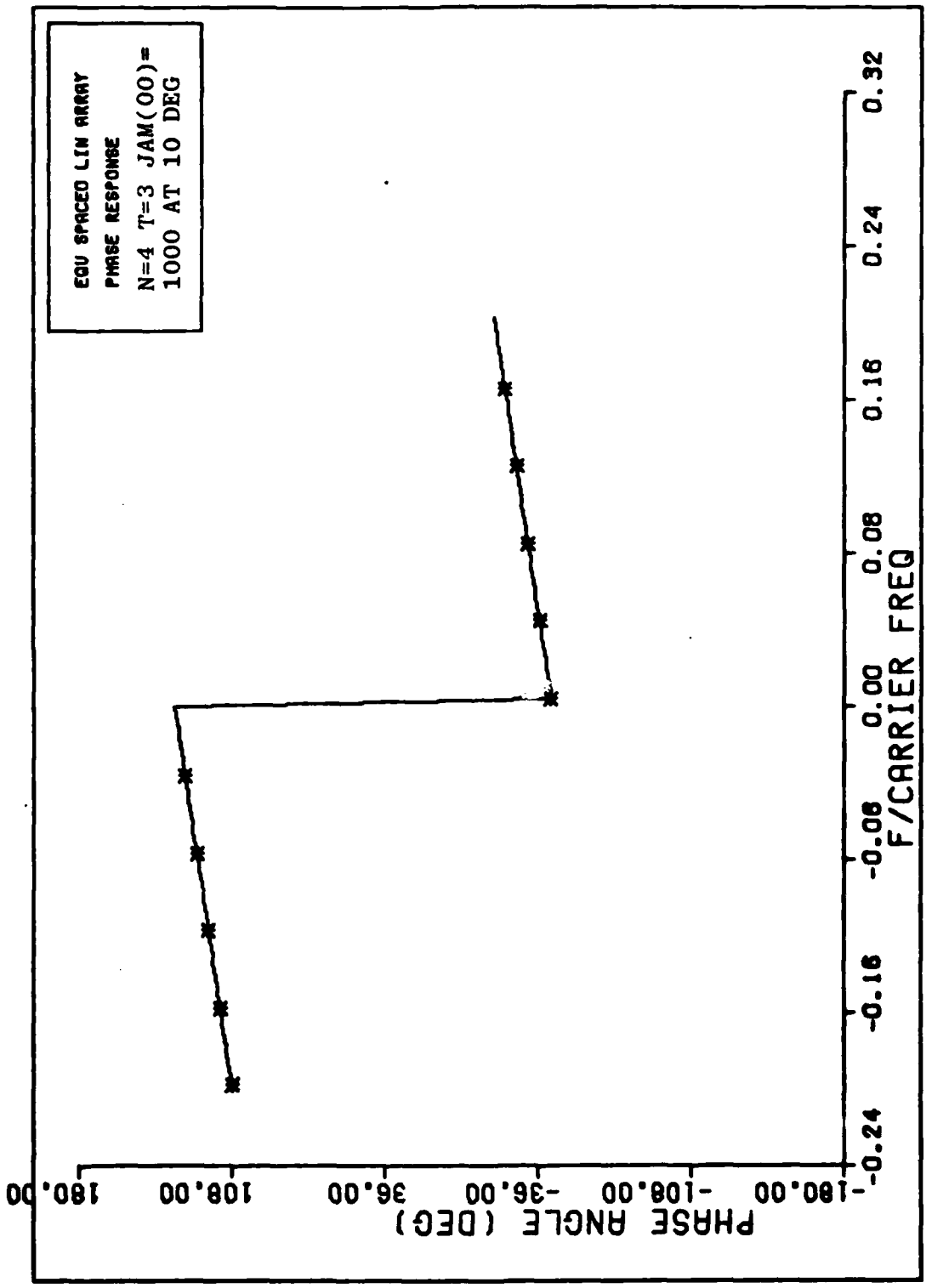

Figure B-4. Phase Response

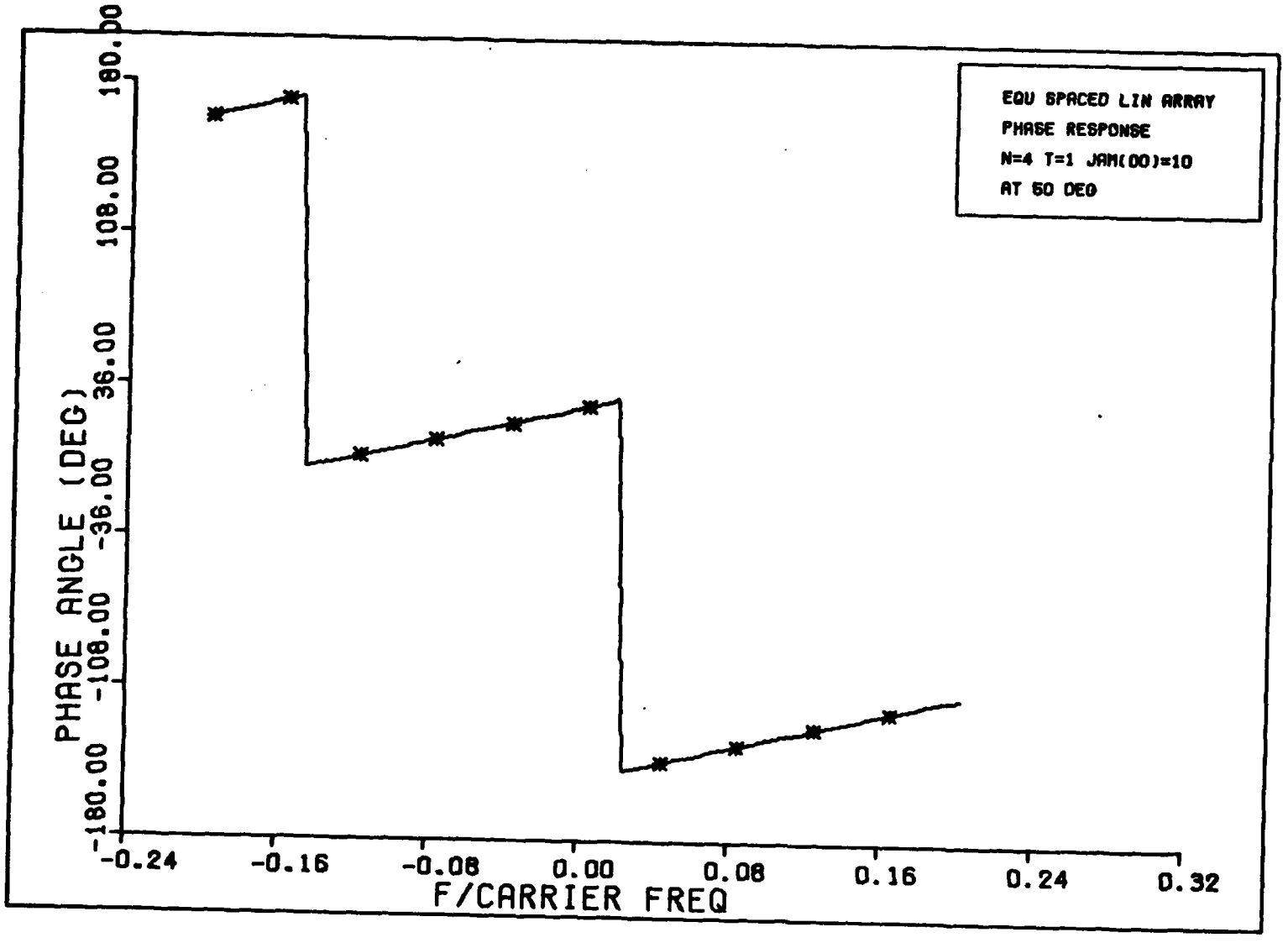

Figure B-5. Phase Response

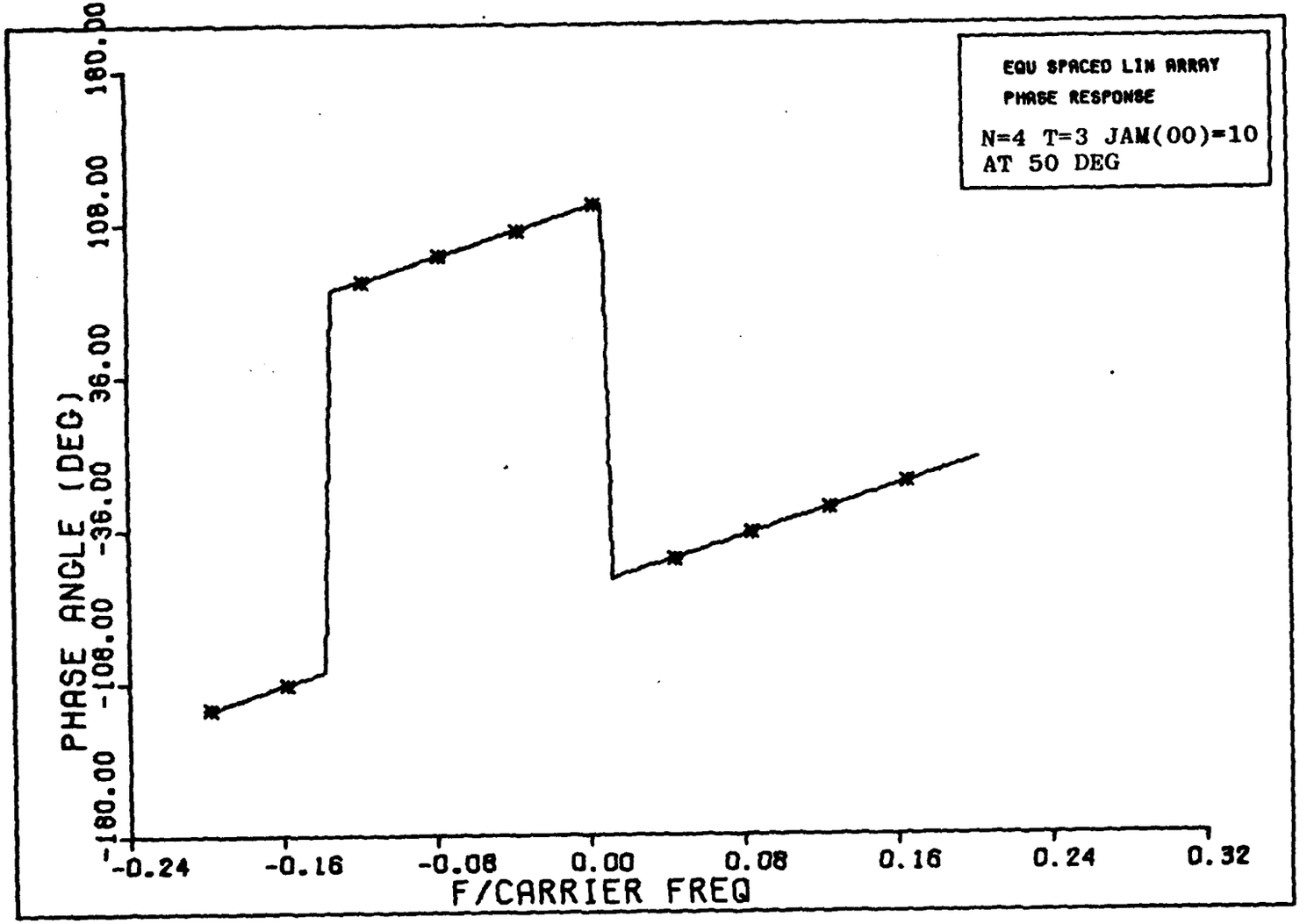

Figure B-6. Phase Response

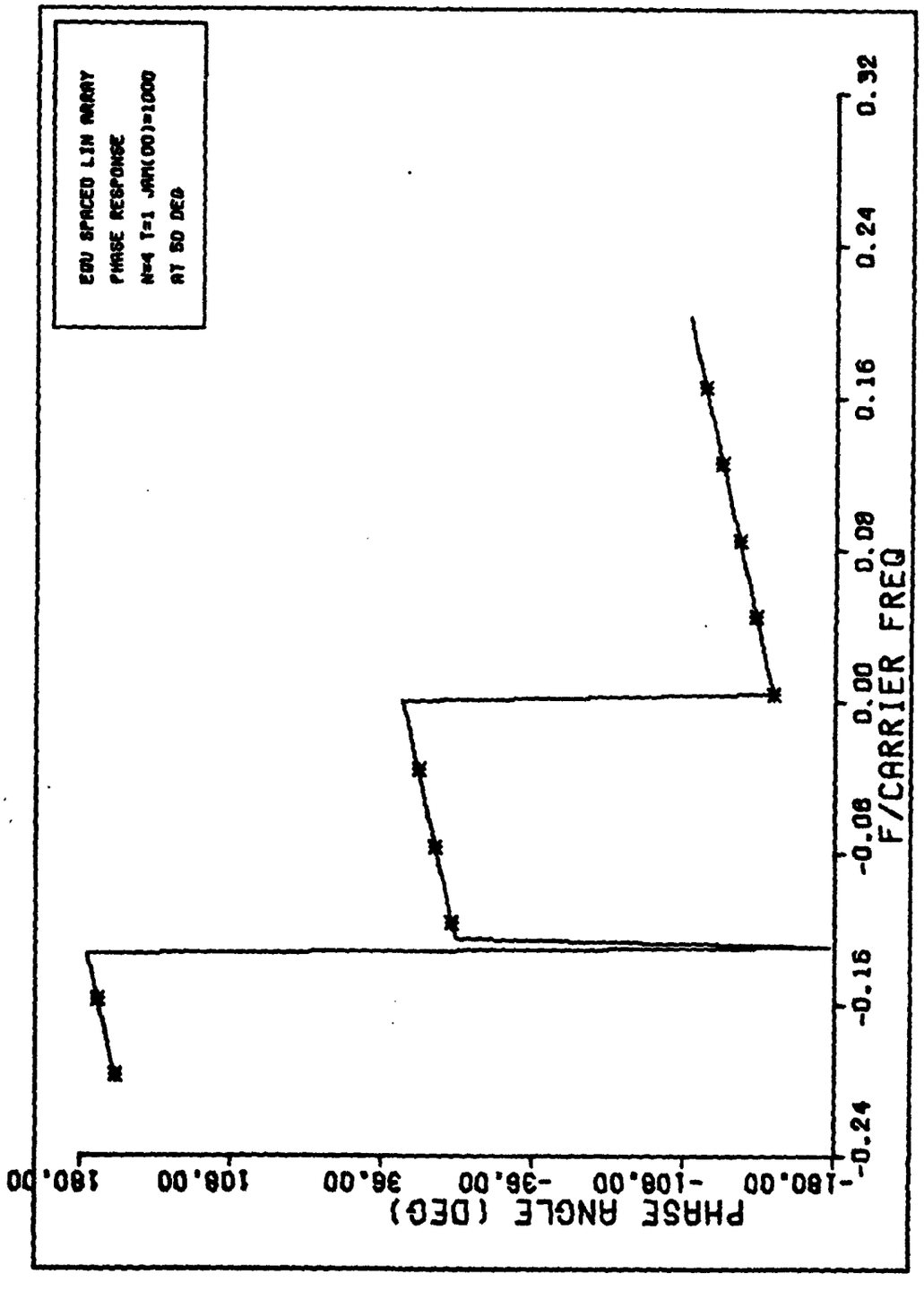

Figure B-7. Phase Response

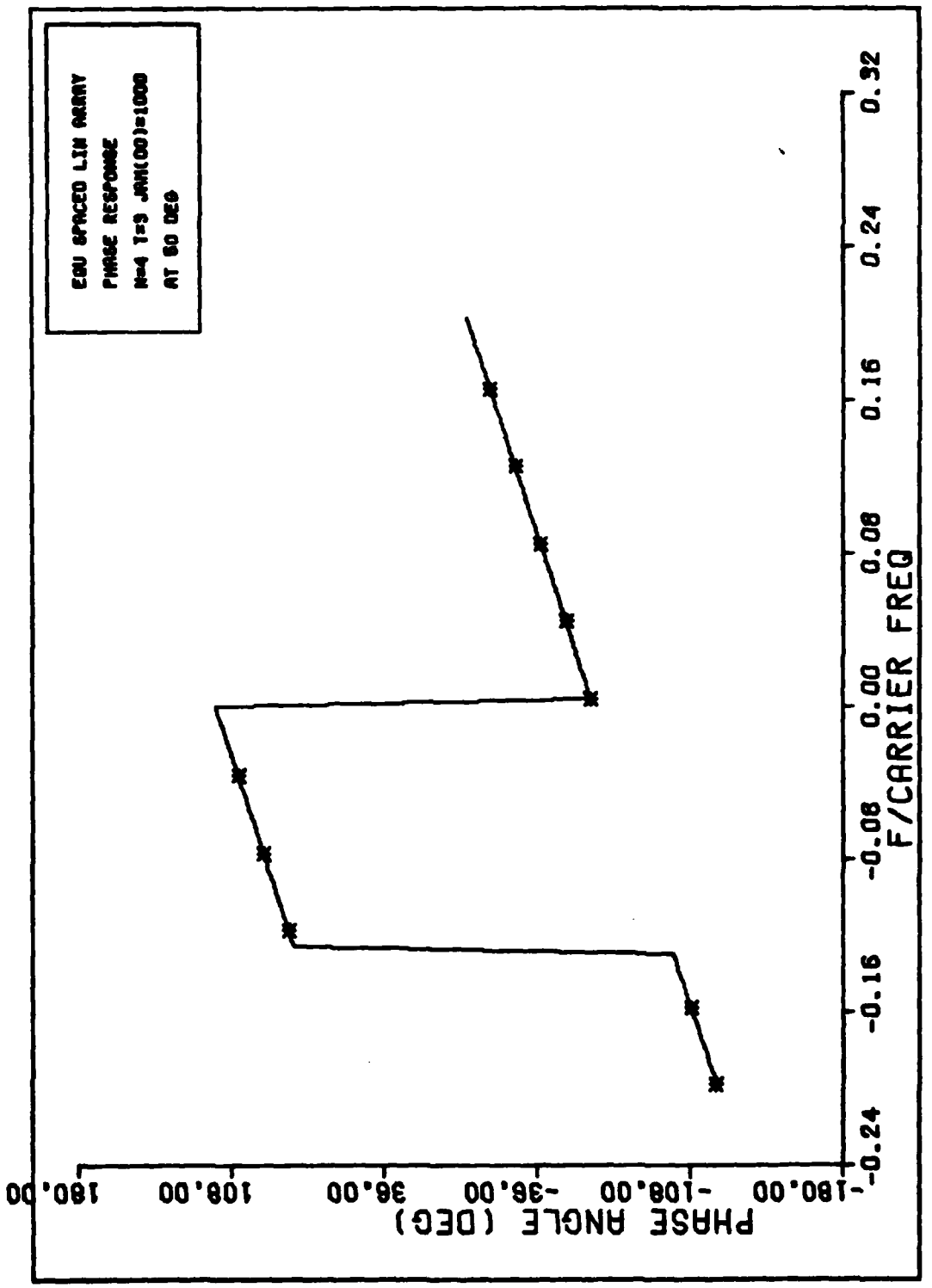

Figure B-8. Phase Response

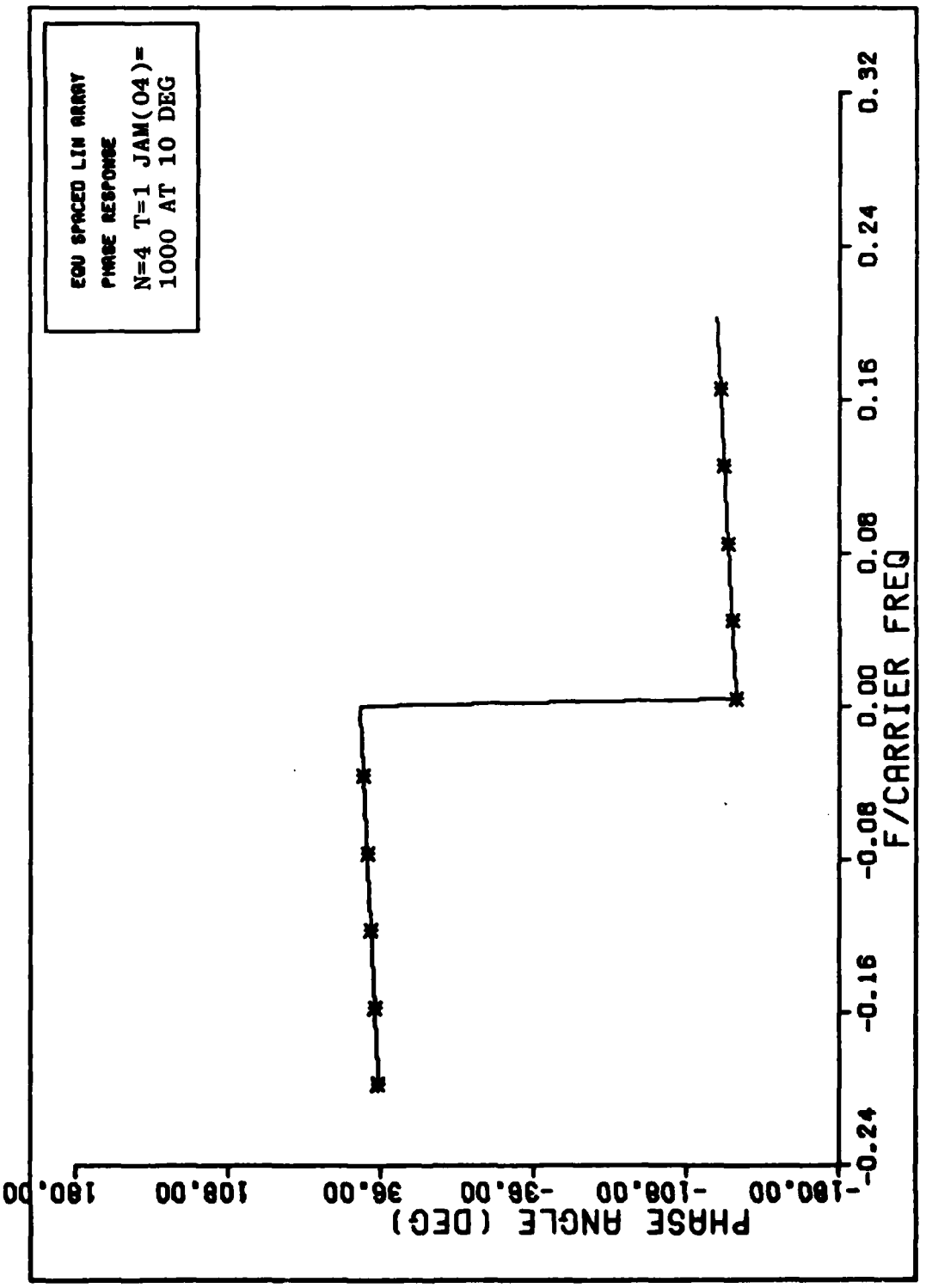

Figure B-9. Phase Response

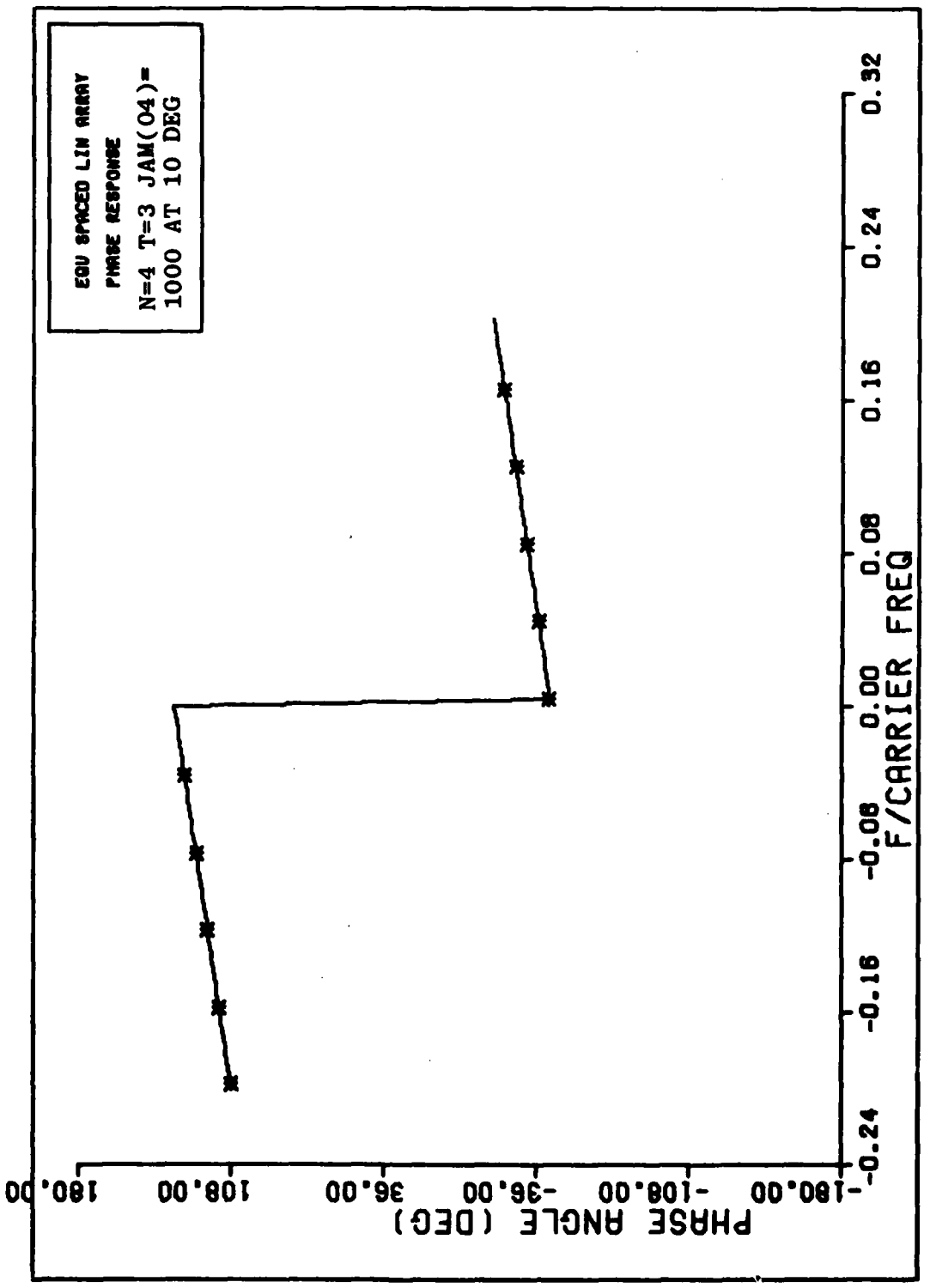

Figure B-10. Phase Response

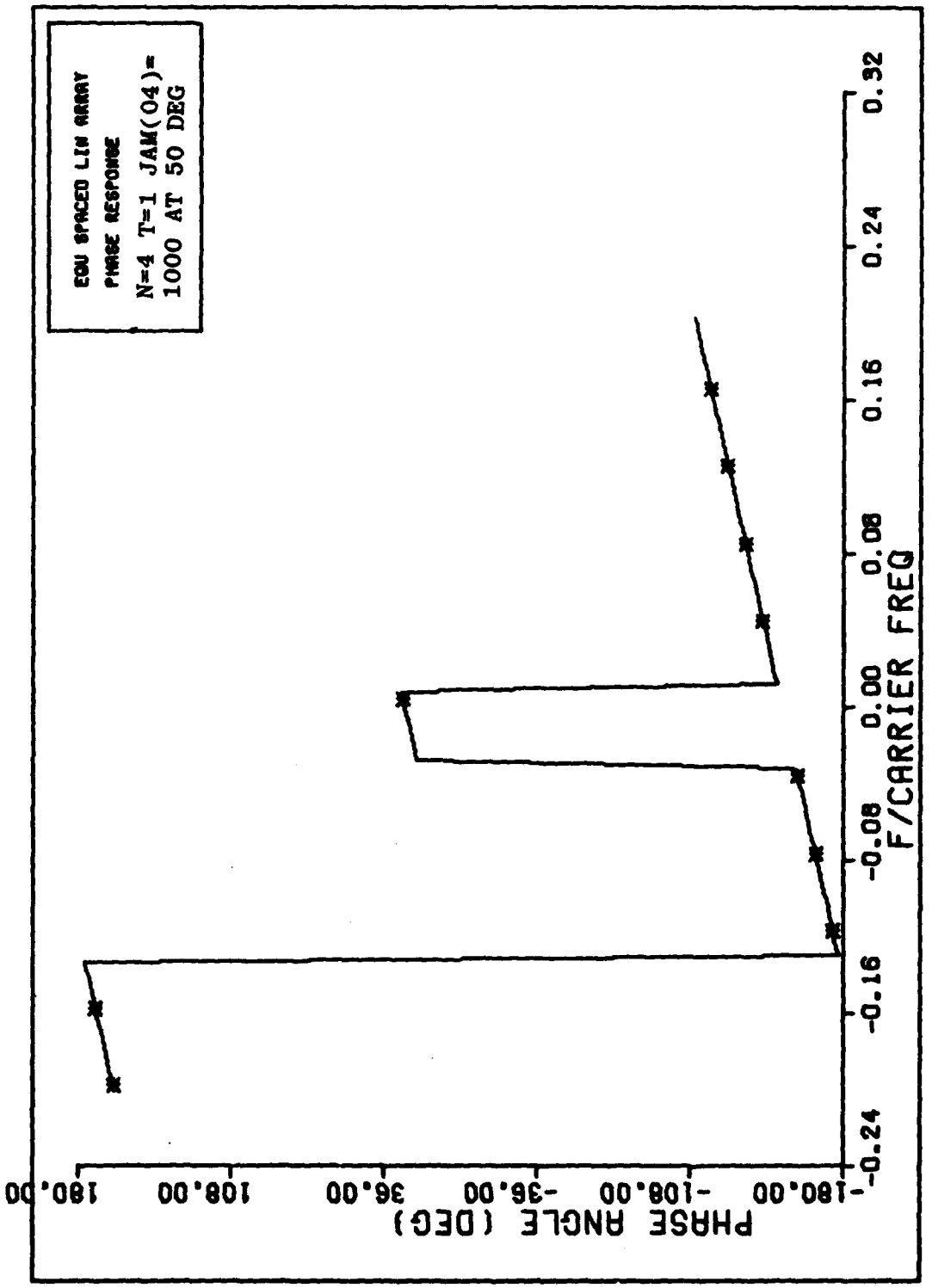

Figure B-11. Phase Response

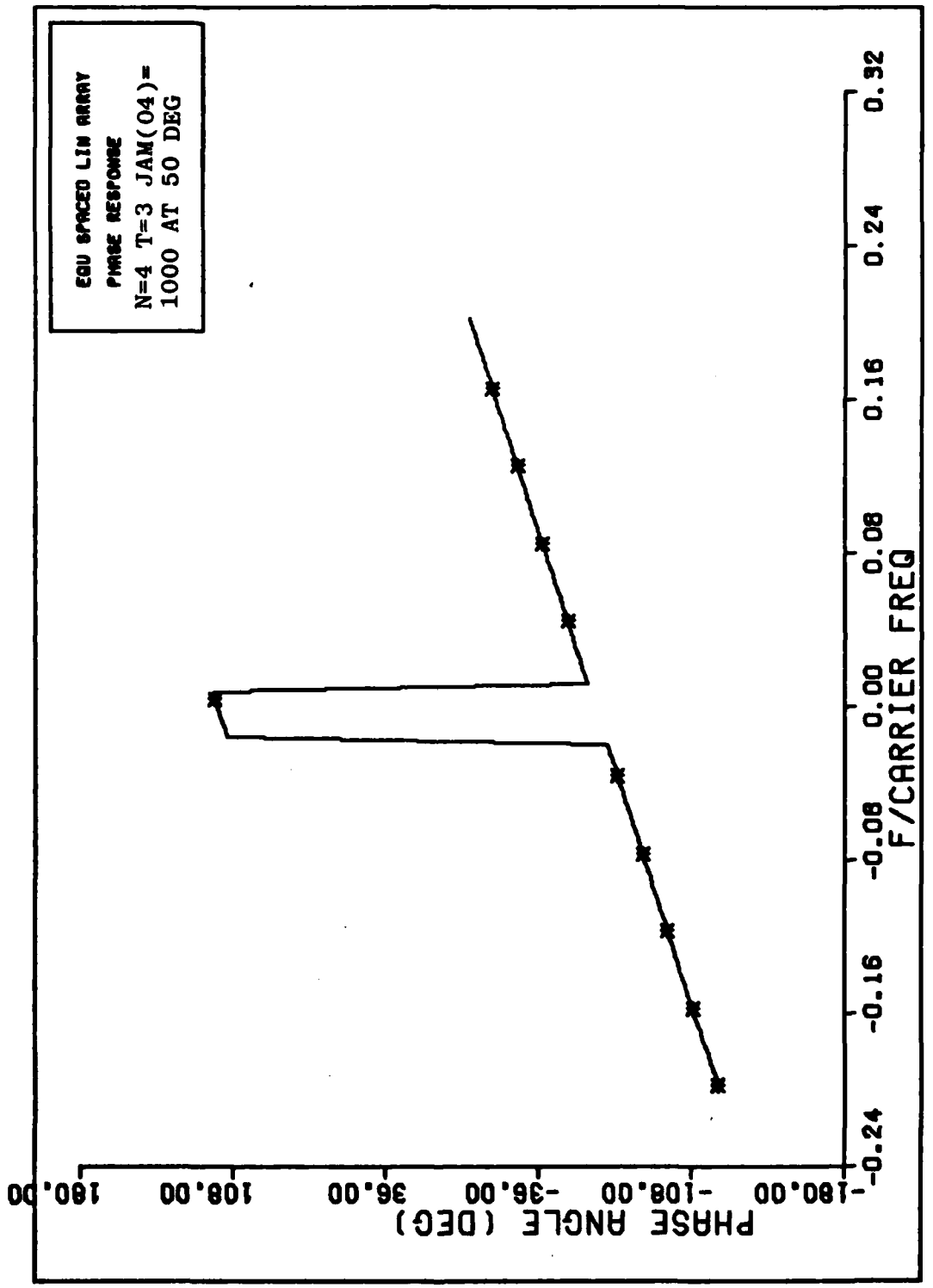

Figure B-12. Phase Response

Appendix C: Frequency Response Figures

This appendix contains frequency response plots which support the conclusions in the body of this paper. Also included are polar plots of some Taylor series coefficients.

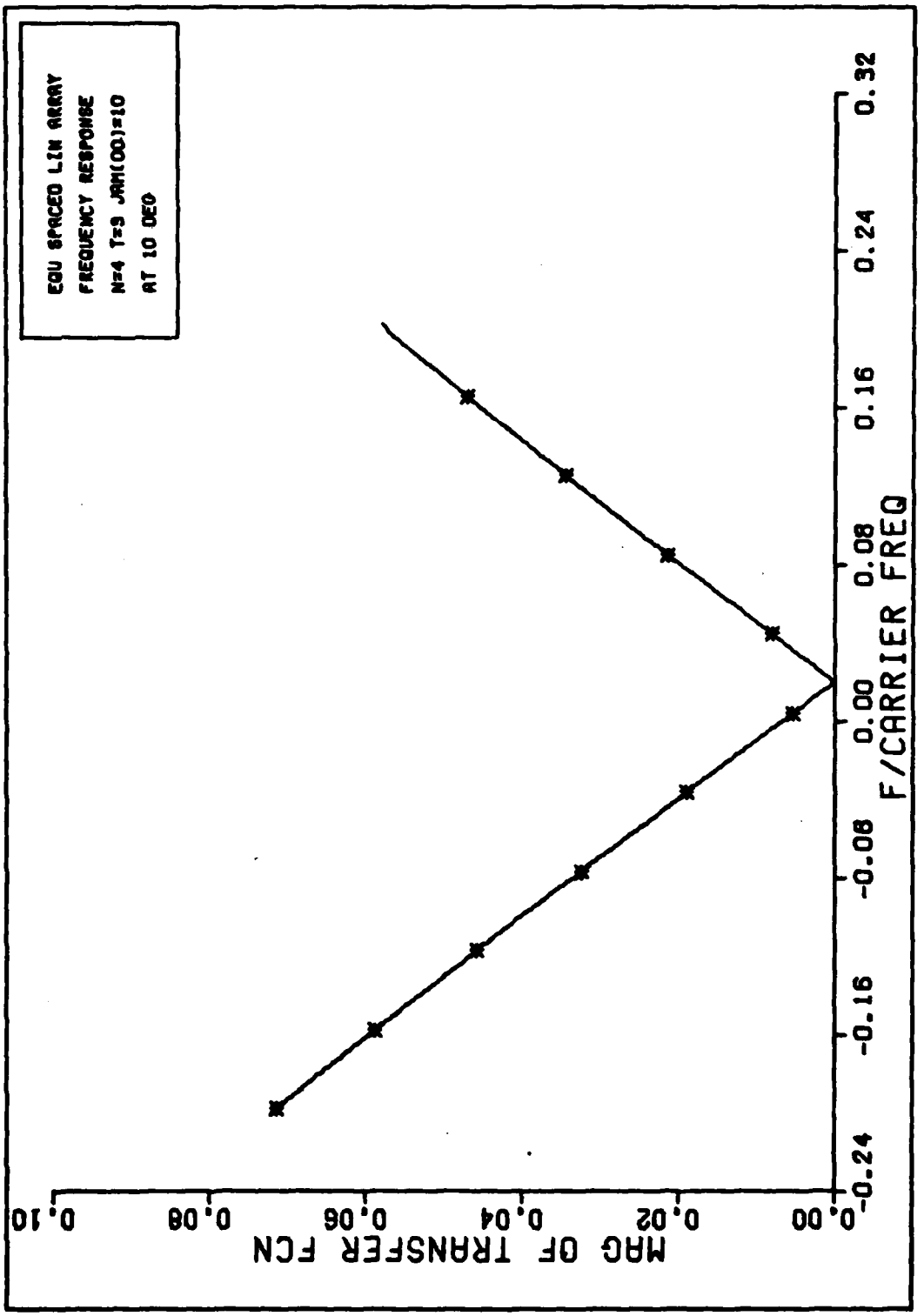

Figure C-1. Frequency Response

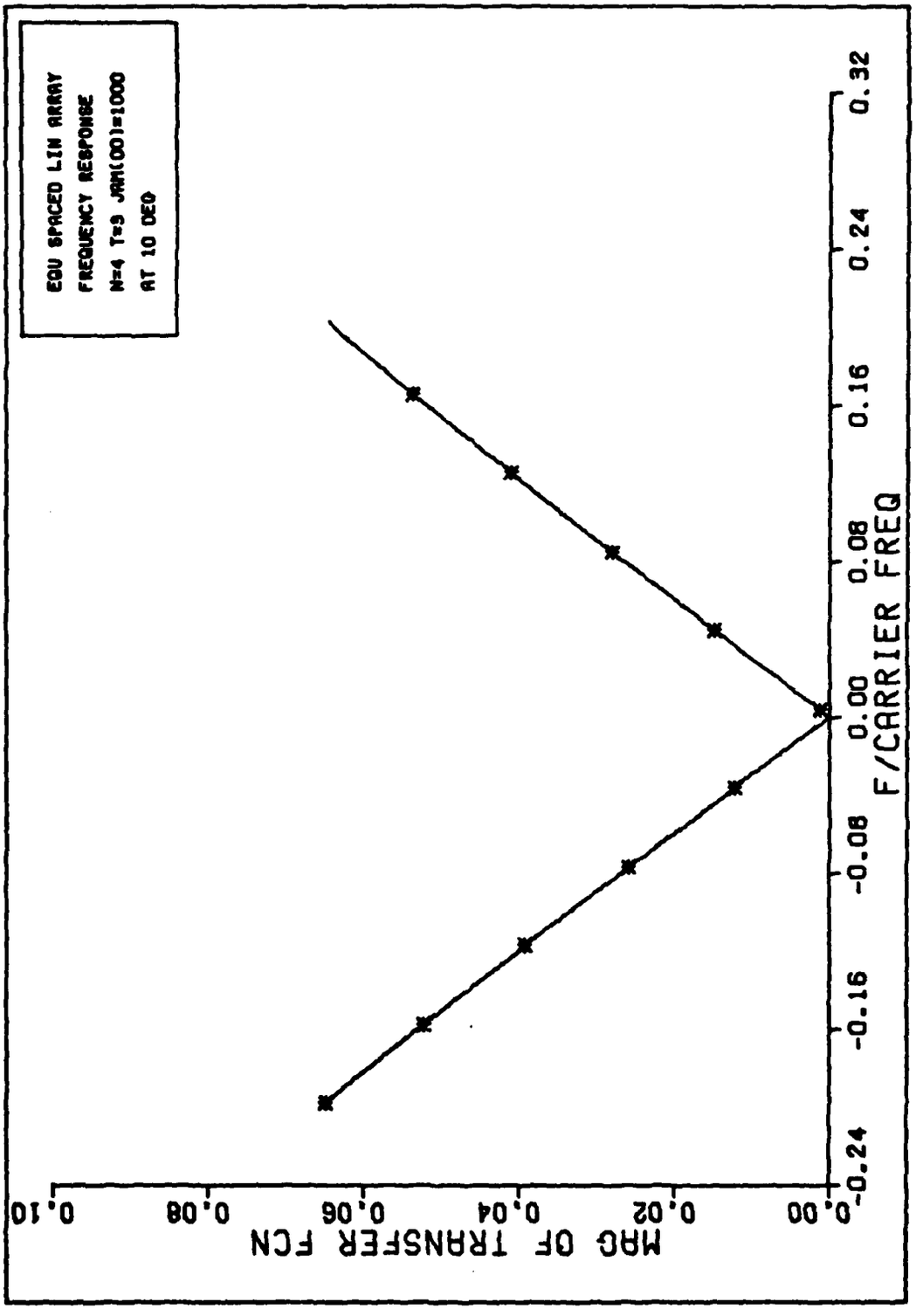

Figure C-2. Frequency Response

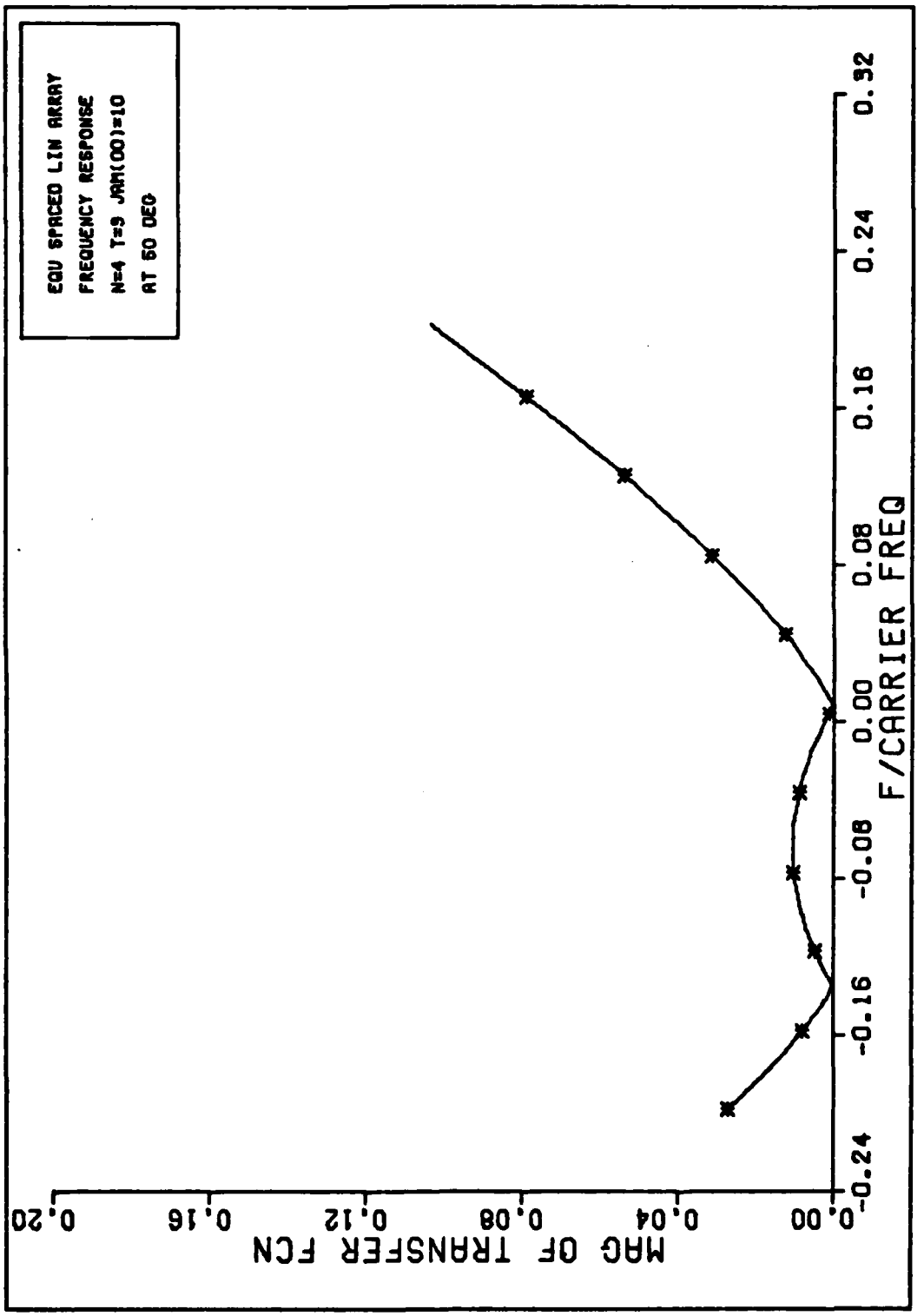

Figure C-3. Frequency Response

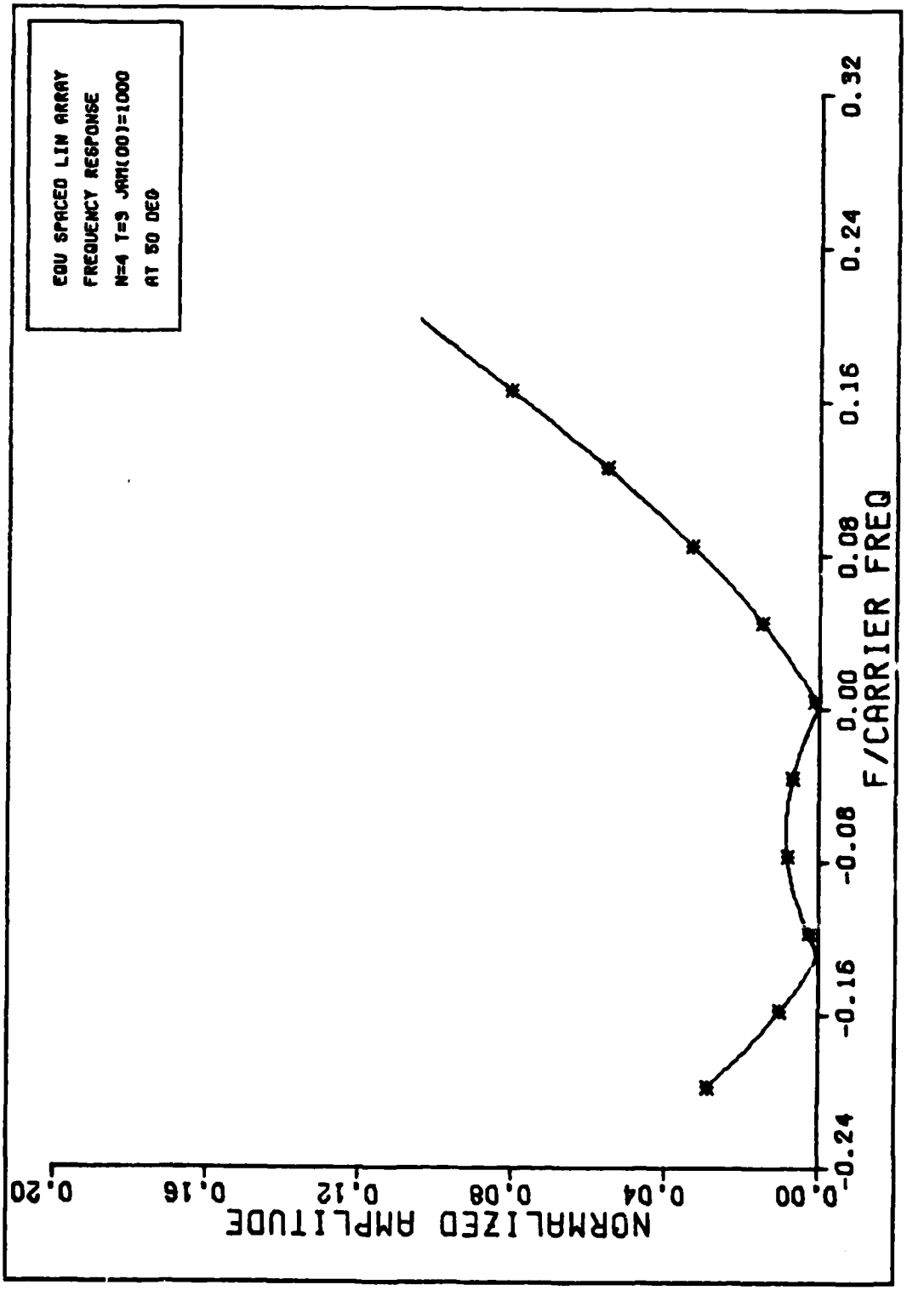

Figure C-4. Frequency Response

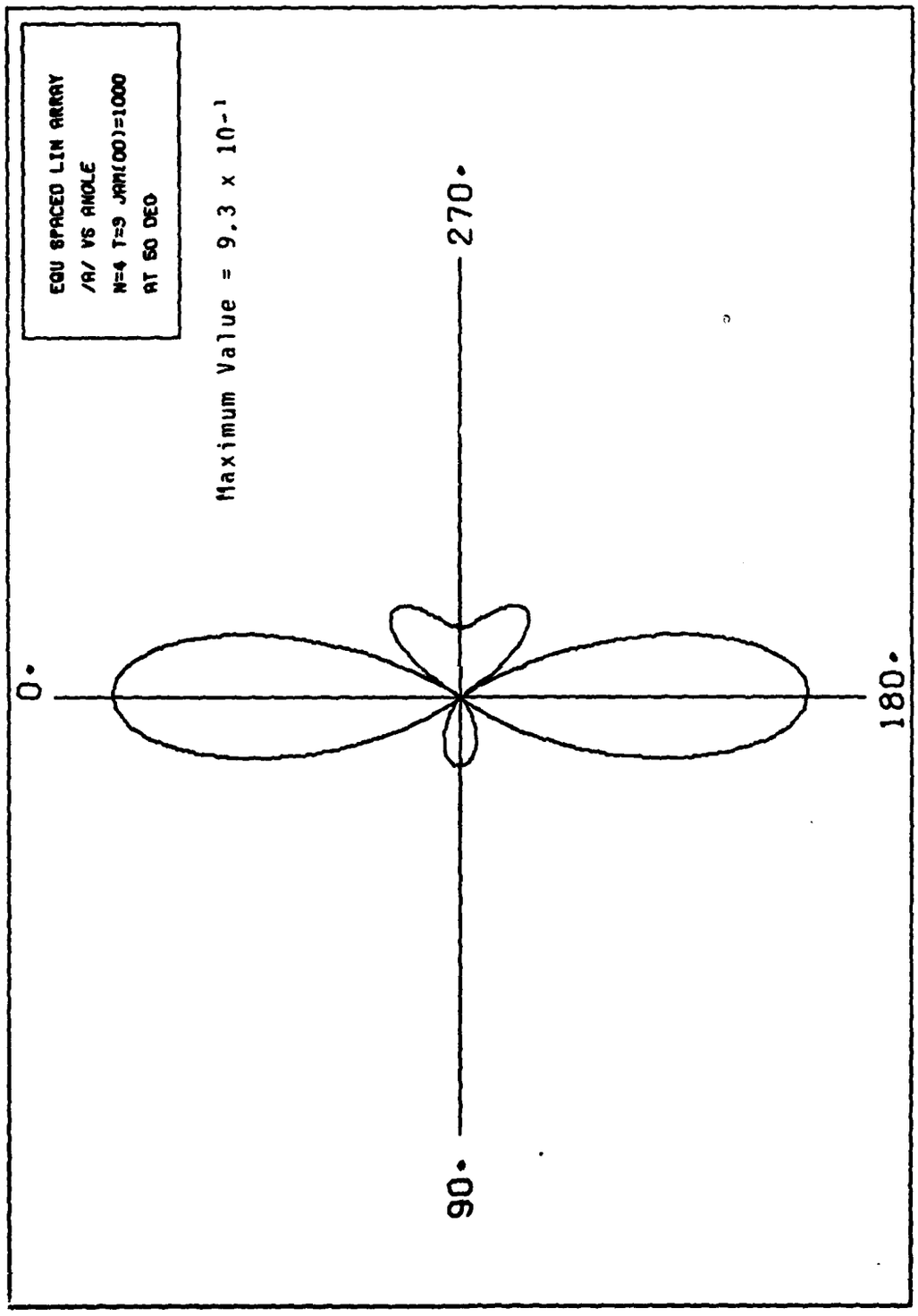

Figure C-5. Polar Plot of $|A(\theta)|$

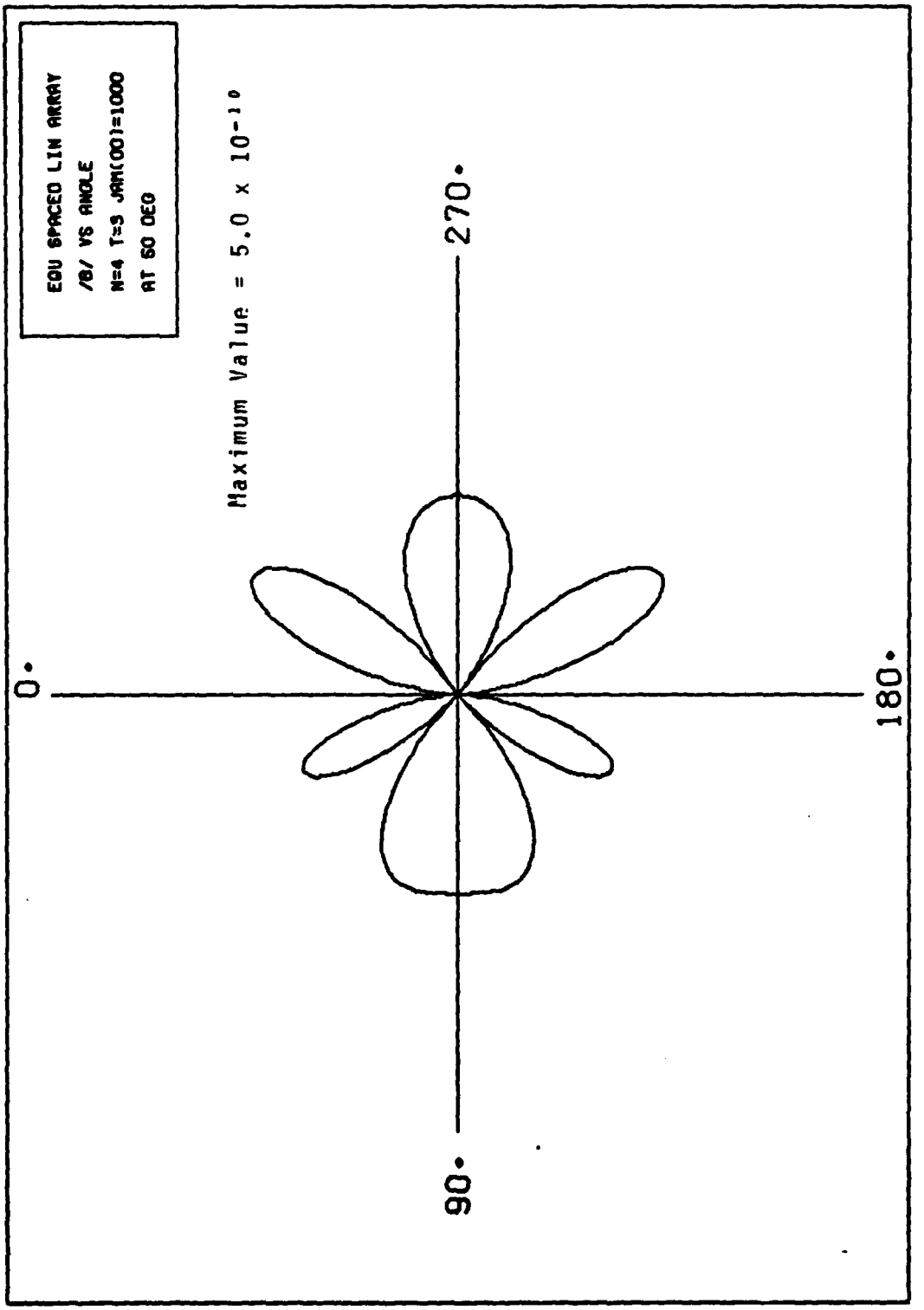

Figure C-6. Polar Plot of $|B(\theta)|$

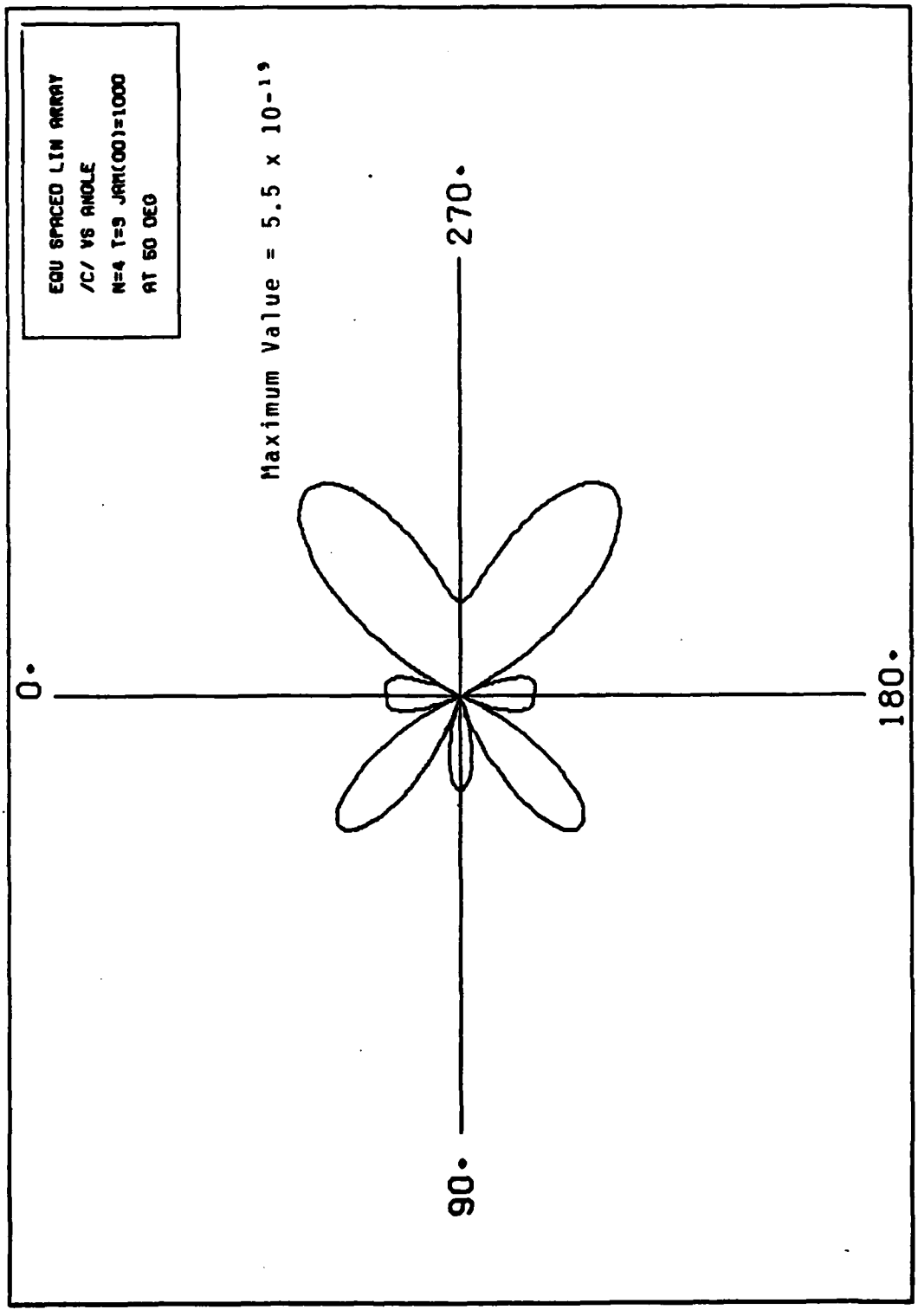

Figure C-7. Polar Plot of $|C(\theta)|$

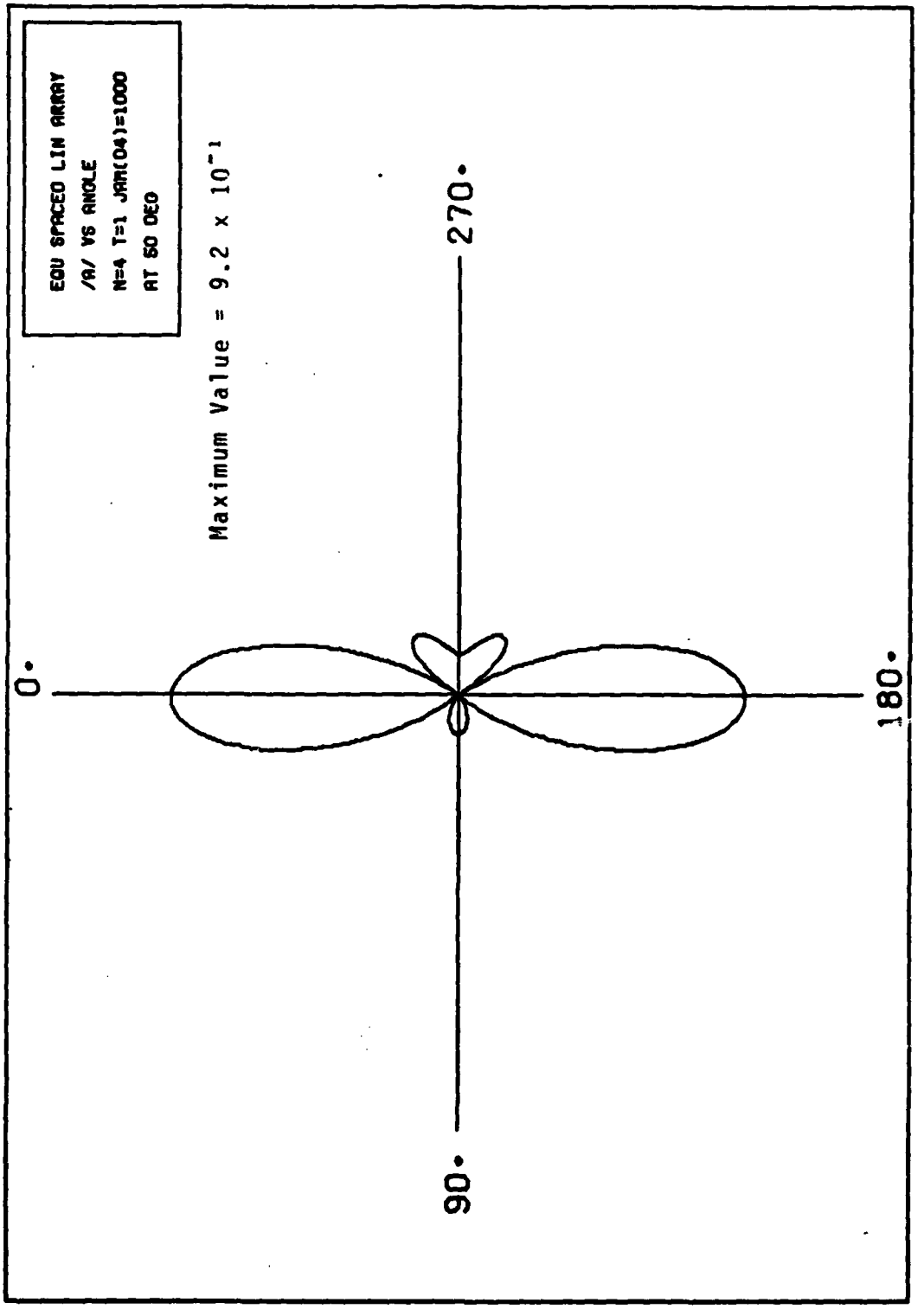

Figure C-8. Polar Plot of |A(θ)|

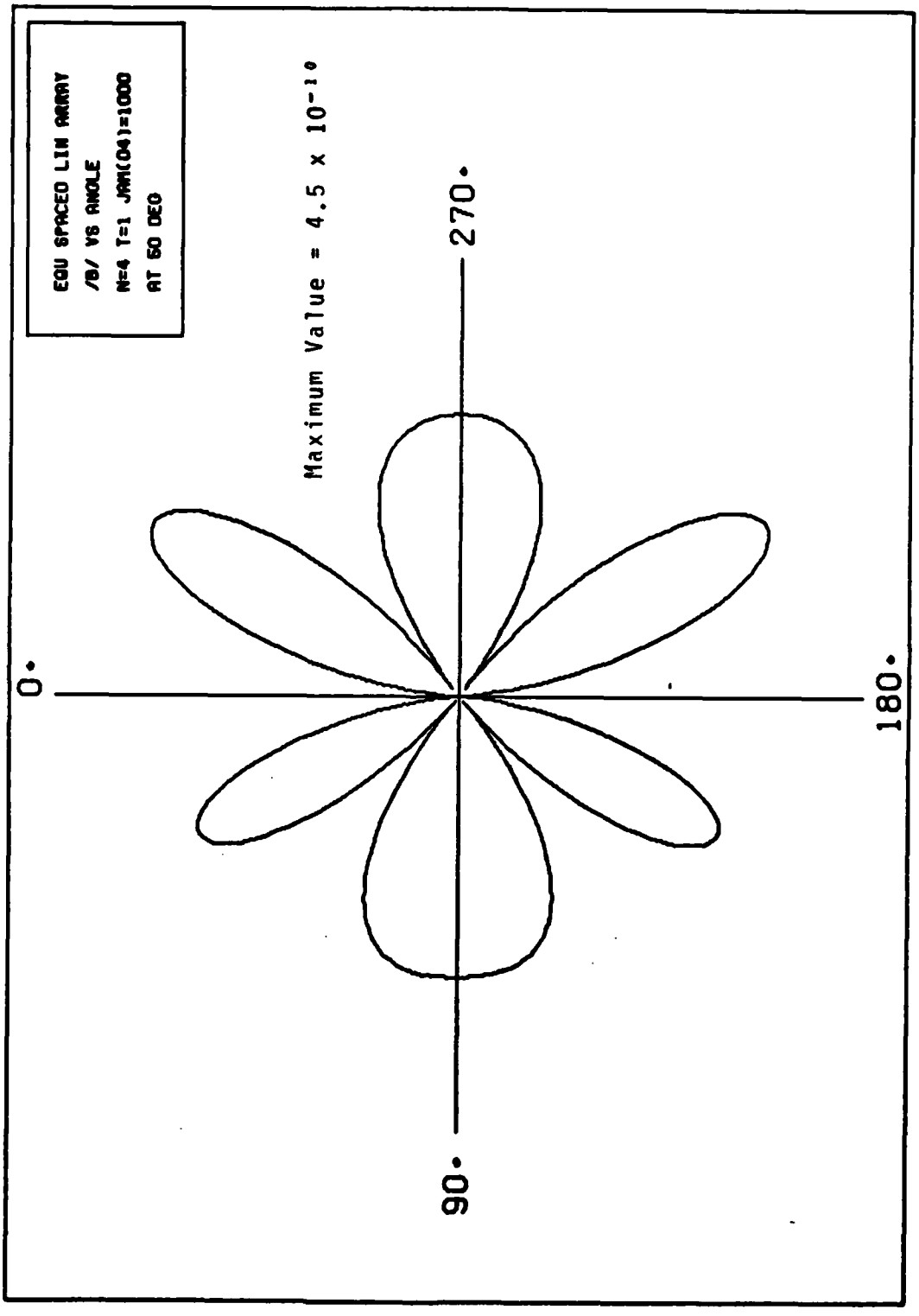

Figure C-9. Polar Plot of $|B(\theta)|$

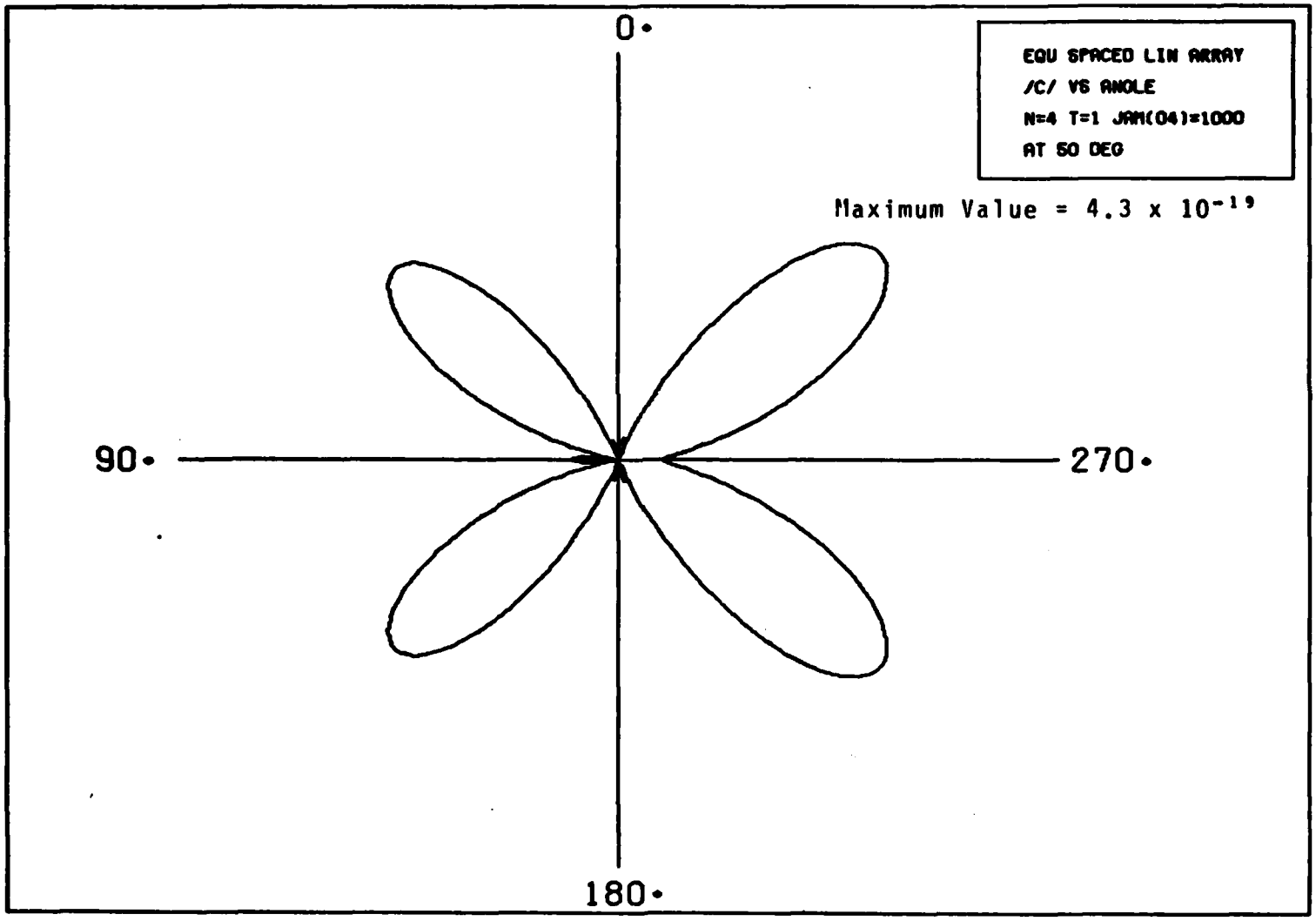

Figure C-10. Polar Plot of |C(θ)|

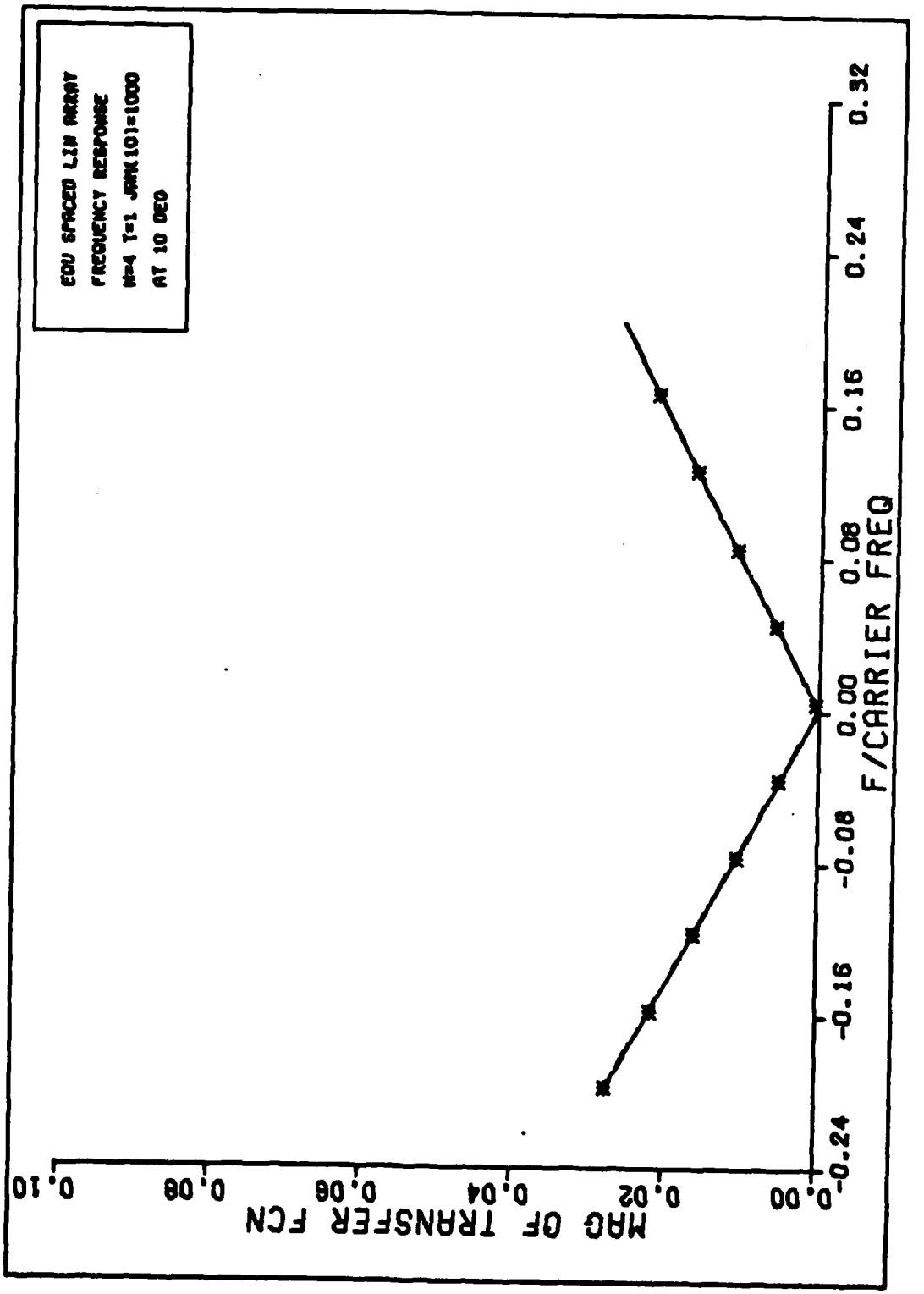

Figure C-11. Frequency Response

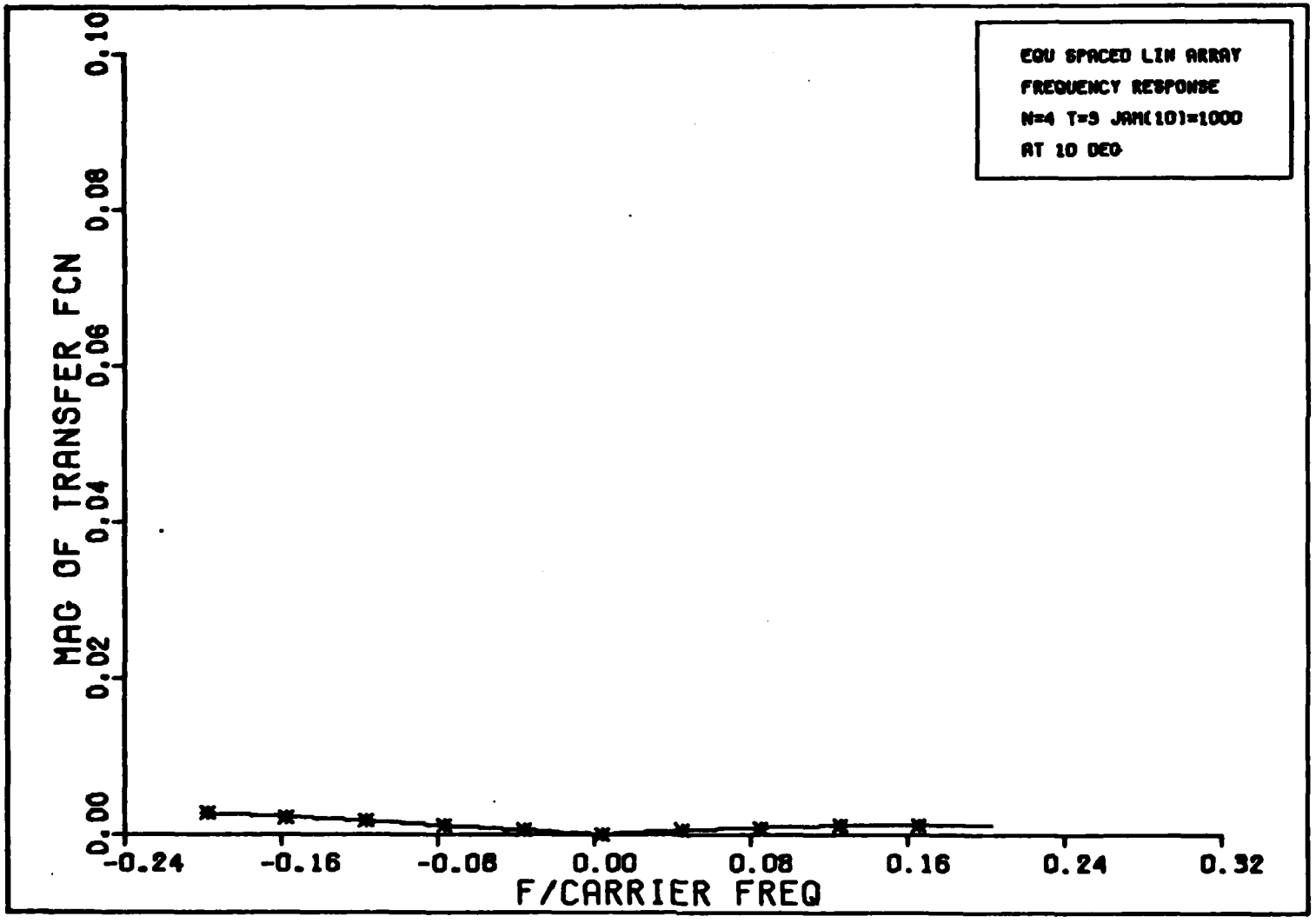

Figure C-12. Frequency Response

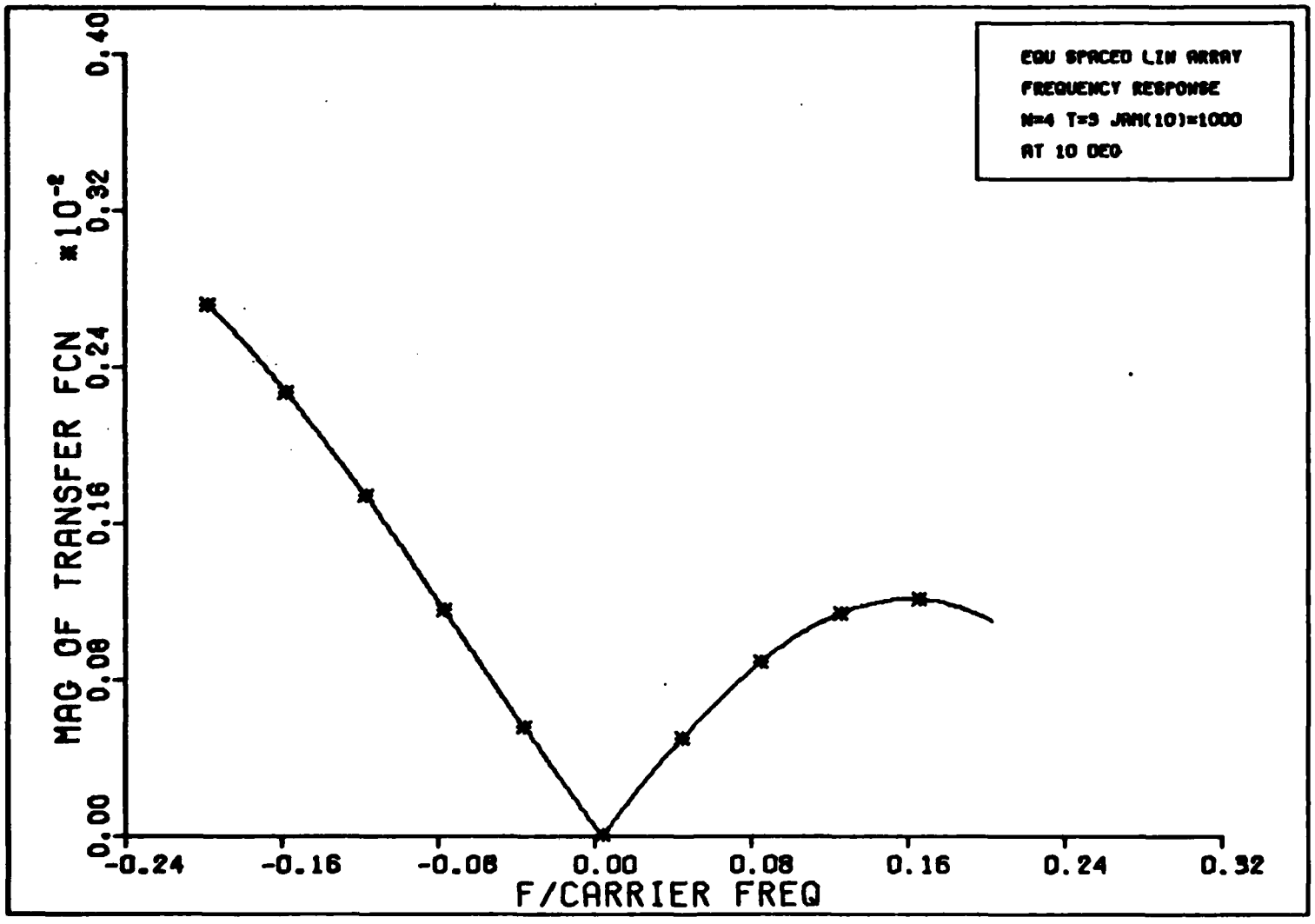

Figure C-13. Frequency Response

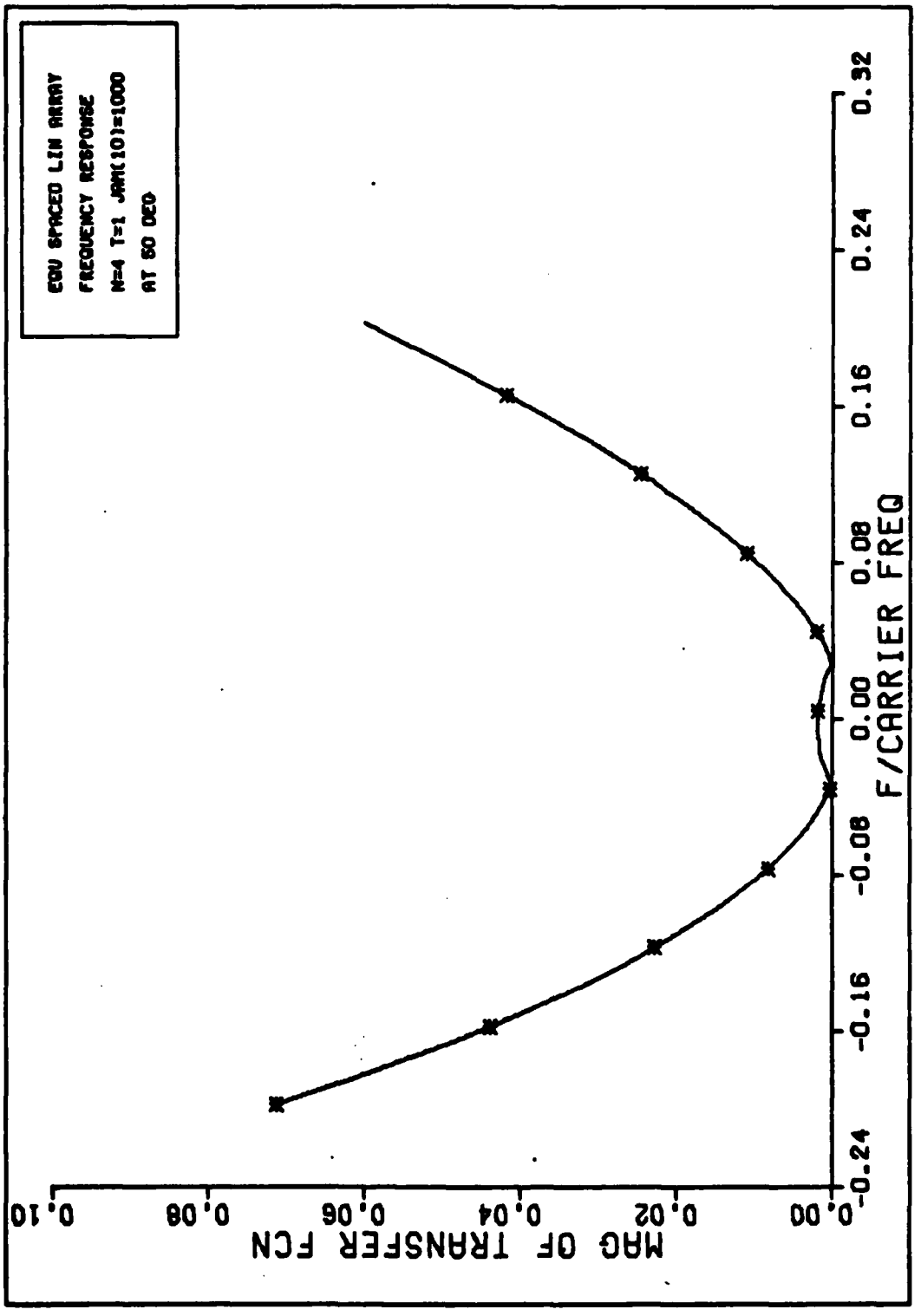

Figure C-14. Frequency Response

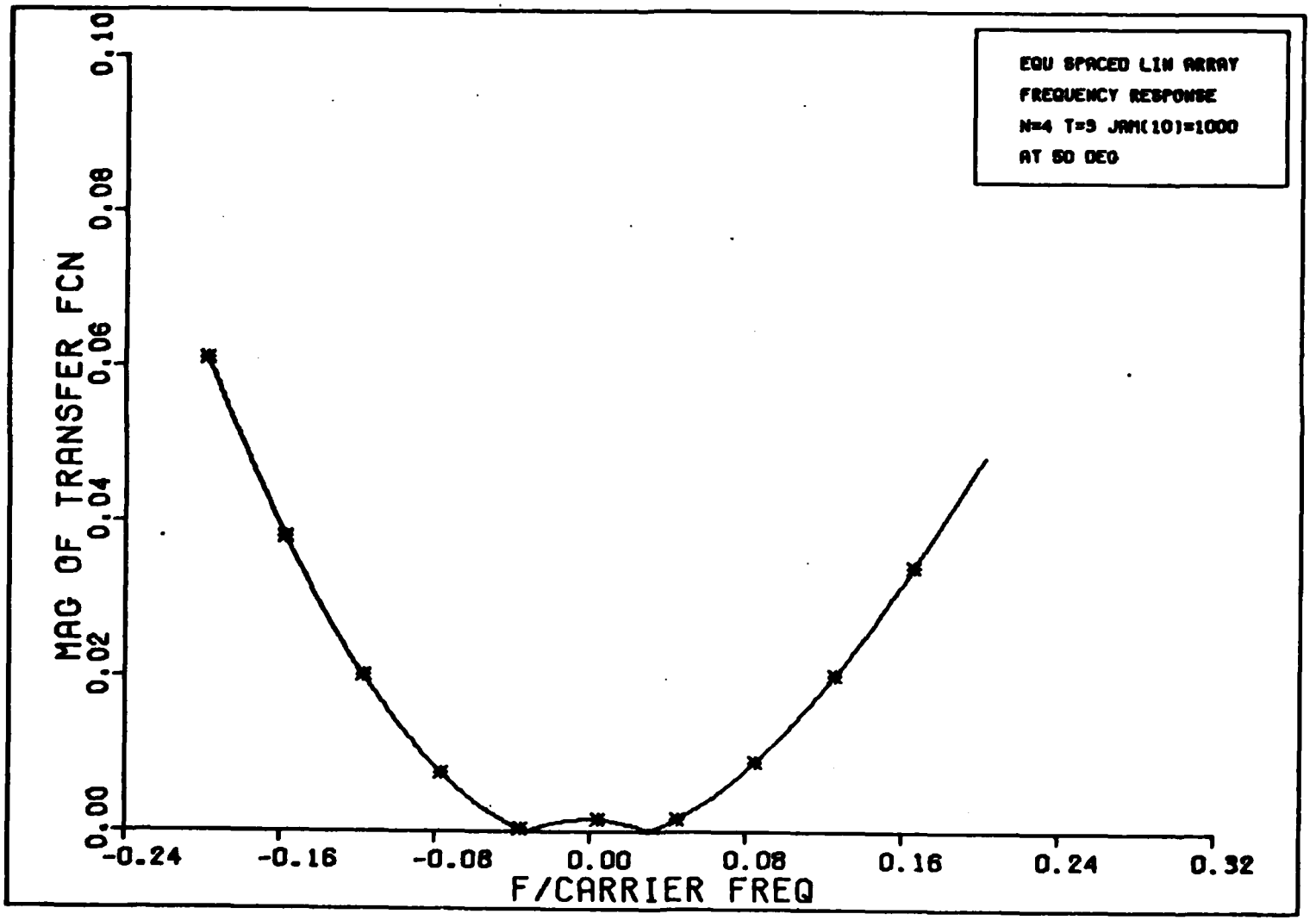

Figure C-15. Frequency Response

VITA

William Artman Riski was born 24 January 1952 in Cleveland, Ohio. He graduated from Wickliffe High School in Wickliffe, Ohio in 1970. He entered The Ohio State University in September of that year and graduated in March 1975 with a Bachelor of Science degree in Electrical Engineering. Upon graduation, he received a commission in the USAF through the ROTC program. He married Laura J. Palmer in April 1975 and was called to active duty in July 1975. From then until June 1978 he worked as a support equipment engineer in the E-3A System Program Office, Electronic Systems Division, Air Force Systems Command at Hanscom AFB, Massachusetts. He entered the School of Engineering, Air Force Institute of Technology, in June 1978.

Permanent address: 1713 Empire Road
Wickliffe, Ohio 44092

REPORT DOCUMENTATION PAGE

READ INSTRUCTIONS BEFORE COMPLETING FORM

1. REPORT NUMBER: AFIT/GE/EE/80-4	2. GOVT ACCESSION NO.: AD-A085708
3. RECIPIENT'S CATALOG NUMBER:	
4. TITLE (and Subtitle): EFFECTS OF ADAPTIVE ANTENNA ARRAYS ON BROADBAND SIGNALS	5. TYPE OF REPORT & PERIOD COVERED: MS Thesis
	6. PERFORMING ORG. REPORT NUMBER:
7. AUTHOR(s): William A. Riski	8. CONTRACT OR GRANT NUMBER(s):
9. PERFORMING ORGANIZATION NAME AND ADDRESS: Air Force Institute of Technology(AFIT/EN) Wright-Patterson AFB, Ohio 45433	10. PROGRAM ELEMENT, PROJECT, TASK AREA & WORK UNIT NUMBERS:
11. CONTROLLING OFFICE NAME AND ADDRESS: Communications & Control Div. (RADC/DCIA) Rome Air Development Center Griffiss AFB, New York 13441	12. REPORT DATE: June 1980
	13. NUMBER OF PAGES: 151
14. MONITORING AGENCY NAME & ADDRESS(if different from Controlling Office):	15. SECURITY CLASS. (of this report): Unclassified
	15a. DECLASSIFICATION DOWNGRADING SCHEDULE:

16. DISTRIBUTION STATEMENT (of this Report)

Approved for public release; distribution unlimited

17. DISTRIBUTION STATEMENT (of the abstract entered in Block 20, if different from Report)

18. SUPPLEMENTARY NOTES

Approved for public release, IAW AFR 190-17

JOSEPH P. HIPPS, Maj USAF
Director of Public Affairs

19. KEY WORDS (Continue on reverse side if necessary and identify by block number)

Antenna Arrays	Adaptive Arrays
Wideband Signals	Tapped Delay Lines
Broadband Signals	Jammers
Spread Spectrum	Interference Sources

20. ABSTRACT (Continue on reverse side if necessary and identify by block number)

This paper develops a complex baseband model for an adaptive array with N isotropic elements and T tapped delay lines behind each element. Three aspects of arrays are represented: spatial and temporal propagation delays and the weighting coefficients. The model is used to determine the steady state effect of arrays on wideband signals. Optimum weights are calculated based on the noise covariance matrix produced by single and multiple narrowband

jammers and single broadband jammers. It is shown that discrete spectral lines can be used to model a broadband jammer. For a jammer with 4% f_0 bandwidth, this approximation yields a correlation function which is accurate to within 0.53%. For a linear, equally spaced adaptive array the output consists of the input signal and its first time derivative. This first derivative distortion is reduced by the addition of tapped delay lines only when the noise environment contains broadband jammers. This performance improvement is quantified by increased null depth. The improvement, for a 4% f_0 bandwidth jammer, was 6.2db with a jammer located at 10^0 and 2.5db for a jammer at 50^0.